2007

Nitrogen Oxides in the North Atlantic Troposphere: Impacts of Boreal Wildfire and Anthropogenic Emissions

Maria Val Martin
Michigan Technological University

Nitrogen Oxides in the North Atlantic Troposphere: Impacts of Boreal Wildfire and Anthropogenic Emissions

By

María Val Martín

A DISSERTATION

Submitted in partial fulfillment of the requirements

for the degree of

DOCTOR OF PHILOSOPHY

(Engineering – Environmental)

MICHIGAN TECHNOLOGICAL UNIVERSITY

July 2007

This dissertation, "Nitrogen Oxides in the North Atlantic Troposphere: Impacts of Boreal Wildfire and Anthropogenic Emissions," is hereby approved in partial fulfillment of the requirements for the degree of DOCTOR OF PHILOSOPHY in the field of Engineering – Environmental.

Department of Civil and Environmental Engineering

Dr. Richard E. Honrath, Dissertation Advisor

Dr. Judith Perlinger, Non-Departamental Program Chair

Date

Abstract

Nitrogen oxides play a crucial role in the budget of tropospheric ozone (O_3) and the formation of the hydroxyl radical. Anthropogenic activities and boreal wildfires are large sources of emissions in the atmosphere. However, the influence of the transport of these emissions on nitrogen oxides and O_3 levels at hemispheric scales is not well understood, in particular due to a lack of nitrogen oxides measurements in remote regions. In order to address these deficiencies, measurements of NO, NO_2 and NO_y (total reactive nitrogen oxides) were made in the lower free troposphere (FT) over the central North Atlantic region (Pico Mountain station, 38°N 28°W, 2.3 km asl) from July 2002 to August 2005.

These measurements reveal a well-defined seasonal cycle of nitrogen oxides (NO_x = NO+NO_2 and NO_y) in the background central North Atlantic lower FT, with higher mixing ratios during the summertime. Observed NO_x and NO_y levels are consistent with long-range transport of emissions, but with significant removal en-route to the measurement site. Reactive nitrogen largely exists in the form of PAN and HNO_3 (∼80–90% of NO_y) all year round. A shift in the composition of NO_y from dominance of PAN to dominance of HNO_3 occurs from winter–spring to summer–fall, as a result of changes in temperature and photochemistry over the region.

Analysis of the long-range transport of boreal wildfire emissions on nitrogen oxides provides evidence of the very large-scale impacts of boreal wildfires on the tropospheric NO_x and O_3 budgets. Boreal wildfire emissions are responsible for significant shifts in the nitrogen oxides distributions toward higher levels during the summer,

with medians of NO_y (117–175 pptv) and NO_x (9–30 pptv) greater in the presence of boreal wildfire emissions. Extreme levels of NO_x (up to 150 pptv) and NO_y (up to 1100 pptv) observed in boreal wildfire plumes suggest that decomposition of PAN to NO_x is a significant source of NO_x, and imply that O_3 formation occurs during transport. Ozone levels are also significantly enhanced in boreal wildfire plumes. However, a complex behavior of O_3 is observed in the plumes, which varies from significant to lower O_3 production to O_3 destruction.

Long-range transport of anthropogenic emissions from North America also has a significant influence on the regional NO_x and O_3 budgets. Transport of pollution from North America causes significant enhancements on nitrogen oxides year-round. Enhancements of CO, NO_y and NO_x indicate that, consistent with previous studies, more than 95% of the NO_x emitted over the U.S. is removed before and during export out of the U.S. boundary layer. However, about 30% of the NO_x emissions exported out of the U.S. boundary layer remain in the airmasses. Since the lifetime of NO_x is shorter than the transport timescale, PAN decomposition and potentially photolysis of HNO_3 provide a supply of NO_x over the central North Atlantic lower FT. Observed $\Delta O_3/\Delta NO_y$ and large NO_y levels remaining in the North American plumes suggest potential O_3 formation well downwind from North America.

Finally, a comparison of the nitrogen oxides measurements with results from the global chemical transport (GCT) model GEOS-Chem identifies differences between the observations and the model. GEOS-Chem reproduces the seasonal variation of nitrogen oxides over the central North Atlantic lower FT, but does not capture the magnitude of the cycles. Improvements in our understanding of nitrogen oxides chemistry in the remote FT and emission sources are necessary for the current GCT models to adequately estimate the impacts of emissions on tropospheric NO_x and the resulting impacts on the O_3 budget.

Acknowledgements

I wish to thank everyone who has contributed to this work. First, I would like to thank Dr. Richard Honrath, my advisor, for all his guidance, his patience and his support throughout this research. In addition, I would also like to thank the members of my committee—Drs. Judith Perlinger, Jim Mihelcic and William Cantrell— for their advice in my PhD proposal and dissertation. Thank you also to my research group for all their help during my years as a graduate student. In particular, I thank Chris Owen for providing the FLEXPART simulations used in Chapter 2 and the HYSPLIT backward trajectories, and for his help in interpreting transport patterns; Dr. Jan Kleissl for supplying the analysis of upslope flow periods; Kateryna Lapina for letting me use her FLEXPART Fire-CO tracer simulations and her comments on boreal wildfire emission factors; and Jessica Strane for her assistance in airflow analyses.

I also appreciate the help of many people involved in the Pico Mountain project. In particular, Mike Dziobak for helping me run the $NO_{x,y}$ system and survive weather conditions at the Pico Mountain. I would also like to thank Dr. Paulo Fialho (Azores University, Portugal) for providing the aerosol black carbon data, Dr. Gabriele Pfister (National Center for Atmospheric Research) for providing the MOZART simulations, Dr. Qinbin Li (Jet Propulsion Lab) for supplying the GEOS-Chem simulations and Dr. Andrea Stohl (Norwegian Institute for Air Research) for providing the FLEXPART stratospheric O_3 tracer simulations used in Chapter 3. I thank the National Science Foundation, the National Oceanic and Atmospheric Administration and the

Civil and Environmental Engineering Department at Michigan Tech for financial support.

Finally, a very special thank you goes to my family, Toni Rubert Godoy and my friends, in particular Domenico Baú, for their support and their encouragement to complete this work, and their belief in my abilities.

Contents

List of Figures

List of Tables

Chapter 1

Introduction

Nitrogen oxides play a central role in the chemistry of the atmosphere since they critically determine levels of ozone (O_3) and acidity [*Levy II*, 1971; *Crutzen*, 1979; *Logan*, 1983]. Ozone is both an important anthropogenic greenhouse gas [*Alley et al.*, 2007] and a regulator of the tropospheric oxidation strength, via controlling the concentration of tropospheric OH [*Logan*, 1983]. In addition, by being a strong oxidant, O_3 has negative effects on human health and ecosystems, at concentrations not far above ambient.

The concentration of NO_x ($NO+NO_2$) in the atmosphere depends on the source strength and the rates of reactions converting NO_x to nitric acid (HNO_3), peroxyacetyl nitrate, (PAN, $CH_3C(O)O_2NO_2$) or other minor compounds and their uptake into precipitation or deposition at the Earth surface [*Logan*, 1983], as shown in Figure 1.1. Collectively, all reactive nitrogen oxides species are denoted as NO_y, which is the sum of NO_x and its oxidation products, *i.e.*, $NO+NO_2+HNO_3+PAN+2N_2O_5+$alkyl nitrates+aerosol NO_3^-+other minor species.

Fossil fuel combustion resulting from anthropogenic activities is the major source of NO_x emissions in the Northern Hemisphere [*Alley et al.*, 2007], with the majority of these emissions located over industrial regions as shown in Figure 1.2. In recent

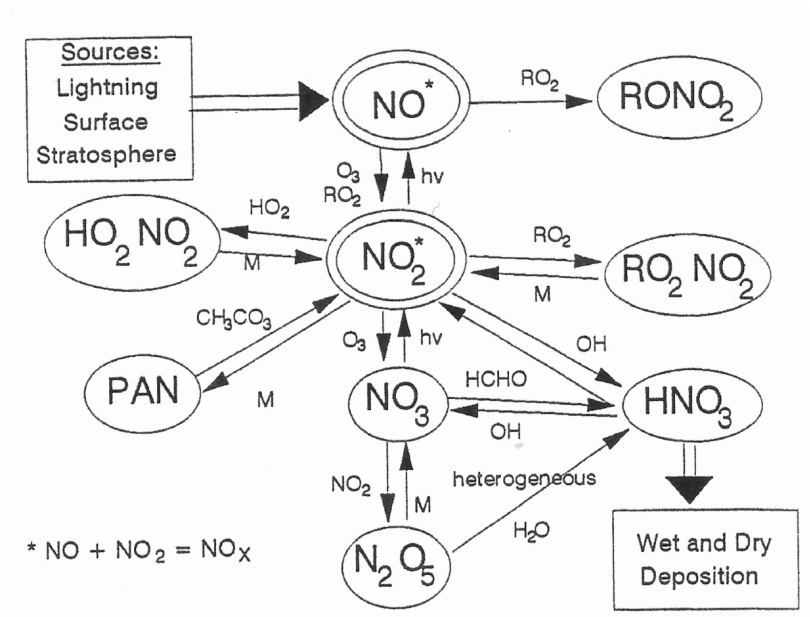

Figure 1.1 Schematic of photochemical cycles among reactive nitrogen species in the troposphere [*Carroll and Thompson*, 1995].

years, as a result of increased area burned and fire frequency over the boreal region [*Kasischke and Turetsky*, 2006], emissions from the boreal wildfires have resulted in a significant source of NO_x to the atmosphere during the summer season [*Goode et al.*, 2000; *Andreae and Merlet*, 2001]. Oxidation of NO_x emitted from these sources takes place on the order of one day within the continental boundary layer (BL). During the day, oxidation of NO_2 to HNO_3 by reaction with OH is the principal sink of tropospheric NO_x. At night, reaction of NO_2 with O_3 followed by heterogeneous hydrolysis of N_2O_5 in aerosols is also an important sink [*Parrish et al.*, 1998; *Brown et al.*, 2006]. HNO_3 leaves the atmosphere by dry or wet deposition, constituting a major component of acid deposition [*Logan*, 1983].

Reaction of NO_2 with peroxyacetyl radical, which is formed by oxidation of ethane, forms PAN:

$$CH_3C(O)O_2 + NO_2 \rightleftharpoons CH_3C(O)O_2NO_2. \tag{1.1}$$

PAN is a key species in the dispersal of NO_x away from the source emissions. The

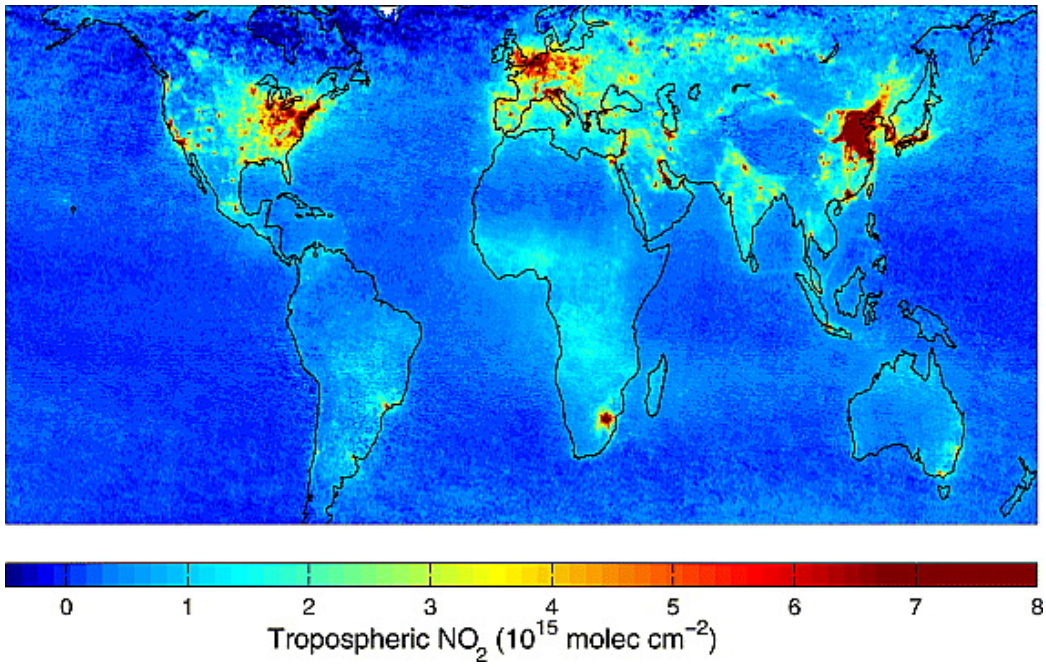

Figure 1.2 Mean tropospheric NO_2 columns retrieved from the SCIAMACHY satellite instrument for May 2004 to April 2005 [*Martin et al.*, 2006].

lifetime of PAN is strongly temperature dependent (∼30 days at -10°C and ∼3 days at 2°C) [*Singh*, 1987]. In the FT, at lower temperatures and pressures, the equilibrium of reaction 1.1 is shifted to the right side. In a later stage, when the airmasses subside or advect to warmer regions, NO_2 and peroxyacetyl radical are released. It has also been suggested that, similar to PAN, the export of HNO_3 followed by photolysis to NO_x can be an important source of NO_x in the troposphere [*Neuman et al.*, 2006].

Quantifying the sources and fate of nitrogen oxides in the troposphere is critical for assessing the influence of anthropogenic and boreal wildfire emissions on global tropospheric O_3. Tropospheric O_3 is controlled by production and reaction processes and is principally limited by the presence of NO_x. The primary loss mechanism of O_3 is via photolysis and subsequent reaction of $O(^1D)$ with H_2O, which occurs in competition with deactivation to $O(^3P)$:

$$O_3 + h\nu \longrightarrow O(^1D) + O_2 \tag{1.2}$$

$$O(^1D) + H_2O \longrightarrow 2OH \quad (1.3)$$

$$O(^1D) \xrightarrow{M} O(^3P), \quad (1.4)$$

where M denotes N_2 or O_2.

The hydroxyl radical (OH) formed in reaction 1.3 oxidizes CO, methane (CH_4), and other hydrocarbons (RH) and thereby produces peroxy radicals ($PO_2 = HO_2 + CH_3O_2 + RO_2$):

$$CO + OH \xrightarrow{O_2} CO_2 + HO_2 \quad (1.5)$$

$$CH_4 + OH \xrightarrow{O_2} CH_3O_2 + H_2O \quad (1.6)$$

$$RH + OH \xrightarrow{O_2} RO_2 + H_2O. \quad (1.7)$$

Peroxy radicals are responsible for the photochemical production or destruction of tropospheric O_3, depending critically on the availability of NO [*Liu et al.*, 1992; *Cox*, 1999]. In regions, where levels of NO_x are higher than 10–50 pptv [*Fishman et al.*, 1979; *Lin et al.*, 1988], PO_2 oxidation of NO results in formation of O_3 through:

$$NO + PO_2 \longrightarrow NO_2 + PO \quad (1.8)$$

$$NO_2 + h\nu \longrightarrow NO + O \quad (1.9)$$

$$O + O_2 \xrightarrow{M} O_3, \quad (1.10)$$

where PO is the alkoxy radical or OH. In remote clean regions, where NO_x mixing ratios are lower than 10–50 pptv, the occurrence of reaction 1.8 is reduced, resulting in reduced O_3 formation and an increased rate of O_3 destruction through reaction 1.11:

$$O_3 + HO_2 \longrightarrow OH + 2O_2. \quad (1.11)$$

In addition to reactions 1.2–1.3 and 1.11, O_3 is also removed by deposition to the surface and heterogeneous loss in clouds, and destroyed to a lesser extent via reaction with OH:

$$O_3 + OH \longrightarrow HO_2 + 2O_2. \quad (1.12)$$

The dependence of O_3 production of NO_x is highly non-linear, *i.e.*, the ozone production efficiency per molecule of NO_x consumed increases rapidly as NO_x concentration decreases [*Liu et al.*, 1987]. As a result, the in-situ production of O_3 in clean remote regions is more efficient than is production in source regions [*Jacob et al.*, 1993]. Regardless of the NO_x level, an increase in NO_x may result in increased O_3, due to either a reduction in the O_3 loss rate (via reaction 1.11) or an increase in the O_3 production rate (via reaction 1.8).

To quantify the impacts of NO_x emissions on tropospheric O_3 at hemispheric scales, it is necessary to quantify both the export of O_3 produced in polluted source regions and the formation of O_3 from the export of precursors (*e.g.*, PAN and HNO_3, which may eventually release NO_x).

Field measurement campaigns have been conducted in the last two decades to characterize the spatial and temporal distribution of tropospheric NO_x and to determine the resulting effect of NO_x emissions on the O_3 budget. However, data composites of results from many of these campaigns show that the spatial and temporal coverage of remote tropospheric NO_x measurements is still quite sparse and reflects a strong seasonal and regional bias [*Emmons et al.*, 1997; *Bradshaw et al.*, 2000; *Emmons et al.*, 2000; *DiNunno et al.*, 2003].

In addition to measurement campaigns, global chemical transport (GCT) models have been developed to derive the global impact of anthropogenic and boreal wildfire emissions on the O_3 budget. However, it is difficult to assess the uncertainty of the resulting estimates, in particular those related to NO_x sources and photochemical processes. The evaluation of GCT models using nitrogen oxides observations in the FT has been limited by a lack of data in remote regions [*e.g. Thakur et al.*, 1999; *Lawrence and Crutzen*, 1999].

Recently, satellite-derived data have been used to derive global and regional NO_x budgets [*e.g. Leue et al.*, 2001; *Martin et al.*, 2004; *Jaeglé et al.*, 2005; *Richter et al.*, 2005] and detect intercontinental transport of nitrogen oxides plumes from boreal

wildfires [*Spichtinger et al.*, 2001] and anthropogenic sources [*Wenig et al.*, 2003; *Stohl et al.*, 2003]. More recently, satellite data have been used to evaluate GCT models [*e.g. Liu et al.*, 2006; *Chandra et al.*, 2004]. However, the limited measurements of nitrogen oxides in the remote lower FT make the evaluation of satellite-derived data difficult [*Leue et al.*, 2001; *Martin et al.*, 2004].

In the central North Atlantic FT, the lack of data is particularly evident. Measurements of O_3 and nitrogen oxides at several Canadian marine sites indicated that O_3 levels in the BL are significantly influence by the export of O_3 and O_3 precursors during spring to fall [*Parrish et al.*, 1998; *Val Martín*, 2002]. During the winter, in the absence of significant photochemistry, O_3 is removed by reaction with NO and NO_2 and deposition [*Parrish et al.*, 1998]. These studies suggested that the ultimate impact of anthropogenic emissions could be even larger as additional in-situ formation of O_3 from these emissions may occur during transit over the ocean. Consistent with this expectation, measurements further downwind, over the Azores, indicated significant O_3 export in U.S. outflow during spring [*Parrish et al.*, 1998], although an absence of transport impacts during the summer [*Peterson and Honrath*, 1999]. However, all these studies were made in the BL and loss of NO_y and O_3 may have resulted in an underestimation of the importance of the impact of anthropogenic emissions [*Derwent et al.*, 1998; *Auvray and Bey*, 2005].

Aircraft measurements over the western North Atlantic region and GCT model simulations indicated that the majority of the NO_x emitted over the U.S. is removed before or during the export out of the U.S. BL [*e.g. Stohl et al.*, 2002; *Parrish et al.*, 2004; *Li et al.*, 2004; *Hudman et al.*, 2007]. The large fraction of NO_x emitted that is removed from the plumes and the large HNO_3/NO_y ratio observed in these studies imply that the potential for future O_3 production in these plumes in the FT must be limited. Further, modeling analyses estimated that most of the O_3 production from North America NO_x emissions occurs near North America.

Although it is believed that most of the photochemical O_3 production takes place

near North America, observations over the North Atlantic Ocean FT showed that it also occurs during long-range transport [*Reeves et al.*, 2002; *Honrath et al.*, 2004]. In fact, the magnitude of the O_3 enhancements observed in U.S. outflow over the central North Atlantic lower FT is unusually large, implying that a significant amount of additional O_3 formation occurs during transport over the ocean [*Honrath et al.*, 2004]. However, the ultimate fate of the nitrogen oxides export and its implication on the O_3 production well downwind is still uncertain due to a lack of nitrogen oxides measurements over this region.

In addition to anthropogenic emissions, attention has recently been paid to the effect of boreal wildfire emissions on the hemispheric NO_x and O_3 budgets. In recent years, as a result of an increase in dry and warm conditions over the boreal region [*Hassol*, 2004], and increase in human-ignited fires [*Mollicone et al.*, 2006], fire activity has increased [*Kasischke and Turetsky*, 2006]. In addition, global circulation model simulations predict a further increase in the near future as a result of climate change [*Stocks et al.*, 1998]. Boreal wildfire emissions have a large degree of variability, and are a function of fuel type (*e.g.*, peat fires versus crown fires) and burning conditions (*e.g.*, smoldering versus flaming) [*Goode et al.*, 2000; *Kasischke et al.*, 2005]. This behavior causes a large uncertainty and variability in the emissions of NO_x.

Boreal wildfires are recognized to be an important source of CO. On a seasonal basis, total boreal wildfire CO emissions can be at times as large as total anthropogenic CO emissions in the midlatitude northern hemisphere[*Kasischke et al.*, 2005]. Boreal wildfires also affect background CO levels in large regions of the northern hemisphere [*Novelli et al.*, 2003; *Honrath et al.*, 2004]. In addition, prior studies have detected enhancements of O_3 in boreal wildfire plumes [*e.g. Lapina et al.*, 2006; *Bertschi and Jaffe*, 2005]. However, the magnitude of the resulting impact of boreal wildfire NO_x emissions on global tropospheric O_3 is not yet well characterized. Thus, an understanding of the impact of boreal wildfires on tropospheric NO_x levels is needed to further understand the influence of this source on tropospheric O_3, both at present

and in the future.

This discussion demonstrates the importance of understanding the impacts of both anthropogenic and boreal wildfire NO_x emissions on the tropospheric NO_x and O_3 budgets. However, the current understanding of these budgets is limited by gaps in our knowledge of nitrogen oxides levels in remote regions. In addition, the paucity of nitrogen oxides observations inhibits the evaluation of the adequacy of GCT models and spaced-based observations.

1.1 Research Objectives and Approach

This research was motivated by the current deficiencies in the understanding of the nitrogen oxides and the resulting influence on the tropospheric O_3 budget in the North Atlantic troposphere. The objectives of this research include to:

1. determine the seasonal variation of NO, NO_x and NO_y levels in the background central North Atlantic lower FT;

2. characterize the composition of NO_y in the background central North Atlantic lower FT;

3. assess the influence of transport of anthropogenic emissions from the U.S. on levels of NO_x and NO_y in the remote central North Atlantic lower FT;

4. determine the impact of boreal wildfire emissions on levels of NO_x and NO_y in the remote North Atlantic lower FT and, the degree to which boreal wildfires affect the annual distribution of nitrogen oxides; and

5. assess the resulting implications of the North American boreal wildfire and anthropogenic emissions for the regional and hemispheric O_3 budget.

To achieve these goals, measurements of NO, NO_2 and NO_y were made at the Pico Mountain station in the central North Atlantic lower free troposphere from July

2002 to August 2005. The Pico Mountain station is located on the summit caldera of the Pico Mountain, at 2225 m, in the Azores Islands, Portugal (38°N, 28°W). The Azores Islands are a remote island group located approximately 1500 km from west of Portugal and 3900 km from the east coast of North America, as shown in Figure 1.3. The Pico Mountain station station was established during the summer 2001, beginning with measurements of CO, O_3, aerosol black carbon and meteorological parameters. Measurements of NO, NO_2, and NO_y began during late summer 2002, and non-methane hydrocarbons began during spring 2004. Due to the remoteness and the difficulty of access to the measurement site, an existing high sensitivity $NO_{x,y}$ system developed at Michigan Tech [*Peterson and Honrath*, 1999] was modified to automatically operate at the Pico Mountain station. Figure 1.4 displays two images of the Pico Mountain station and the $NO_{x,y}$ system, and Table 1.1 summarizes the measurements and the tools used to address the objectives of this work.

1.2 Dissertation Overview

The following chapters present analyses, results and conclusions of the nitrogen oxides measurements made at the Pico Mountain station. Chapter 2 covers the seasonal variation of nitrogen oxides over the central North Atlantic lower FT and impacts of the transport of pollution on the nitrogen oxides levels, with a focus on eastern North American pollution. This chapter presents analyses of measurements made from July 2002 to August 2005. Chapter 3 presents the impacts of boreal wildfire emissions on the nitrogen oxides levels based on analysis of data from summer 2004. The last chapter summarizes the main results and conclusions. The appendix contains the documentation of the nitrogen oxides data reduction and information on the performance of the system.

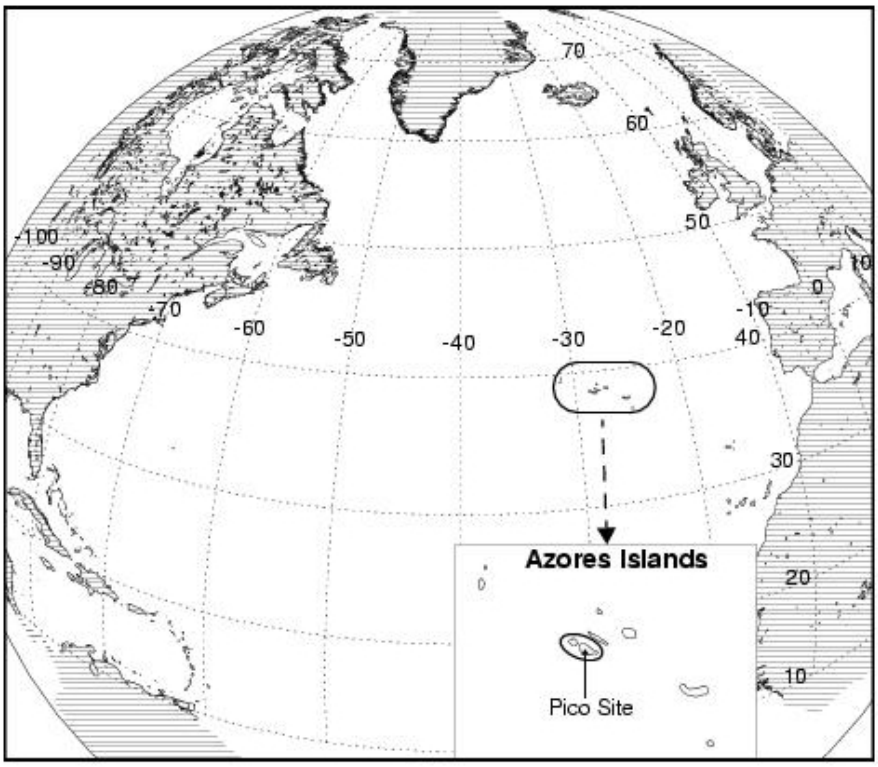

Figure 1.3 Location of the Pico Mountain station.

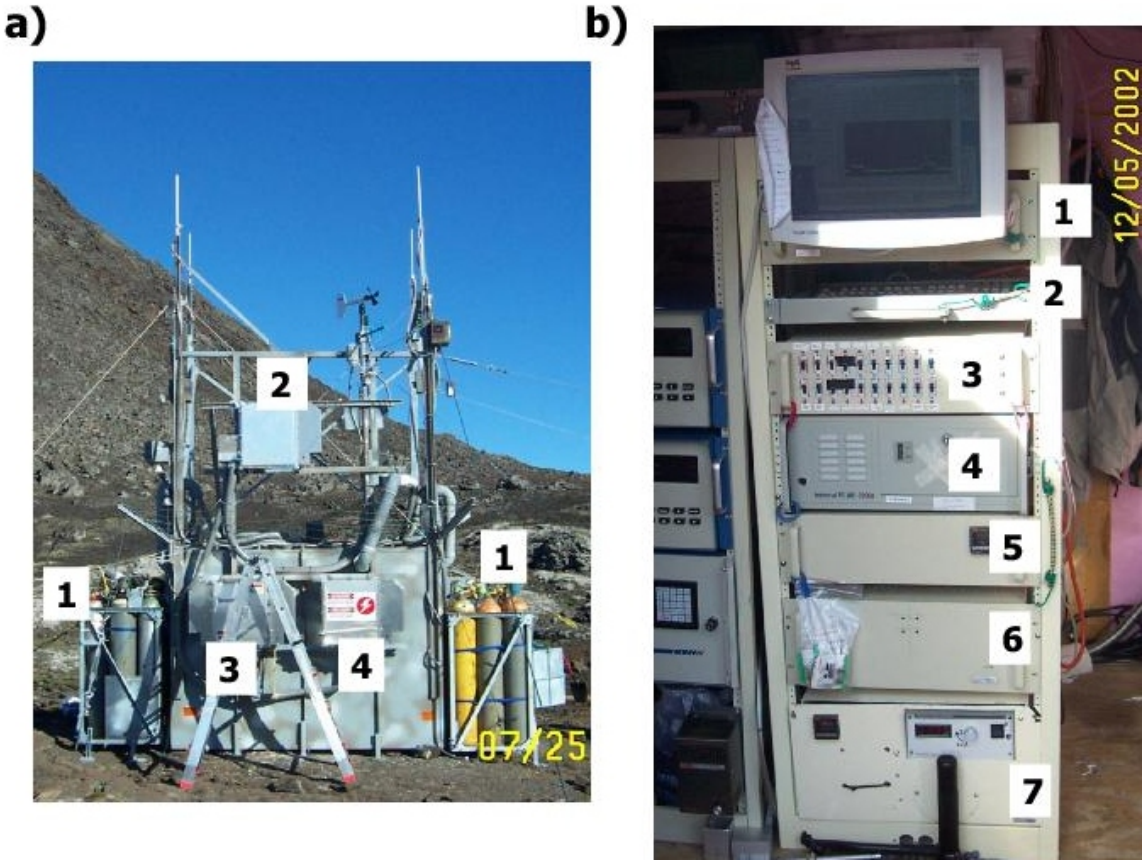

Figure 1.4 $NO_{x,y}$ system at the Pico Mountain station: a) Components outside the station: 1.Calibration and reagent gases, 2.NO_x inlet (to sample NO or NO_2) and NO_y inlet, and NO_y converter 3.NO_2 converter, and 4.NO_2 lamp power supply ; b) Components inside the station: 1.Ozone generator, 2.Computer keyboard, 3.Analog and Digital Input/Output box, 4.Computer, 5.CH_3CN calibration source, 6.System power supplies, and 7.NO detector.

Table 1.1 Measurements at the Pico Mountain station and other tools used in this work.

Measurement/Tool	Technique/Source
NO	O_3 chemiluminesce (developed at Michigan Tech)
NO_2	NO_2 photolysis (developed at Michigan Tech)
NO_y	Au-catalytic reduction (developed at Michigan Tech)
CO	Non-dispersive IR (TEI 48C-TL)
O_3	UV absorption (TEI 49C)
Aerosol black carbon[a]	UV-vis absorption (AE31 Aethalometer)
Wind speed and direction	standard (R.M. Young 05103)
RH and Temperature	standard (Rotronic TM12R)
Pressure	standard (R.M. Young 61201)
Global Chemical Transport Models	
MOZART	National Center for Atmospheric Research
GEOS-Chem	Jet Propulsion Lab
Transport Models	
FLEXPART	Michigan Tech/Norwegian Institute for Air Research
HYSPLIT	Michigan Tech

[a]University of the Azores.

Chapter 2

Seasonal Variation of Nitrogen Oxides in the Central North Atlantic Lower Free Troposphere and Impacts of Transport of Pollution[†]

Reactive nitrogen species are critical for the chemistry of the atmosphere. Photochemical production of O_3 depends on the concentration of NO_x ($NO+NO_2$), which in turn, influences the concentration of tropospheric OH. Species that affect OH are important, as reaction of OH provides the dominant path for removal of a variety of atmospheric pollutants [*Crutzen*, 1979; *Logan*, 1983]. In addition, nitric acid, the primary end product of NO_x oxidation, is one of the major components of acid deposition.

[†]This chapter is based on material to be submitted, with minor changes, as Val Martín M., R. Honrath, R. C. Owen, K. Lapina and Q. Li (2007), Seasonal variation of nitrogen oxides in the central North Atlantic lower free troposphere, *J. Geosphys. Res.*

Understanding the impact of NO_x on tropospheric O_3 on a global scale is important for several reasons. Ozone is considered the third most important anthropogenic greenhouse gas [*Alley et al.*, 2007]. In addition, slightly elevated levels of O_3, at concentrations not far above ambient, pose a serious concern because of their effects on the human respiratory system and ecosystems. In particular, there is an increasing concern regarding intercontinental transport of O_3 pollution since it appears to be changing the composition of the background troposphere [*Simmonds et al.*, 2004; *Jaffe et al.*, 2003] and make difficult for the countries downwind to achieve their air quality standards [*Li et al.*, 2002; *Derwent et al.*, 2004].

In the Northern Hemisphere, emissions of nitrogen oxides are dominated by anthropogenic sources in urban and industrial regions [*Logan*, 1983]. The impact of NO_x emissions from these regions on global O_3 is limited as oxidation of NO_x to HNO_3, peroxyacetyl nitrate (PAN) and other minor compounds occurs in less than one day in the continental boundary layer (BL). However, the dependence of O_3 production of NO_x is highly non-linear [*Liu et al.*, 1987]. This means that the number of O_3 molecules produced per molecule of NO_x consumed, known as the O_3 production efficiency, increases as NO_x concentration decreases. As a result, the export of small fractions of emitted NO_x may lead to significant O_3 production in the remote troposphere [*Jacob et al.*, 1993]. The export of NO_x away from the source regions is facilitated by the export of PAN, a thermally unstable, non-water-soluble species, out of the continental BL, followed by the transport of PAN on a global scale at cold temperatures, and decomposition to NO_x as the airmasses become warmer [*Moxim et al.*, 1996]. It has been suggested that, similar to PAN, the export of HNO_3 followed by photolysis to NO_x can be an important source of NO_x in the troposphere [*Neuman et al.*, 2006]. Thus, quantifying the export of nitrogen oxides and their chemical evolution is fundamental to understand the impact of anthropogenic emissions on the global O_3 budget.

Previous studies, based on NARE and ICARTT aircraft measurements [*e.g. Par-*

rish et al., 2004; *Li et al.*, 2004; *Hudman et al.*, 2007], have estimated that less than 20% of the NO_x emitted over eastern U.S. is exported to the North Atlantic free troposphere (FT) as NO_y (the sum of NO_x and its oxidation products). Further analyses on the composition of the NO_y indicate that NO_y exported in the airmasses out of the North America BL is mostly HNO_3 ($\gtrsim$50%), with $\sim$35% as PAN and less than 10% as NO_x [*e.g. Parrish et al.*, 2004; *Singh et al.*, 2007]. The large fraction of emitted NO_x that is removed from the plumes and the large HNO_3/NO_y ratio imply that the potential for future O_3 production in these plumes in the FT must be limited.

In addition to the field studies, several model simulations have examined the export of NO_y from North America [*e.g. Horowitz et al.*, 1998; *Liang et al.*, 1998]. Model simulations indicate that about 30% of the NO_x emitted in the U.S. is exported out of the U.S. boundary layer as NO_y (25% in summer, 35% in winter) and that 60-80% of this export is in the form of NO_x and PAN, leading to an increased importance of downwind O_3 production relative to direct export of O_3 produced over North America [*Liang et al.*, 1998]. Results from NARE and ICARTT apparently contradict these model analyses. *Li et al.* [2004] reconciled these results, suggesting that these previous model simulations underestimated NO_y scavenging during export from the North America boundary layer. In this work, *Li et al.* [2004] showed that the potential O_3 production due to exported NO_x and PAN is comparable in magnitude to the direct export of O_3 pollution from North America and that more than half of the O_3 production from transported NO_x and PAN occurs over the continent or nearby downwind regions.

While net photochemical O_3 production typically takes place near the source regions, observations over the North Atlantic Ocean have indicated that it can also occur during long-range transport [*Reeves et al.*, 2002; *Honrath et al.*, 2004]. However, the large-scale impacts of the long-range transport of emissions on the tropospheric O_3 production over the North Atlantic region is uncertain. Simulations from two global chemical transport (GCT) models [*Auvray et al.*, 2007] and a photochemical box

model constrained by observations [*Reeves et al.*, 2002] of the impact of U.S. outflow over the North Atlantic region indicate that the export of NO_x emissions from the U.S. lead to a perturbation of the chemistry over this region through changes in the O_3 production rate. As a consequence, long-range transport events significantly affect the O_3 photochemical production over the entire North Atlantic troposphere all year round [*Auvray et al.*, 2007]. However, other studies indicate that the North Atlantic region is in a state of net O_3 destruction all year round [*Klonecki and Levy*, 1997], or in a state of net O_3 destruction during the summer and net O_3 production during the winter [*Yienger et al.*, 1999].

In addition to anthropogenic emissions, wildfires over the boreal region can also result in a substantial source of nitrogen oxides to the atmosphere during the summer seasons [*Goode et al.*, 2000; *Andreae and Merlet*, 2001]. Recently, it has been shown that NO_x emissions from the boreal wildfires can be efficiently transported to the North Atlantic region [*Val Martin et al.*, 2006; *Singh et al.*, 2007; *Real et al.*, 2007]. Boreal wildfire NO_x emissions may be comparable in magnitude to the total eastern North America anthropogenic NO_x emissions during the boreal fire season [*Val Martin et al.*, 2006]. Observations and GCT model simulations indicate that significant photochemical O_3 production occurs in the fire plumes during transport, likely as a result of decomposition of PAN to NO_x [*Val Martin et al.*, 2006; *Pfister et al.*, 2006; *Real et al.*, 2007]. The ultimate impact of the boreal wildfire NO_x emissions on the O_3 budget can be significant. For example, emissions from boreal wildfires may result in a monthly ozone production on the order of 10 to 20% of the net photochemical O_3 production in the northern middle and high latitudes [*Val Martin et al.*, 2006], and may increase the O_3 burden in the Northern Hemisphere by up to 4% [*Pfister et al.*, 2006]. However, due to the poorly constrained current estimates of NO_x emissions and the uncertainty in the injection height of the wildfire plumes [*e.g. Leung et al.*, 2007], questions still remain regarding the impact of boreal wildfire emissions on nitrogen oxides and ozone levels over the Northern Hemisphere.

In the last decade, GCT models and space-based observations have provided useful information to study the fate and distribution of nitrogen oxides at regional to global scales [*e.g. Richter et al.*, 2005; *Hudman et al.*, 2007]. However, the evaluation of model predictions and satellite observations are severely limited by an inadequate coverage of nitrogen oxides observations in remote regions [*e.g. Emmons et al.*, 1997; *Thakur et al.*, 1999; *Martin et al.*, 2004].

The data presented in this paper constitute a multi-year record of NO, NO_x and NO_y in the North Atlantic lower FT made at the Pico Mountain station. These data are analyzed with two purposes: to characterize the seasonal and diurnal variation of nitrogen oxides in the background lower FT over the North Atlantic region, and to assess the degree to which transport of anthropogenic and boreal wildfire emissions affect nitrogen oxides levels and the resulting implications for the hemispheric NO_x and O_3 budgets.

2.1 Methodology

Measurements of NO, NO_2, NO_y were made at the Pico Mountain station from July 2002 to August 2005. We present here measurements of nitrogen oxides analyzed in combination with measurements of CO and O_3 also made at the Pico Mountain station. Because the Pico Mountain station and measurement details have already been described elsewhere [*Honrath et al.*, 2004; *Kleissl et al.*, 2007; *Owen et al.*, 2006; *Val Martin et al.*, 2006], only a brief summary of the most relevant experimental aspects is presented here.

2.1.1 Measurement Site

The Pico Mountain station is located on the summit of Pico mountain (2.2 km asl) in the Azores Islands, Portugal (38° N, 28° W). The station is well above the regional marine boundary layer during all seasons, which is typically less than 1 km in height

from May to September and 1.4 km from October to April [*Kleissl et al.*, 2007]. Upslope flow can bring air from lower altitudes to the station, including occasionally from the marine BL. However, upslope flow affects the Pico Mountain station much less than it does many other mountain observatories. An intensive study of the occurrence of upslope flow indicated that, from May to September, less than 25% of the measurement time presents the meteorological conditions required for an airmass from below the mountain to reach the summit via buoyant uplifting, *i.e.*, weak synoptic winds and strong insolation. From October to April, buoyant upslope flow is unusual, but strong synoptic winds have the potential for mechanical uplifting. This potential mechanical upslope flow has a strong seasonal cycle, which depends on stronger winds and higher marine BL heights during winter. As a result, the potential frequency of marine BL lofting to the summit is 35–60% from October to April, whereas it is less than 20% from May to September. However, at the Pico Mountain station, impacts of mechanical and buoyant upslope flow on nitrogen oxides, CO and O_3 are small [*Kleissl et al.*, 2007], indicating that the air sampled at the site is negligibly influenced by island pollution. For example, mean NO_x was 33 ± 5 pptv (mean$\pm$2-standard error of the mean) in periods with potential mechanical and/or buoyant upslope flow, whereas it was 30 ± 1 pptv for the non-upslope flow periods.

The Azores are situated over a region that is frequently impacted by continental emissions. They are often impacted by large-scale transport patterns in the lower FT, which can transport emissions from North America to the Azores in 5 to 7 days [*Owen et al.*, 2006]. Episodically, emissions exported from the eastern U.S. in warm conveyor belts with the associated convection, followed by subsidence, impact the Azores [*Owen et al.*, 2006]. In addition, the Azores are affected by outflow from high latitudes, which can carry emissions from boreal wildfires in Canada, Alaska and Siberia and carry them to the Azores 6 to 15 days later [*Honrath et al.*, 2004; *Val Martin et al.*, 2006].

2.1.2 Measurements

NO, NO_2, and NO_y were determined by an automated $NO_{x,y}$ system, which used established techniques for high sensitivity detection: NO detection by O_3 chemiluminescence [*Ridley and Grahek*, 1990], NO_2 by conversion to NO via ultraviolet photodissociation [*Kley and McFarland*, 1980; *Parrish et al.*, 1990], and NO_y by Au-catalyzed reduction to NO in the presence of CO [*Bollinger et al.*, 1983; *Fahey et al.*, 1985]. A detailed description of the $NO_{x,y}$ system including operation, sensitivities, conversion efficiencies, precision and artifacts can be found in *Val Martin et al.* [2006] (Chapter 3).

Measurements were recorded as 30-s averages (NO and NO_2) and 20-s averages (NO_y) every 10 min, and further averaged to obtain the 30-min averages used in this work. The instrumental detection limit (2-σ) of the 30-min averages was 6.5 to 16 pptv for NO, 13 to 17 pptv for NO_2, 14 to 21 pptv for NO_x and 7.5 to 21 pptv for NO_y based on the artifact correction uncertainty and the precision (2-σ) of the instrument. Ninety percent of the measurements had detection limits less than 6.5 pptv for NO, 16 pptv for NO_2 and NO_x, and 19 pptv for NO_y. Measurement accuracy was estimated to be 5% (July 20, 2002–July 17, 2003), 7% (July 17, 2003–May 1, 2004) and 4% (May 1, 2004–August 27, 2005) based on total uncertainty of the sample and calibration mass flow controllers and the NO standard calibration gas mixing ratio.

Accuracy of the NO_y measurements depends on the effective conversion of NO_y compounds and the lack of significant conversion of non-NO_y compounds [*Fahey et al.*, 1985; *Kliner et al.*, 1997; *Kondo et al.*, 1997], in addition to the accurate determination of the resulting NO. Based on regular calibrations and standard addition tests with NO_2, i-propyl nitrate and HNO_3 in ambient air, the observed NO_y included 80–100% of the actual NO_2 level (typically >97%), with similar values expected for PAN [*Fahey et al.*, 1985], 62–100% of the actual HNO_3 level (typically >80%), and 61–100% of the actual i-propyl nitrate (typically >80%). Due to occasional degra-

dation of the NO_y converter, measurements of NO_y were corrected for non-unity NO_y conversion by using the NO_2 conversion efficiencies measured at the system. A maximum correction of 20% was applied to a few of the measurements made before March 2003 and a maximum correction of 8% was applied to measurements made from mid-July to mid-August 2004. No correction was made after mid-August 2004 as the NO_2 conversion efficiency was constant to the expected value of 97–100%. In addition, NO_y observations in March–May 2003 and May–June 2004 presented an additional uncertainty of 13% and 5% due to uncertainty in the NO_y sensitivity determination. Based on the NO_y composition estimated at the Pico Mountain station (section 2.2.3.1) and the uncertainty of NO determination, the total NO_y uncertainty mainly due to potentially incomplete conversion to NO, was estimated to be at worst ∼55%, from March to May 2003 (less than 3% of the total dataset). During most periods, total measured uncertainty was $\lesssim$ 20% at NO_y levels of 100 pptv and $\lesssim$ 15% at NO_y levels of 500 pptv. Interference of non-NO_y species was not a problem in this study as inferred from the very low conversion efficiencies (always less than 0.5%; typically 0.3%) during regular testing using standard addition of CH_3CN.

As discussed by *Val Martin et al.* [2006], unexpected spikes were sometimes observed in ambient NO_x and NO_y, and were attributed to volcanic emanations. To avoid including these observations in our analysis, we used methods similar to but slightly more stringent than those used previously [*Val Martin et al.*, 2006]. First, we excluded measurements made during calm winds (wind speed below 2 m s^{-1}) and when wind data were not available. Two exceptions were made. The fire-impacted period of September 1–5, 2004, which did not present the typical spikes associated with volcanic emissions [*Val Martin et al.*, 2006] was included, although wind speeds were lower than 2 m s^{-1}. During the periods of October–May and June 2004, wind data were scarce due to ice blockage or malfunctioning of the sensor and observations when wind data were not available were included. However, including these observations did not compromise our results as the nitrogen oxides levels in the limited

calm wind periods during these months were not significantly different than those in the overall data. (For example, from October to May, mean NO_x was 26 ± 2 pptv (mean±2-standard error of the mean) in periods with wind speeds below 2 m s^{-1}, whereas it was 28 ± 1 pptv for the overall period.) Second, we excluded observations that exhibited high ambient variability. For this purpose, periods with high ambient variability were defined as those when the standard deviation of the 30-s points in a 30-min period (SD) was above 8 pptv for NO or above 20 pptv for NO_2 and NO_x, or the NO_y SD exceeded 20 pptv $+ 0.5([NO_y] - 50)$, where the second term was included to allow increased variability during periods of high $[NO_y]$. Observations made within ±3 hours of the identified high variability observation were also excluded. The wind speed criterion removed about 20% of the measurements from the overall dataset, and the ambient variability screen criterion removed an additional 20% for NO_y and 34% for NO_x. Finally, with the purpose of identifying additional periods with potential influence of volcanic emissions, we excluded observations made during buoyant upslope flow as described by *Kleissl et al.* [2007]. These periods were characterized by a strong radiation and low wind speeds, conditions in which volcanic emissions may potentially be detectable. This screening removed an additional 6% and 3% of the NO_y and NO_x measurements, respectively, mostly during the summer.

In remote regions, nighttime NO values are expected to be zero due to the rapid oxidation of NO by O_3 and the expected absence of local sources [*Ridley et al.*, 1998; *Peterson et al.*, 1998]. This was true for all seasons, with the exception of summer 2004, which presented a nighttime median of 3 pptv. It was not possible to conclusively determine the reason for the generally non-zero nighttime NO levels during summer 2004. However, the weather at Pico that summer was unusual since it was dominated by high relative humidity (RH) and calm wind periods. This may have resulted in a very small but detectable flux of NO from soil bacteria around the station. This unclear source could not be removed by any screening criteria and systematically affected the measurements during this season. These emissions

would presumably affect NO during the daytime and NO_x both day and night as well. However, the interference from this source does not appear to compromise the results: if we exclude the 2004 NO summertime observations, the diurnal cycle and seasonal variation presented below do not significantly change. For example, summer daytime median NO was 7.9 pptv in 2002–2005, whereas it was 7.7 pptv excluding the summer 2004 dataset.

As will be discussed in section 2.2.1, observations of NO_2 were also influenced by a small unknown source during the daytime. We could not find any consistent indication of the presence of a source in the vicinity of the station. We thus hypothesize that the excess NO_2 may be due to the interference from PAN decomposition to NO_2 in the sampling lines or the photolysis cell since relatively elevated temperatures were registered in the NO_2 converter during the day. Using the maximum temperature registered (39°C), the residence time in the photolysis lamp ($\sim$ 8 sec) and the typical levels of PAN estimated at the measurement site (section 2.2.3.1), we calculate that the contribution of PAN decomposition may account for about 2–4 pptv to the NO_2 observations, mainly during the summer. This small interference may partially explain the additional source of NO_2 detected in our observations during the summer and early fall. However, it is small and does not compromise the results presented below.

We also analyzed measurements of CO and O_3 made from July 2002 to August 2005 and from July 2003 to August 2005, respectively. The CO and O_3 instruments are described in detail elsewhere [*Owen et al.*, 2006; *Honrath et al.*, 2004].

2.1.3 FLEXPART and GEOS-Chem Simulations

To investigate the sensitivity of our measurements to upwind emissions, we used the FLEXPART particle dispersion model version 6.2 [*Stohl*, 1998; *Stohl et al.*, 2005]. FLEXPART was driven with data from the European Centre for Medium Range

Weather Forecasts (ECMWF) [*ECMWF*, 2005] with a 1°x 1° horizontal resolution, 60 vertical levels and a temporal resolution of three hours, using meteorological analyses at 0000, 0600, 1200, and 1800 UTC, and ECMWF 3-hr forecasts at 0300, 0900, 1500 and 2100 UTC.

We ran FLEXPART in its backward mode to create retroplumes. Retroplumes were initiated every three hours with 4,000 particles released over a one-hour time interval into a 1°x 1° grid box centered on the Pico Mountain station, over the altitude range of 2000–2500 m asl. Particles were followed backward in time for 20 days. To account for differences in air density between the release cell and upwind sources, the residence time of the particles was normalized by the air density in each cell to yield the specific volume weighted residence time (SVWRT).

To evaluate the contribution of anthropogenic emissions, anthropogenic CO tracers at the Pico Mountain station from North American, Asian and European emissions were calculated by multiplying the upwind-time-integrated SVWRT in the footprint layer (0–300 m) with emissions, using the approach of *Seibert and Frank* [2004]. These tracers are referred as FLEXPART NA-CO, FLEXPART Asia-CO and FLEXPART Euro-CO in the remainder of this paper. Anthropogenic emissions were based on the EDGAR 3.2 Fast Track 2000 dataset [*Olivier and Berdowski*, 2001].

A fourth CO tracer, from the boreal wildfire emissions in North America (referred as FLEXPART Fire-CO) was calculated to assess the magnitude of fire impact at the Pico Mountain station. For this purpose, SVWRT in the column 0-7500 m was multiplied with emissions distributed according to air density in the column. Boreal wildfire CO emissions were based on an inventory created by the Boreal Wildland-Fire Emissions Model [*Kasischke et al.*, 2005]. Further details on the boreal wildfire inventory and the FLEXPART Fire-CO are presented elsewhere [*Lapina al.*, Evidence of late-season decrease in NO_x/CO emission ratios from boreal fires, manuscript in preparation, 2007 (hereinafter *Lapina et al.*, in preparation)].

To study the influence of stratospheric transport to the measurement site, we

ran FLEXPART in its forward mode to create a stratospheric O_3 tracer. This was done by first determining the potential vorticity (PV) of each particle upon creation. Particles with a PV greater than 2.0 pvu were given a specific mass according to $MO_3 = Mair \times PV \times C$, where Mair was the mass of air represented by a particle and $C = 60 \times 10^{-9}$ pvu^{-1} was the ozone/PV relationship [*Stohl et al.*, 2000]. Particles were then allowed to advect through the stratosphere and into the troposphere according to the winds. At any one time, approximately 4 million particles were present in the model for the stratospheric tracer runs. Particles were carried in the model for 20 days before being removed. This tracer is referred here as FLEXPART Strat-O_3.

Simulations from the global chemical transport model GEOS-Chem were also used to further analyze the nitrogen oxides observations. GEOS-Chem version 7.01 was driven by 3-hourly assimilated meteorological fields from the Goddard Earth Observing System of NASA [*Bey et al.*, 2001]. The spatial resolution of the model was 2° latitude by 2.5° longitude with 26 levels between the surface to 0.1 hPa. Global anthropogenic emissions were determined following the procedure described by *Bey et al.* [2001]. Over the continental U.S. and Europe, the anthropogenic emissions were based on the U.S. EPA NEI-97 [*EPA*, 1997] and the European Monitoring and Evaluation Program for European countries [*EMEP*, 1997]. Biomass burning emissions were obtained from *Duncan et al.* [2003] with monthly mean estimates relocated using Moderate-resolution Imaging Spectroradiometer fire counts. More information on these emissions and additional sources (*e.g.*, lightning, stratospheric injection) is presented elsewhere [*Bey et al.*, 2001].

2.2 Results and Discussion

Figure 2.1 presents an overview of the nitrogen oxides measurements at the Pico Mountain site from July 2002 to August 2005. All 30-min averages of daytime NO,

NO_x and NO_y are shown as time series, and bar plots represent the distribution of the data by season and year.

Significant variability is apparent in the data at all times of the year. A large number of factors contribute to the magnitude and the changes of the nitrogen oxides levels. In this section, five aspects of the data are analyzed: diurnal cycle, seasonal variation, partitioning of NO_y, impacts of anthropogenic pollution and influence of boreal wildfire emissions. These aspects are not entirely independent but provide a structure for the discussion.

2.2.1 Diurnal Cycles

Diurnal cycles of nitrogen oxides can be caused by photochemical, transport and emission processes whose strength vary between day and night. Table 2.1 summarizes the statistical parameters of the diurnal cycles of NO, [NO]/[NO_2], NO_2 and NO_y for each season. As an example, Figure 2.2 displays the diurnal variation for the springtime measurements. (Similar variation was present in the other seasons.) For the [NO]/[NO_2] analysis, values that deviated from the mean by more than three times of the standard deviation were removed. This was done because NO_2 and NO measurements are related as the calculation of NO_2 includes the NO mixing ratio. Hence, rare outliers in the NO measurements may result in NO_2 outliers, which produces unrealistic [NO]/[NO_2] values that may significantly affect the mean [*Yang et al.*, 2002].

To test for the existence of a consistent diurnal variation, we examined both the median and the mean of the data in the nighttime and daytime subsets. Nighttime values were observations made between 23:00 and 5:00 UTC; daytime values were those made when the solar zenith angle was below 62°. These cutoffs were chosen to allow significant number of data points in both subsets while ensuring daylight and nighttime conditions in all seasons. As expected, Table 2.1 indicates that robust

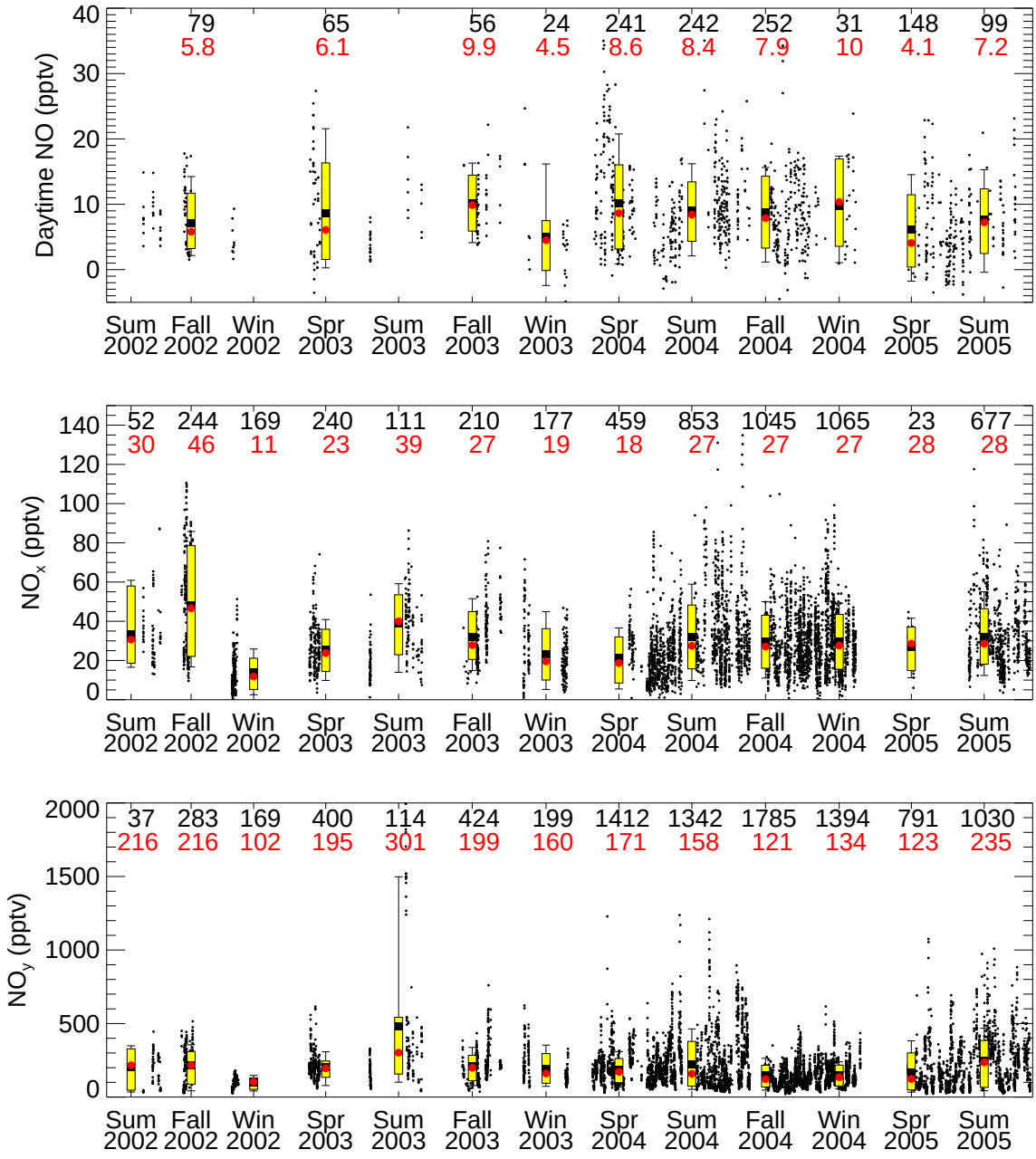

Figure 2.1 Time series of daytime NO (top), NO_x (middle) and NO_y (bottom) from July 20, 2002 to August 25, 2005 at the Pico Mountain station. Daytime NO are observations when the solar zenith angle was below 62° (see text for explanation). Each data point represents a 30-min average. Bar plots indicate the distribution of the data for each season and year. The medians (red circles) and the means (black squares) are shown along with the central 67% (yellow box) and the central 95% (thin black lines). The number of 30-min average measurements (in black) and the median (in red) included in each distribution are given above the plot for each bar. Distributions with fewer than 20 data points are not shown.

Table 2.1 Statistical parameters of the nitrogen oxides diurnal cycle. Reported average, standard deviation (SD), median and number (N) of the 30-min average observations in pptv for NO, NO_2 and NO_y.

		Daytime[a]			Nighttime[a]			Amplitude[b]	
Season	Data	Mean±SD	Median	N	Mean±SD	Median	N	Δmean	Δmedian
Spring[c]	NO	9 ± 8	7	448	1 ± 3	1	886	8 ± 2	7
	NO/NO_2	0.4 ± 0.5	0.3	81	0.1 ± 0.4	0.0	274	0.3 ± 0.3	0.3
	NO_2	20 ± 11	20	135	19 ± 12	18	307	1 ± 5	2
	NO_y	184 ± 123	178	702	184 ± 111	166	905	-1 ± 24	12
Summer[c]	NO	9 ± 5	8	350	2 ± 4	2	918	6 ± 1	6
	NO/NO_2	0.4 ± 0.3	0.3	221	0.1 ± 0.3	0.0	614	0.3 ± 0.1	0.3
	NO_2	25 ± 13	22	279	28 ± 15	24	695	-3 ± 4	-3
	NO_y	221 ± 181	163	536	248 ± 208	204	1098	-27 ± 40	-41
Fall[c]	NO	9 ± 5	8	371	1 ± 3	0	652	8 ± 1	7
	NO/NO_2	0.3 ± 0.2	0.3	244	0.0 ± 0.1	0.0	392	0.3 ± 0.1	0.3
	NO_2	28 ± 16	24	276	30 ± 16	26	430	-1 ± 5	-2
	NO_y	161 ± 102	142	506	164 ± 108	136	733	-3 ± 24	6
Winter[c]	NO	7 ± 6	5	64	0 ± 2	0	561	7 ± 3	5
	NO/NO_2	0.4 ± 0.3	0.4	40	0.0 ± 0.2	0.0	440	0.4 ± 0.2	0.4
	NO_2	24 ± 13	24	50	25 ± 16	23	455	-1 ± 8	1
	NO_y	156 ± 79	145	76	152 ± 88	128	511	4 ± 39	17

[a]Daytime are observations when the solar zenith angle was $< 62°$; Nighttime are observations made between 23:00–5:00 UTC.

[b]Amplitude is expressed as the difference between the means (Δmean) and the medians (Δmedian) of daytime and nighttime. Uncertainty (2-σ) is based on propagation of errors.

[c]Seasons are: spring (March, April, May), summer (June, July, August), fall (September, October, November) and winter (December, January, February).

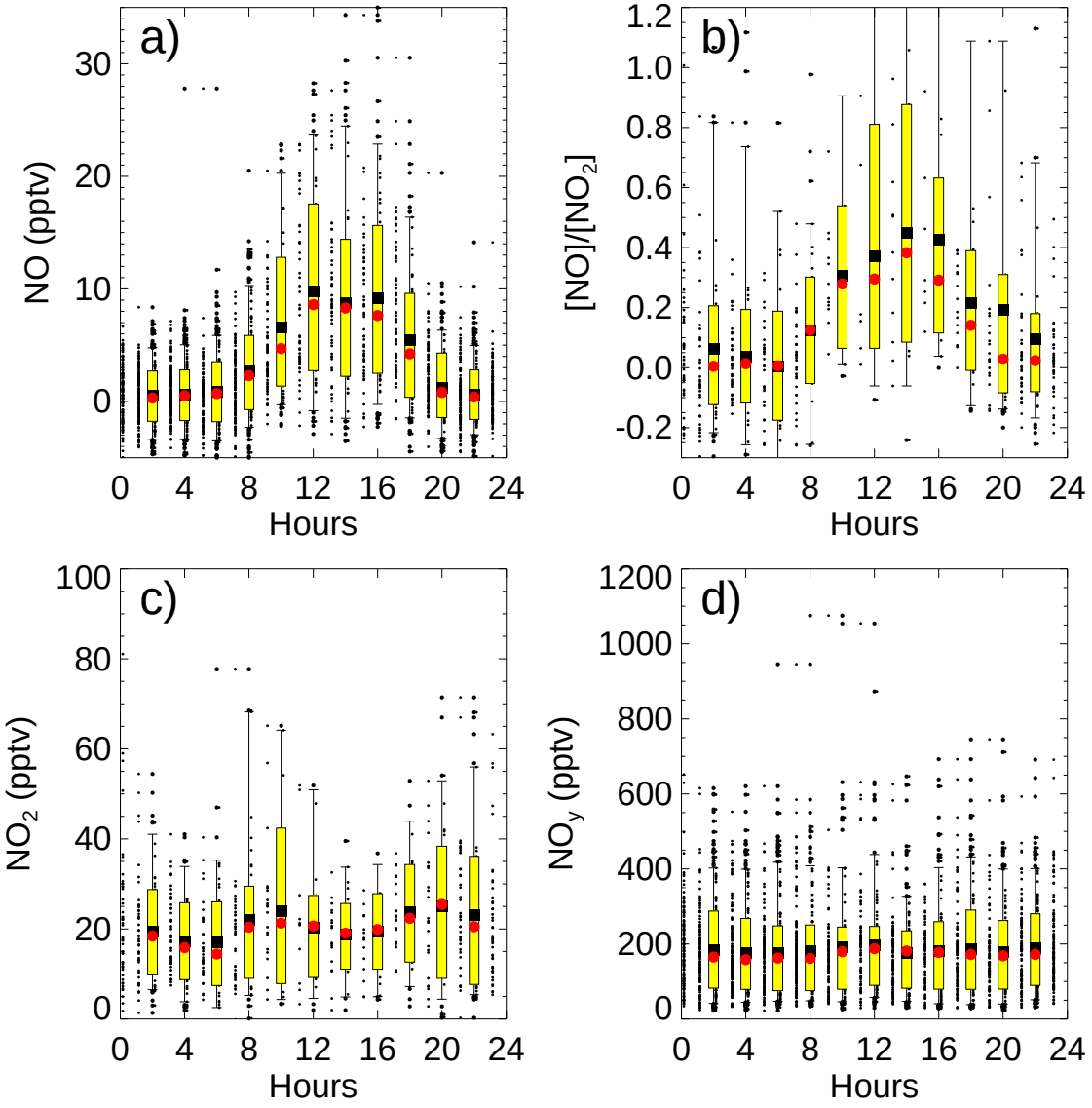

Figure 2.2 Springtime diurnal cycles of (a) NO, (b) [NO]/[NO_2], (c) NO_2 and (d) NO_y. All 30-min average data are plotted centered in each hour, with the exception of [NO]/[NO_2] (see text for explanation). Few data points outside the plot boundaries are not shown to make the cycle more apparent (25 for NO and NO/NO_2, 8 for NO_2 and 1 for NO_y). Symbols and error bars are the same as in Figure 2.1.

diurnal cycles exist for NO and [NO]/[NO_2] ratios in all seasons, with median diurnal amplitudes of 5–7 pptv and 0.3–0.4, respectively. The phase of these cycles is consistent with photochemical causes: the maximum occurs around the time of maximum insolation, during the local solar noon time (14:00 UTC for spring; Figure 2.2), indicating a dominance of production of NO from photolysis of NO_2, whereas the minimum occurs at nighttime, indicating dominance of NO destruction by reaction with O_3.

Given the observed NO cycle amplitude, a negative amplitude of similar magnitude should be present in the NO_2 cycle as NO_2 is photolyzed to NO during daytime. Figure 2.2c and Table 2.1 indicate that a very weak negative diurnal variation or no variation was present for NO_2, with median diurnal amplitudes of -3 to 1 pptv. This small negative or non-existent amplitude suggests the presence of a small source of NO_2 during daytime. As discussed in section 2.1, this may be partially the result of interference of PAN decomposition in the photolysis cell, mainly during summer and early fall.

Consistent with our expectation that diurnal varying upslope flow does not affect the measurements [*Kleissl et al.*, 2007], Figure 2.2d and Table 2.1 show that no significant diurnal variation was present for NO_y, with the exception of the summer, which exhibited a negative median amplitude of -41 pptv. This may be due to the strong removal nature of summertime NO_y, which is composed primarily by HNO_3 (section 2.2.3.1). Summertime RH measurements at the Pico Mountain station indicate that the percentage of NO_y observations made in the presence of clouds (RH above 96%, section 2.2.3.1) was larger during the daytime (24%) than at nighttime (16%), which may result in a stronger wet removal of HNO_3 during the day.

Comparisons of the diurnal variation observed at the Pico Mountain station to those observed at other remote marine FT stations are not straightforward. As opposed to the Pico Mountain station, ground-based mountaintop stations (*e.g.*, Mauna Loa Observatory (MLO) over the North Pacific Ocean and Izaña over the eastern At-

lantic Ocean) are typically characterized by a diurnal downslope-upslope flow regime [*Ridley et al.*, 1998; *Fischer et al.*, 2004]. However, spring diurnal amplitudes of ∼8 pptv for NO and ∼0.4 for NO/NO_2 were observed at MLO during a rare event in which free tropospheric air was sampled all day [*Ridley et al.*, 1998], similar to the spring amplitude observed at the Pico Mountain station for NO (8 ± 2 pptv) and for $[NO]/[NO_2]$ (0.3 ± 0.3).

2.2.2 Seasonal Variation

Figures 2.3a-c present the annual cycle of nitrogen oxides at the Pico Mountain site. NO_y measurements were influenced by washout processing, as indicated by the lower NO_y values in higher RH conditions shown in Figure 2.4 for fall. (Similar behavior was found in the other seasons.) To avoid a potential bias in the seasonal variation due to washout, Figure 2.3c shows the seasonal cycle of NO_y determined in dry conditions (RH below 60%). In Figure 2.3d, the annual cycle of CO is also shown for comparison. The distribution of all measurements is displayed by monthly periods independently of the year of study. Additionally the monthly median for years with more than 20 observations is also identified by the numerals next to the bars. The statistics of all observations are further summarized in Table 2.2.

It is clear from Figures 2.3a-d that there is a large interannual variability in the CO and nitrogen oxides monthly medians within some months. Large variability of CO at hemispheric scales is known to occur, and has mainly been associated with variations in biomass burning emissions [*e.g.*, *Novelli et al.*, 2003; *Edwards et al.*, 2004; *Honrath et al.*, 2004]. Although interannual variability is apparent for the nitrogen oxides, we find that in some cases this variability may also be due to the limited number of observations available and the fact that the measurements are variable within each month, *i.e.*, events. For example, NO_x in October 2002 was significantly higher (47 ± 3 pptv; mean±2-standard error of the mean) than in 2003 (28 ± 1 pptv)

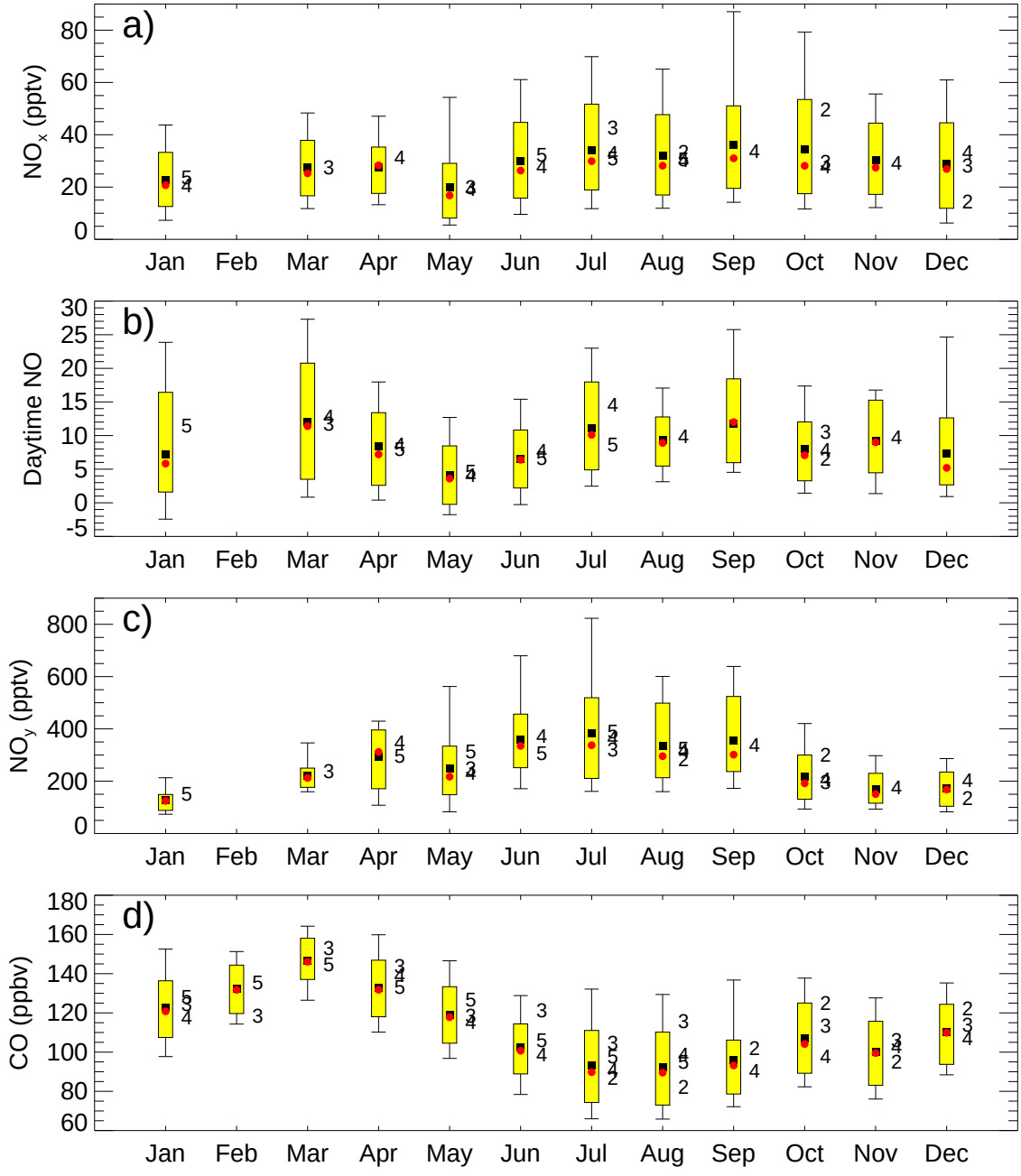

Figure 2.3 Seasonal cycle of (a) NO_x, (b) daytime NO, and (c) NO_y in dry conditions (see text for explanation) and (d) CO. Bar plots indicate the distribution of the data for each month. Symbols and error bars are the same as in Figure 2.1. Months with fewer than 20 data points are not shown. The median for each month and year are plotted by numerals to the right of the bar plots (2: year 2002, 3: year 2003, 4: year 2004 and 5: year 2005). Medians with fewer than 20 data points are not shown.

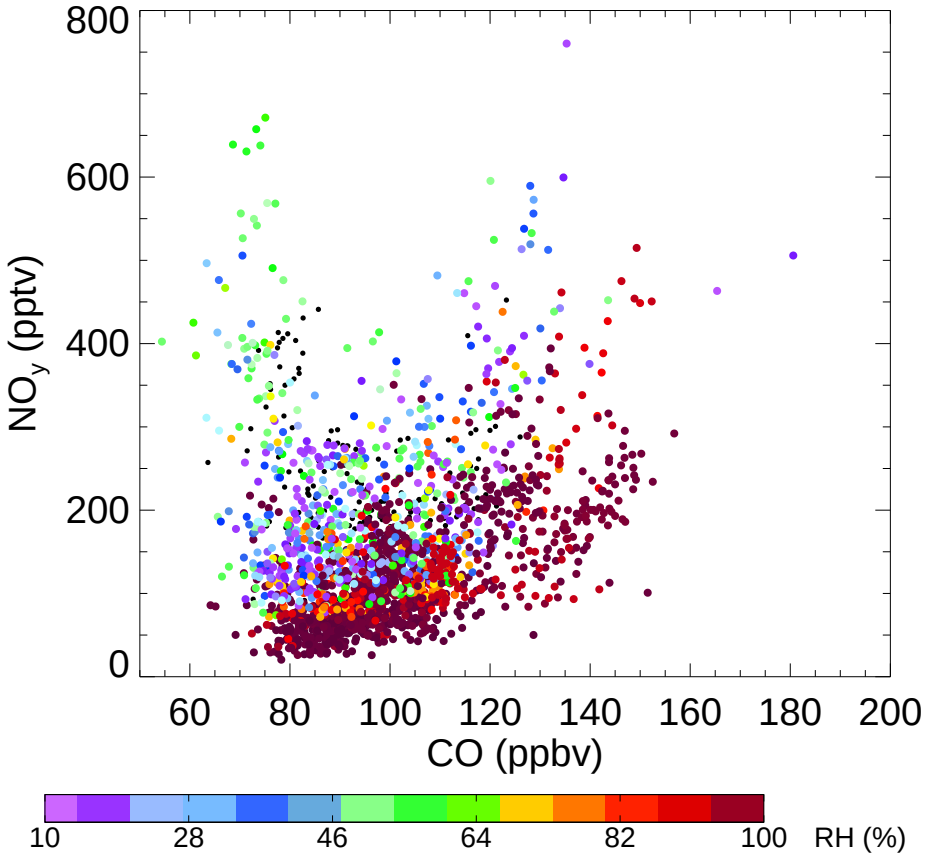

Figure 2.4 Relationship between NO_y and CO during fall. Dots represent simultaneous 30-min averages. Where data are available, the dots are color-coded according to simultaneous 30-min averages of RH as indicated in the color bar.

Table 2.2 Summary of monthly mixing ratios of nitrogen oxides and CO at the Pico Mountain station. Reported are the average, standard deviation of all 30-min average observations (SD), median and number (N) of the 30-min average observations in pptv for daytime NO, NO_x and NO_y and in ppbv for CO.

	Daytime NO			NO_x			NO_y[a]			CO		
Month	Mean±SD	Median	N	Mean±SD	Median	N	Mean±SD	Median	N	Mean±SD	Median	N
Jan	7 ± 7	6	38	23 ± 11	21	436	129 ± 44	125	137	123 ± 18	121	1968
Feb	NA	NA	NA	NA	NA	NA	NA	NA	NA	132 ± 12	132	1139
Mar	12 ± 8	11	184	27 ± 12	25	197	220 ± 54	212	105	147 ± 11	146	748
Apr	8 ± 8	7	135	28 ± 10	28	81	292 ± 116	312	163	133 ± 15	132	2037
May	4 ± 4	4	135	20 ± 15	17	444	249 ± 127	217	247	119 ± 15	118	3185
Jun	7 ± 5	6	124	30 ± 17	26	385	357 ± 132	335	295	102 ± 17	101	2246
Jul	11 ± 6	10	79	34 ± 18	30	637	383 ± 192	338	331	93 ± 22	90	4753
Aug	9 ± 4	9	166	32 ± 17	28	671	333 ± 143	296	338	92 ± 20	90	4089
Sep	12 ± 6	12	26	36 ± 23	31	152	357 ± 141	301	172	96 ± 24	93	1097
Oct	8 ± 6	7	256	34 ± 21	28	809	216 ± 103	192	432	107 ± 17	104	3458
Nov	9 ± 5	9	105	30 ± 14	27	538	171 ± 67	151	305	100 ± 16	99	1933
Dec	7 ± 6	5	26	29 ± 17	27	975	174 ± 76	168	564	110 ± 16	110	2579

NA, non available.

[a] NO_y determined in dry conditions.

and 2004 (31±3 pptv) because NO_x observations were only available for about 10 days in 2002, which happened to coincide with North American outflow.

Figure 2.3d shows a sharp seasonal cycle for CO, with a minimum median of 90 ppbv in July–August and a maximum median of 146 ppbv in March. CO is oxidized by OH. Thus, annual variation of CO is driven to a large extent to the annual change in OH, which is closely related to the water vapor and the solar intensity cycle [*Novelli et al.*, 1992]. In addition to photochemical processes, seasonal variation in synoptic flow patterns, and the associated changes in source regions and transport times to the measurement site can also affect the background levels of CO. Based on a clustering analysis of backward trajectories to the Pico Mountain station [*Strane et al.*, Major source regions to the Pico Mountain station: Transport, chemical observations, and interannual variability, manuscript in preparation], more frequent transport from the Atlantic basin and longer transit times from the North American continent in summer may also explain the lower observed summertime CO. This effect was also noted for the non-methane hydrocarbons (NMHC) sampled at the Pico Mountain station [*Helmig et al.*, Analysis of transport and oxidation chemistry in the North Atlantic region from interpretations of NMHC measurements at Pico Mountain, Azores, submitted to *J. Geophys. Res.*, 2007 (hereinafter *Helmig et al.*, submitted)].

In contrast to CO, the seasonal variation of nitrogen oxides is more complex. The variation of nitrogen oxides in the troposphere remote from sources of NO_x depends largely on the partitioning of NO_y [*Atlas et al.*, 1992; *Ridley et al.*, 1998], which in turn, is controlled to a larger extent by the rate of loss of the reservoir species and by the recycling of NO_x from these reservoirs. Moreover, since the loss processes differ among compounds, each process may result in a different effect on NO_y. For example, thermal decomposition of PAN regenerates NO_2, which changes the partitioning of NO_y but not the total NO_y, whereas wet and dry deposition of HNO_3 results in a change in total NO_y as nitrogen is removed from the atmosphere.

Figure 2.3a shows that NO_x observations exhibited a distinct seasonal cycle, with

the overall variability at all percentiles larger from July to October than in the other months. However, monthly medians did not reveal a distinct pattern. Similar monthly medians were present all year round (17–31 pptv). (To avoid the possible interference from additional daytime NO_2 (section 2.2.1), we also compared nighttime NO_x medians and found similar results: 16–28 pptv). Because the lifetime of NO_x in the lower FT (on the order of $\lesssim$ 1 day [*Liu et al.*, 1987]) is shorter than the transit time from NO_x source regions to the measurement site, it is clear that in-situ sources of NO_x are required to provide these NO_x levels all year round. This implies that PAN decomposition and potentially photolysis of HNO_3 in the airmasses that reach the Pico Mountain station provides a supply of NO_x to the lower FT in this region, in particular during summer seasons.

Due to the rapidly increasing solar insolation and decreasing O_3 concentrations from spring to fall, one may expect a shift of NO_x partition toward NO as photolysis of NO_2 increases and the rate of the reaction of NO with O_3 decreases. In our observations, the actual situation was somewhat different. Figure 2.3b shows that daytime NO mixing ratios presented a small broad peak from July to September, with medians of 9–12 pptv. The increase in NO during these months is consistent with the increase in solar radiation and generally lower O_3 concentrations observed at the Pico Mountain station (not shown). However, a peak was also present in March, with a median of 11 pptv. Although not fully understood, this behavior may be the result of a slower rate of reaction of NO with peroxy radicals, which may be present in low concentrations during this month due to a reduced availability of OH.

As shown in Figure 2.3c, NO_y observations exhibited a well-defined seasonal cycle, with larger values in June–September (medians 296–338 pptv) than in October–May (medians 125–312 pptv). There are several causes that may be responsible for this behavior.

First, synoptic-scale changes in the lofting mechanisms over the continents may result in seasonal changes in the export of emissions. *Parrish et al.* [2004] proposed

that shallow venting of the continental BL to the lower FT, driven by surface heating and associated with fair weather cumulus breaking through the afternoon BL, may provide an important lofting mechanism for anthropogenic emissions over the eastern U.S. This mechanism, which is expected to be most frequent in summer, results in a significant export of nitrogen oxides to the North Atlantic region [*e.g. Parrish et al.*, 2004; *Li et al.*, 2004; *Hudman et al.*, 2007], and is likely to contribute to the larger summertime levels of NO_y observed at the Pico Mountain station.

Second, boreal wildfires have been recently recognized to be a significant source of nitrogen oxides to the North Atlantic troposphere [*Val Martin et al.*, 2006; *Singh et al.*, 2007]. NO_y means from July to September —typically the boreal fire season— exceeded the medians by 13–18%, showing extreme excursions from the median in the positive direction. As will be shown in section 2.3.2, the higher variability of NO_y in these months reflects the high but varying influence of boreal wildfire emissions. Thus, summertime wildfire emissions result in higher levels of NO_y.

Finally, variation in the input from stratospheric or upper tropospheric sources could also contribute to changes in nitrogen oxides. NO_x production by lightning varies seasonally, with the maximum production occurring in the Northern Hemisphere during summer [*Nesbitt et al.*, 2000]. Stratospheric injection is found to be more important during springtime [*e.g. Parrish and Fehsenfeld*, 2000; *Merrill and Moody*, 1996], although injections are also frequent in summer [*Thompson et al.*, 2007]. To assess the impact of stratospheric and upper tropospheric transport to the Pico Mountain station, we used FLEXPART Strat-O_3 values from July 2002 to August 2005. This analysis indicated that stratospheric O_3 occasionally impacts the measurement site, but the overall impact is rather small: the average$\pm$2-standard deviation of all FLEXPART Strat-O_3 values was 7 ± 9 ppbv, without significant variation on a seasonal basis. On an event basis, we did not find any consistent correlation between nitrogen oxides levels and FLEXPART Strat-O_3, *i.e.*, enhancements of NO_y were not correlated with increases in the FLEXPART Strat-O_3 values. We thus con-

clude that stratospheric air did not significantly contribute to the changes in the nitrogen oxides observed at the Pico Mountain station.

Table 2.3 compares the mixing ratios of nitrogen oxides at the Pico Mountain station with observations from previous aircraft studies in the North Atlantic troposphere and from two ground-based stations, MLO over the North Pacific Ocean and Jungfraujoch (JFJ) station over central Europe. Values are compiled by seasons. The majority of these studies were made during the summer season. Thus, we focus here on summertime observations, unless indicated otherwise.

It is evident that nitrogen oxides levels at the Pico Mountain station (median 322 pptv for NO_y and 29 pptv for NO_x; Table 2.3 rows 2 and 12) are lower than those observed at other studies over the western North Atlantic at 0.5–6 km altitudes (652–1000 pptv for NO_y and 40–55 pptv for NO_x; Table 2.3 rows 5–7 and 15–17). Lower NO_y and NO_x at the Pico Mountain station indicate that removal of NO_y and rapid oxidation of NO_x in the airmasses may occur as a result of longer transport times over the ocean. In addition, lower NO_y and NO_x levels may also indicate a smaller influence of stratospheric and upper tropospheric transport. NO_x and NO_y typically exhibit a C-shaped profile near source regions with high concentrations near the surface decreasing through the FT and then with a sharp rise at altitudes generally above 6 km [*e.g. Singh et al.*, 2007]. This is the result of the combination of atmospheric oxidation with the location of the emissions (BL and upper troposphere) and convection.

Nitrogen oxides levels observed at MLO (median 168–374 pptv for NO_y and 25–36 pptv for NO_x; Table 2.3 rows 3 and 13) were similar to those observed at the Pico Mountain station (147–322 pptv for NO_y and 21–29 pptv for NO_x) all year round. Similar to the Pico Mountain station, MLO is a remote marine observatory, in which well-aged airmasses are sampled during downslope conditions [*Ridley et al.*, 1998]. Thus, observed levels at MLO also reflect the strong removal of NO_y and rapid oxidation of NO_x in the airmasses during transport. In contrast, larger NO_x and

Table 2.3 Observation of nitrogen oxides in the lower free troposphere of remote regions.

	Sampling	Altitude	Spring		Summer		Fall		Winter		
Year	Location	(km)	Mean±SD	Median	Mean±SD	Median	Mean±SD	Median	Mean±SD	Median	Source[a]
NO_y (pptv)											
2002–2005[b]	C Atl	2.2	257 ± 115	229	358 ± 160	322	228 ± 121	195	165 ± 73	147	[1]
1991–1992	N Pac	3.4	368 ± 109	374	203 ± 99	188	177 ± 70	168	204 ± 82	187	[2]
1997–1999	W Eur	3.6	748 ± 614	581	653 ± 570	529	553 ± 477	422	501 ± 659	350	[3]
2004	W Atl	2–4	—	—	809 ± 610	652	—	—	—	—	[4]
1988–1993	W Atl	0.5–3	—	—	817 ± 104	850	—	—	675 ± 248	675	[5]
		3–6	—	—	969 ± 65	1000	—	—	467 ± 76	450	[5]
1993	C Atl	1	—	—	495 ± 214	480	—	—	—	—	[6]
1993	E Atl	2.4	—	—	390 ± 100	390	—	—	—	—	[7]
2000	N Ame	2–3	—	275–450	—	—	—	—	—	275–300	[8]
NO_x (pptv)											
2002–2005	C Atl	2.2	23 ± 14	21	32 ± 17	29	33 ± 19	28	27 ± 16	24	[1]
1991–1992	N Pac	3.4	39 ± 15	36	29 ± 12	28	26 ± 9	25	32 ± 11	31	[2]
1997–1999	W Eur	3.6	183 ± 289	98	191 ± 482	133	205 ± 355	115	203 ± 454	87	[3]
2004	W Atl	2–4	—	—	64 ± 63	52	—	—	—	—	[4]
1988–1993	W Atl	0.5–3	—	—	73 ± 67	40	—	—	—	—	[5]
		3–6	—	—	55 ± 21	55	—	—	—	30	[5]
1993	E Atl	2.4	—	—	50 ± 20	50	—	—	—	—	[7]
2000	N Ame	2–3	—	15–50	—	—	—	—	—	28	[8]

—: Not reported; N Pac: North Pacific; N Ame: North America; W Atl: Western North Atlantic; C Atl: Central North Atlantic; E Atl: Eastern North Atlantic; W Eur: Western Europe.

[a]Observations from *Emmons et al.* [1997] are average±SD of several field campaigns over western Atlantic Ocean; observations at MLO and Izaña are for downslope conditions and at JFJ for undisturbed conditions. Observations from *Peterson et al.* [1998] are average±SD of two periods in the FT. [1]: Pico Mountain: *This work*, [2]: MLO (*Ridley et al.* [1998]), [3]: JFJ (*Zellweger et al.* [2003]), [4]: ICARTT (*Singh et al.* [2007]), [5]: *Emmons et al.* [1997], [6]: NARE (*Peterson et al.* [1998]), [7]: IZANA (*Fischer et al.* [2004]) and [8]: TOPSE (*Wang et al.* [2003]).

[b]NO_y at the Pico Mountain station determined in dry conditions.

NO_y medians present at the continental JFJ observatory (350–581 pptv for NO_y and 87–133 pptv for NO_x; Table 2.3 rows 4 and 14) suggest the input of relatively fresh NO_x emissions from the continental BL [*Zellweger et al.*, 2003].

2.2.3 Average Partitioning of NO_y

To better understand the changes on the nitrogen oxides over the central North Atlantic lower FT, we examined the partitioning of NO_y into its three principal components: NO_x, HNO_3 and PAN.

2.2.3.1 Estimation of NO_y Partition

We used NO_x, NO_y and RH measured at the Pico Mountain station on a regular basis to determine the partitioning of NO_y. Several studies have demonstrated the rapid and efficient scavenging of nitric acid within clouds [*e.g. Chameides*, 1984; *Peterson et al.*, 1998; *Garrett et al.*, 2006]. For example, *Chameides* [1984] showed that HNO_3 levels decreased by two orders of magnitude in less than 100 s after marine cloud formation. Consistent with those studies, NO_y measurements at the Pico Mountain station were affected by the presence of clouds (section 2.2.2). Thus, measurements of NO_y levels during in- and out-of-cloud periods can be used to estimate the mixing ratio of cloud-scavenged NO_y species, *i.e.*, HNO_3, by assuming that HNO_3 is scavenged into clouds droplets during in-cloud periods [*Peterson et al.*, 1998]. (Even for the smallest observed orographic clouds ($\sim$1500 m radius) and typical higher wind speeds ($\sim$12 m s^{-1}; 95th percentile of wind speed observations when NO_y was available), there was enough time ($\sim$125 s) for HNO_3 to be scavenged into the cloud droplets before air reached the measurement site.) For this purpose, we subdivided the observations into periods above 96% RH and below 60% RH in order to identify in- and out-of-cloud intervals at the site, respectively. The RH cutoffs were selected so as both subsets contained similar numbers of data points and, at

the same time, cloud and cloud-free periods were present at the measurement site. Archived photos of the conditions at the station confirmed cloud and cloud-free periods under those cutoffs. Monthly HNO_3* values were determined by subtracting the monthly averages of NO_y observed during "in-cloud" periods from those observed during "out-of-cloud" periods; [PAN*] was determined by subtracting NO_x from NO_y in simultaneous observations during "in-cloud" periods, and [NO_x] and [NO_y] were determined using direct observations made during "out-of-cloud" periods. (The terms HNO_3* and PAN* are used here to indicate estimated, not directly measured values of these species.) Table 2.4 summarizes the NO_y levels during "in-cloud" and "out-of-cloud" periods, and the derived fraction of reactive nitrogen species on a seasonal basis, *i.e.*, [HNO_3*]/[NO_y], [PAN*]/[NO_y] and [NO_x]/[NO_y]. Figure 2.5a shows the monthly variation of the [HNO_3*]/[NO_y], [PAN*]/[NO_y] and [NO_x]/[NO_y]. A limited number of more direct estimates of [HNO_3*] were also made, using alternated measurements of [NO_y]-[HNO_3] and NO_y. Measurements of [NO_y]-[HNO_3] were made in August 2004 and 2005 by removing HNO_3 from NO_y before sampling using a nylon filter attached to the NO_y inlet [*e.g. Parrish et al.*, 1986; *Yamamoto et al.*, 2001]. [HNO_3] was determined by difference from NO_y; [PAN*] was determined as ([NO_y]-[HNO_3]) minus [NO_x]. Results from these tests are also presented in Table 2.4. These measurements provide an additional method to test the consistency of our approach. The fraction of reactive nitrogen species estimated directly from these tests (53–62% HNO_3, 23–34% PAN* and 9–16% NO_x) is similar to that deduced for the summer ($71 \pm 9\%$ HNO_3*, $21 \pm 8\%$ PAN* and $12 \pm 8\%$ NO_x).

To confirm that the changes in RH used in this analysis were independent of the origin and the chemical history on the airmasses, we inspected the variation of CO in the "in-cloud" and "out-of-cloud" periods when NO_y measurements were available. As shown in Figure 2.5b, CO did not exhibit a clear relationship with RH, *i.e.*, monthly CO averages were variable all year round, independent of "in-cloud" and "out-of-cloud" conditions. However, significant larger monthly CO means for the

Table 2.4 Partitioning of NO_y at the Pico Mountain station.

		Out-of-Cloud/ Without Filter[a]		In-Cloud/ With Filter[b]					
Season	Test Period	NO_y[c]	NO_x[c]	NO_y[c]	[PAN*][c]	[HNO_3*][c]	[HNO_3*]/[NO_y][d]	[PAN*]/[NO_y][c]	[NO_x]/[NO_y][e]
Spring		259 ± 120	23 ± 11	132 ± 101	117 ± 81	127 ± 31	0.49 ± 0.13	0.45 ± 0.12	0.11 ± 0.05
		(451)	(227)	(351)	(114)				
Summer		365 ± 163	37 ± 17	105 ± 110	76 ± 130	260 ± 30	0.71 ± 0.09	0.21 ± 0.08	0.12 ± 0.08
		(841)	(550)	(475)	(295)				
	Aug 26, 2004	395 ± 47	45 ± 13	182 ± 21	212 ± 52	132 ± 24	0.54 ± 0.15	0.34 ± 0.07	0.13 ± 0.04
	09:48–15:27	(18)	(30)	(17)					
	Aug 26–27, 2004	218 ± 39	19 ± 7	70 ± 16	148 ± 42	51 ± 17	0.62 ± 0.23	0.23 ± 0.09	0.09 ± 0.03
	20:29–06:58	(36)	(26)	(28)					
	Aug 18–19, 2005	278 ± 20	44 ± 13	130 ± 31	149 ± 33	85 ± 36	0.53 ± 0.23	0.31 ± 0.07	0.16 ± 0.05
	21:04–08:58	(28)	(63)	(35)					
Fall		223 ± 114	38 ± 20	117 ± 67	65 ± 41	101 ± 20	0.47 ± 0.10	0.29 ± 0.04	0.19 ± 0.07
		(721)	(479)	(981)	(408)				
Winter		157 ± 74	28 ± 13	115 ± 70	63 ± 36	42 ± 17	0.27 ± 0.11	0.40 ± 0.06	0.19 ± 0.06
		(557)	(485)	(500)	(277)				

[a]Out-of-Cloud: observations of NO_y and NO_x made with RH$<$ 60%; Without filter: observations of NO_y and NO_x made in the alternated [NO_y]–[HNO_3] and NO_y tests. (See text for explanation.)

[b]In-Cloud: observations made with RH$>$ 97%. With filter: observations of [NO_y]–[HNO_3] made in the alternated [NO_y]–[HNO_3] and NO_y tests. (See text for explanation.)

[c]Reported are average$\pm$standard deviation of the 30-min average observations (in pptv) for the "out-of-cloud"/"in-cloud" analysis and average$\pm$standard deviation of the 20-sec or 30-sec average observations for the "without filter"/"with filter" tests, for NO_y, NO_x and PAN*. (See text for explanation.) Uncertainties for [HNO_3*] are based on propagation of errors (2-σ). In parentheses, number of the 30-min average, 20-sec or 30-sec observations.

[d]Ratios of the means. Uncertainty is based on propagations of errors (2-σ).

[e]Mean of ratios. Uncertainty is the 2-standard error of the mean.

"out-of-cloud" periods from July to September may indicate a dominance of boreal region outflow, which is characterized by low RH and elevated CO levels [*Val Martin et al.*, 2006]. This influence of boreal emissions during "out-of-cloud" conditions may have resulted in an overestimation of HNO_3 and underestimation of PAN levels during summer, since NO_y is enhanced during boreal wildfire events.

In this analysis, we neglected the possible influence of aerosol and alkyl nitrates. The $NO_{x,y}$ system inlet used at the Pico Mountain station excludes large aerosol particles, but allowed sampling of the $\lesssim$10 micron aerosol fraction [*Hangal and Willeke*, 1990; *Peterson and Honrath*, 1999]. However, sub-micron size aerosol nitrates are not efficiently measured in our system as conversion efficiency for these compounds are low [*Miyazaki et al.*, 2005]. The contribution of alkyl nitrates to NO_y in the remote marine troposphere is very small [*Singh et al.*, 2007; *Reeves et al.*, 2007]. For example, alkyl nitrates accounted for less than 2% of the tropospheric NO_y in the lower FT over the North Atlantic Ocean during the ICARTT study [*Singh et al.*, 2007]. Thus, although the presence of alky nitrates may introduce a bias in our estimation of PAN, this bias is expected to be very small.

2.2.3.2 Variation of NO_y Partitioning

From Figure 2.5a, it is evident that although reactive nitrogen is principally emitted as NO, it largely exists in its secondary reservoir forms in the central North Atlantic lower FT all year round. Low NO_x/NO_y ratios (9–19%; Table 2.4) are consistent with long-range transport and photochemical processing times to the measurement site. Because of the relatively short lifetime of NO_x compared to NO_y, NO_x/NO_y is expected to decrease with increasing airmass age. In the remote lower FT, typical NO_x/NO_y values of 10–17% have been observed all year round [*Ridley et al.*, 1998; *Atlas et al.*, 1992; *Singh et al.*, 2007], consistent with the values observed at the Pico Mountain station.

The shift from dominance of PAN in winter–spring to dominance of HNO_3 in

summer–fall in Figure 2.5a is noteworthy. The small contribution of PAN during the summer (21–34%; Table 2.4) is attributed to the strong thermal decomposition of PAN to NO_x in the North Atlantic lower FT. Conversely, the large fraction of HNO_3 (53–71%; Table 2.4) is directly related to the efficient formation of HNO_3 from reaction of NO_x with OH, as conversion of NO_x to HNO_3 is 5 times faster during summer than winter [*Logan*, 1983]. Indirectly, the strong decomposition of PAN during the summer may result in the formation of HNO_3 as NO_x is ultimately converted to HNO_3.

To evaluate the effect of temperature on PAN, we examined the lifetime of PAN with respect to thermal decomposition in the airmasses during transit to the Pico Mountain station. For this purpose, we extracted the average temperature from the HYSPLIT model output [*Draxler and Rolph*, 2003] for the 10-day backward trajectories arriving at the measurement site. More information on the HYSPLIT backward trajectories is presented elsewhere [*Honrath et al.*, 2004; *Val Martin et al.*, 2006]. We calculated the average temperature in the airmasses from the measurement site to 3 days upwind. This average temperature is the typical temperature that the airmasses encounter before arriving at the Pico Mountain station. We then used those average values to calculate the lifetime of PAN. Figure 2.5a shows the lifetime of PAN in the airmasses determined from the monthly average upwind temperatures from July 2002 to August 2005. The average lifetime of PAN under those conditions ranged from 5 days in March (average temperature -4.4°C) to 0.5 days in August (average temperature 8.9°C). Therefore, the dominance of PAN in NO_y in winter–early spring is consistent with the longer lifetime of PAN in the airmasses, whereas the rapid decomposition of PAN in the airmasses during the summer results in the lower PAN fraction observed during that season. Due to the rapid oxidation of NO_x by OH in the summer ($\lesssim$ 1 day), PAN decomposition may result in the formation of HNO_3 before the airmasses reach the Pico Mountain station.

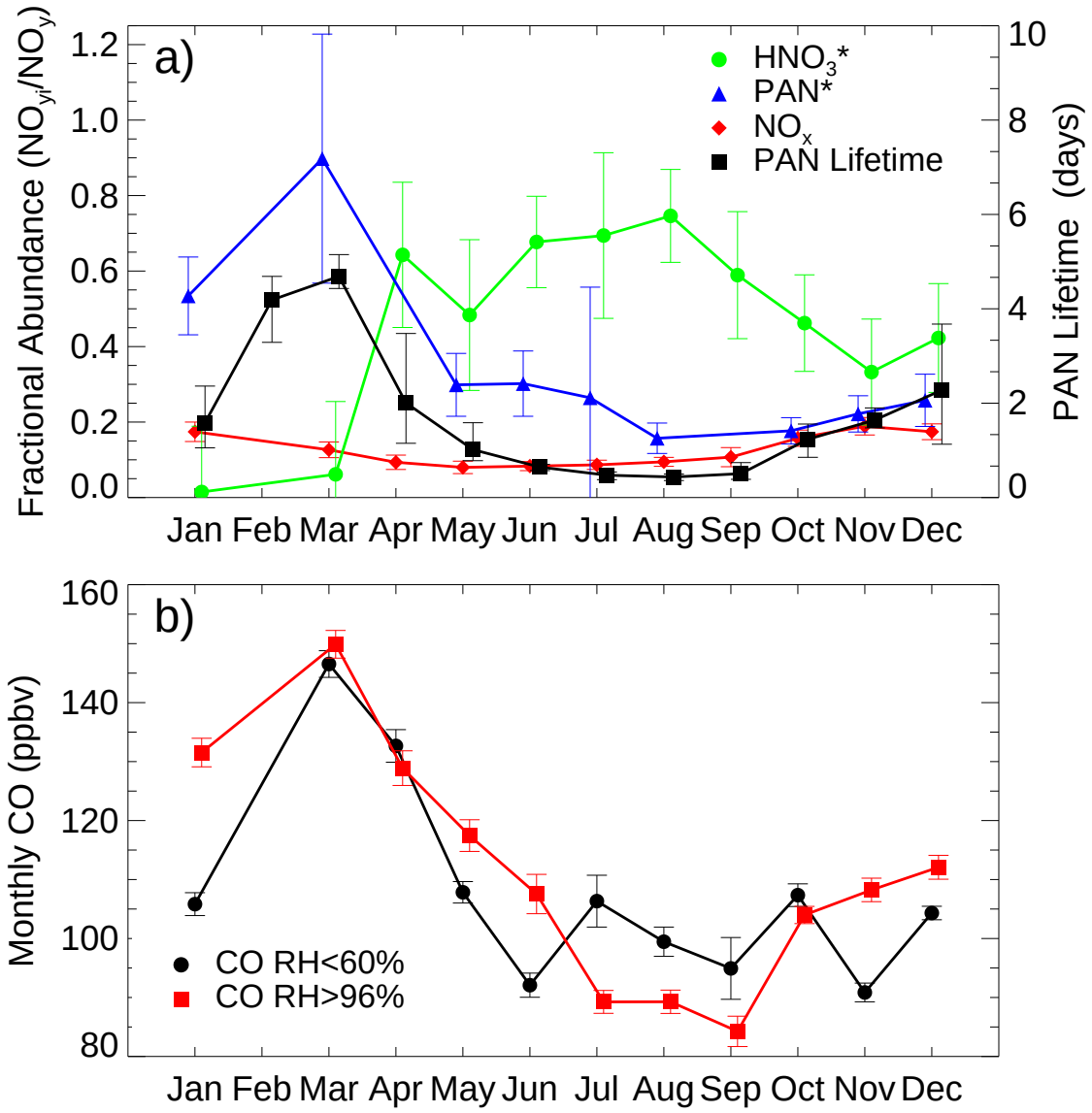

Figure 2.5 Seasonal cycle of a) partitioning of reactive nitrogen (HNO_3*, PAN* and NO_x) and average lifetime of PAN with respect to thermal decomposition in the air arriving at the Pico Mountain station, and b) CO in "in-cloud" (RH$>$ 96%) and "out-of-cloud" (RH$<$ 60%) periods. (See text for explanation.) Symbols represent monthly averages for HNO_3* (green circles), PAN* (blue triangles), NO_x (red diamonds), CO RH$>$ 96% (red squares) and CO RH$<$ 60% (black circles) and average of the monthly means for PAN lifetime (black squares). Error bars indicate the 2-standard error of the mean for CO, NO_x and PAN*, the uncertainty (2-σ) based on propagation of errors for HNO_3* and the minimum and maximum estimated monthly PAN lifetime.

2.2.3.3 Comparison to Previous Observations

A comparison of the distribution of NO_y species at the Pico Mountain station to those collected over the western North Atlantic Ocean during the NARE and ICARTT aircraft campaigns from spring to fall [*Parrish et al.*, 2004; *Li et al.*, 2004; *Singh et al.*, 2007; *Hudman et al.*, 2007] allows for some speculation on the behavior of nitrogen oxides across the North Atlantic region. Table 2.5 compares the fractions of reactive nitrogen species measured during the ICARTT and NARE campaigns with those estimated at the Pico Mountain station.

Our spring–fall estimates of the fraction of NO_x (9–19%), PAN* (21–45%) and HNO_3* (47–71%) are similar to those observed over the western Atlantic Ocean in those other studies (8–13% for NO_x, 34–47% for PAN and 40–57% for HNO_3; averages in 2–8 km and 2.5–6.5 km altitudes from Table 2.5). However, as discussed in section 2.2.2, levels of NO_y at the Pico Mountain station are 2–3 times lower than those over the western Atlantic region (section 2.2.2), indicating the significant removal of HNO_3 during transport to the measurement site. These results suggest that to maintain the observed fractions of NO_x and HNO_3* at the Pico Mountain station, decomposition of PAN to NO_x and further oxidation of NO_x to HNO_3 must occur in the airmasses.

2.2.3.4 Comparison to GEOS-Chem

Figures 2.6a-c compares the measurements with results obtained from the global chemical transport model GEOS-Chem for NO_y, HNO_3*, PAN* and NO_x. Additionally, the model-data comparison for CO is shown in Figure 2.6d. GEOS-Chem simulations were available from January to December, 2005, whereas data from the Pico Mountain station in 2005 were available only from January to August. To be able to compare a full year cycle, we compared GEOS-Chem simulations to all data in 2002–2005. To account for any interannual variability that could bias our comparison,

Table 2.5 Partitioning of NO_y (%) and NO_y export efficiency (%) estimates reported from ICARTT, NARE and Pico Mountain studies.

Study	Altitude (km)	Season	$[NO_x]/[NO_y]^a$	$[PAN]/[NO_y]^a$	$[HNO_3]/[NO_y]^a$	Export Efficiency[b]	Source
Pico Mountain	2.2	Spring	11	45	49	3 ± 2	[1]
		Summer	9–16	21–34	53–71	5 ± 2	
		Fall	19	29	47	3 ± 1	
		Winter	19	40	27	2 ± 1	
NARE 96	2–8	Spring	11	42	47	11 ± 6	[2]
			—	—	—	5	[3]
NARE 97	2–8	Fall	8	34	57	9 ± 5	[4]
	2–8		—	—	—	3	[3]
ICARTT	2.5–6.5	Summer	13	47	40	16 ± 10	[5]
	2.5–3.5		—	—	54	18 ± 11	
	3.5–6.5		14	53	33	12 ± 6	
ICARTT	2–8	Summer	8	35	44	—	[6]
	2–4		8	26	60	—	
	4–6		7	43	43	—	

—, Not reported.

[a]NO_y composition reported is: For Pico Mountain, average percentages in spring, fall and winter, and minimum and maximum average percentages in summer (Table 2.4); For NARE and ICARTT, average percentages [*Parrish et al.*, 2004; *Li et al.*, 2004; *Hudman et al.*, 2007] or percentages calculated using means reported every 2 km altitude bins [*Singh et al.*, 2007]. [1]: *This work*, [2]: *Parrish et al.* [2004], [3]: *Stohl et al.* [2002], [4]: *Parrish et al.* [2004] and *Li et al.* [2004], [5]: *Hudman et al.* [2007] and [6]: *Singh et al.* [2007].

[b]Export efficiencies reported are: For Pico Mountain, average and uncertainty (2-σ) for the U.S. plumes above the marine BL (section 2.3.1.3). For NARE and ICARTT, average and uncertainty reported in each study and for *Stohl et al.* [2002], estimates above 3 km altitude.

we also compared GEOS-Chem simulations to the data available in 2005 only. The model-data comparison focuses mainly on the median since this value is less affected by the variability resulting from large episodic events, with the exception of HNO_3* and PAN*, which are based on the estimated averages.

From Figure 2.6a, it is apparent that GEOS-Chem reproduces the annual variation of NO_y observed at the Pico Mountain station. However, GEOS-Chem tends to overestimate NO_y. As shown in Figure 2.6b, this overestimation is mainly due to an excess of HNO_3. For example, during summer, GEOS-Chem produces monthly HNO_3 medians 50–150 pptv greater than NO_y medians at the Pico Mountain station and it also overestimates HNO_3 by about a factor of two during that season. This problem is known to occur in current GCT models [*e.g. Lawrence and Crutzen*, 1998; *Bey et al.*, 2001; *Singh et al.*, 2007], and may be related to an overestimation of OH concentrations [*Singh et al.*, 2007], to insufficient scavenging in the model [*Bey et al.*, 2001] or a combination of these and other causes.

Because of the scavenging scheme used in GEOS-Chem, it has been suggested that the model allows for significant escape of nitrogen oxides to the lower FT and it simulates reasonably well the shallow convection from the U.S. BL to the lower FT during the summer [*Li et al.*, 2004; *Hudman et al.*, 2007]. Thus, GEOS-Chem suggests that the export of NO_y out of the U.S. BL may be partially responsible for the increased summertime NO_y levels over the central North Atlantic lower FT, consistent with our hypothesis (section 2.2.2). However, the large values produced by GEOS-Chem indicate an inability to capture the actual magnitude of NO_y over the North Atlantic lower FT.

Figure 2.6b shows the comparison between simulated PAN levels and observations. The model produces an annual variation of PAN similar to that estimated at the Pico Mountain station. However, GEOS-Chem tends to underestimate PAN, in particular from July to September, when GEOS-Chem values are a factor of 6–7 times lower than the observations. This behavior may be related to causes such as

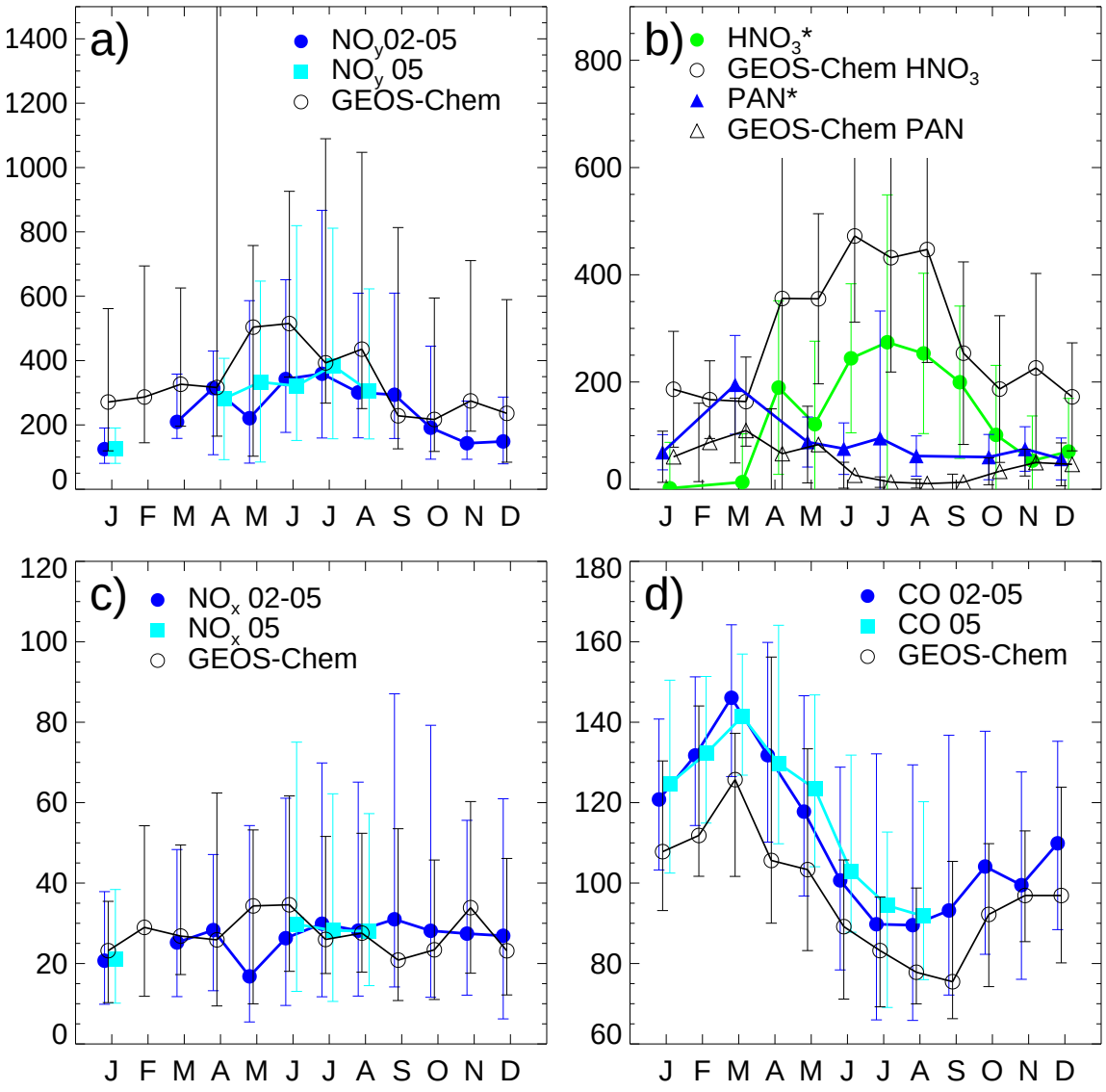

Figure 2.6 Comparison of observations a) NO_y in dry conditions (see section 2.2.2 for explanation), b) HNO_3* and PAN*, c) NO_x and d) CO to GEOS-Chem simulations. Symbols represent monthly medians in 2002–2005 (blue solid circles) and in 2005 (cyan solid squares) for NO_y, NO_x and CO; monthly medians in 2005 for GEOS-Chem NO_y, NO_x and CO (black open circles); monthly averages in 2002–2005 for HNO_3* (green solid circles) and PAN* (blue solid triangles) and in 2005 for GEOS-Chem HNO_3 (black open circles) and GEOS-Chem PAN (black open triangles). Error bars indicate the 10th and 90th percentile for observed and simulated NO_y, NO_x and CO, the standard deviation of all estimates of PAN* and GEOS-Chem simulations of HNO_3 and PAN, and the uncertainty (2-σ) based on propagation of errors for HNO_3*.

an excessive decomposition of PAN in the model or underestimation of NO_x and/or NMHC emissions. Finally, the model-data difference may also be related to a low removal efficiency for HNO_3 within the clouds present at the Pico Mountain station, resulting in an overestimation of PAN*, since PAN* was calculated by assuming complete removal of HNO_3 in the presence of clouds at the station. Were this the case, it would also reduce the HNO_3 model-data difference during summer, but only by 20%, not changing the conclusion that [HNO_3] exceeds the simulated values.

A comparison of simulated and observed NO_x levels is shown in Figure 2.6c. Similar to our measurements, GEOS-Chem does not simulate a clear seasonal cycle for the median NO_x values. GEOS-Chem simulations produce monthly medians (21–35 pptv) similar to those observed at the Pico Mountain station (21–30 pptv in 2005 and 16–29 pptv in 2002–2005). However, the model does not capture the very large variability in the NO_x mixing ratios, particularly that associated with transport of boreal wildfires in summer 2005.

Figure 2.6d shows observed and modeled CO values. GEOS-Chem CO exhibits a seasonal variation similar to that observed at the Pico Mountain station, but systematically underestimates the CO observations in 2005 by 10 to 25 ppbv. This behavior has been noted previously [*Bey et al.*, 2001], and may be related to an excess of OH in the model and/or to the underestimation of the CO emissions. During July–September, this difference is more apparent. GEOS-Chem simulates a sharp decrease of CO through these months, whereas observed CO remain stable. This may be related to the strong impact of boreal wildfire emissions during these months in both 2004 and 2005, which it is not simulated by the fire emission inventory used in this GEOS-Chem simulation.

This comparison shows that, although current GCT models have become more sophisticated [*Singh et al.*, 2007], uncertainties in simulating nitrogen oxides in the remote lower FT remain. These uncertainties are clearly related to errors in emission sources and limitations in our understanding of the nitrogen oxides chemistry in the

remote troposphere.

2.3 Influence of Transport of Pollution

In this section, we determine the influence of transport of pollution on the nitrogen oxides levels over the central North Atlantic lower FT. We first assess the impacts of transport of anthropogenic emissions from eastern North America and examine the resulting implications for the tropospheric O_3 budget. Second, we determine the impact of boreal wildfire emissions on the distribution of the nitrogen oxides levels.

2.3.1 Impacts of North American Anthropogenic Emissions

To assess the influence of North American anthropogenic emissions over the central North Atlantic lower FT, we compare the enhancements of CO and nitrogen oxides in North American outflow to levels observed in clean marine air without the input of recent emissions. The following section describes the identification of North America outflow periods and presents two example episodes.

2.3.1.1 Identification of North American Anthropogenic Impact

We identified periods potentially impacted by upwind anthropogenic emissions by selecting those in which the hourly average of CO was at least 20 ppbv higher than the CO background in each season and year, and the average of FLEXPART NA-CO during the event was at least 10 ppbv. An exception was made for April 20–24, 2005: although our criteria identified two episodes (April 20 20:30 UTC–April 23 10:30 UTC and April 23 21:30 UTC–April 24 10:30 UTC), elevated CO levels recorded between the events indicated that both periods were part of a continuous event. For the analysis, we considered as background the 20th percentile of all hourly CO observations for each season and year. This value represents clean marine levels without the influence

of emissions at the measurement site. Hourly averages of CO were used to smooth the variability of the CO measurements for comparison to the cutoff values. The average of FLEXPART NA-CO values within the periods was used instead of the individual 3-hour step values to allow for variability in the timing of the FLEXPART-simulated events. The FLEXPART NA-CO cutoff of 10 ppbv corresponds to approximately the 80th percentile of all model simulated values. Although the choice of these criteria is somewhat arbitrary, the cutoff values were designed to be conservative and ensure that the selected data represent significantly polluted airmasses from the U.S..

In addition to outflow strictly from the eastern North America, flow patterns passing over North America can also bring air that originated from the boreal regions. During these periods, air sampled at the Pico Mountain station may contain a mixture of anthropogenic and boreal wildfire emissions. To exclude the interference of boreal wildfire emissions, we removed those periods in which the corresponding average FLEXPART Fire-CO was above the 10th percentile of all simulated values for each season. This resulted in the removal of 30% of the events in summer and early fall. Additionally, transported emissions from North American sources may also be mixed with air containing anthropogenic emissions from Europe and Asia. To limit the events studied to those dominated by North American anthropogenic emissions, we also excluded those periods in which the average FLEXPART Asia-CO or FLEXPART Euro-CO was greater than 50% of the average FLEXPART NA-CO. This screening resulted in removal of an additional 2% of events.

2.3.1.2 Example Episodes

Figure 2.7 presents two example episodes of transport of anthropogenic pollution from the eastern North America to the Pico Mountain station. These two episodes illustrate two different transport mechanisms from North America. Figure 2.8 shows an example of FLEXPART retroplumes and the source contribution map for each episode.

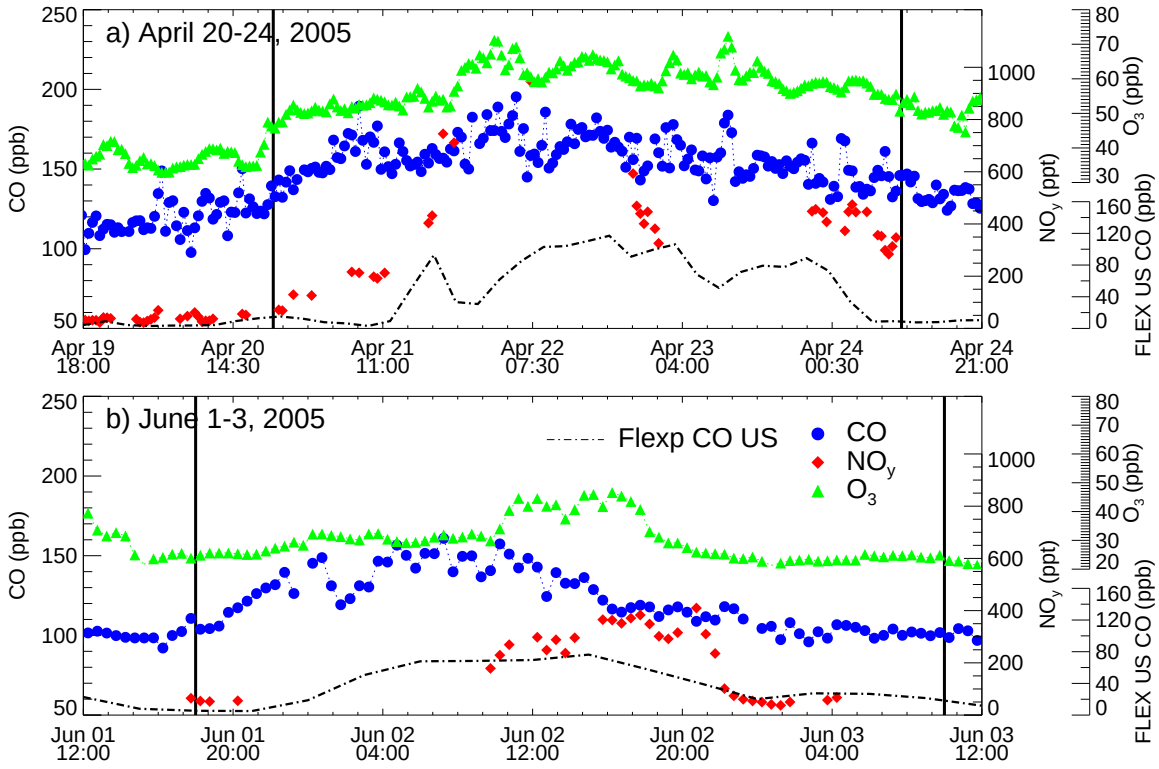

Figure 2.7 Time series of 30-min average CO, NO_y and O_3 measurements, and FLEXPART NA-CO at the Pico Mountain station during two North America outflow events: a) April 20–24, 2005 and b) June 1–3, 2005. NO_x measurements are not available. CO is plotted with blue circles, NO_y with red diamonds, O_3 with green triangles and FLEXPART NA-CO with a dash-dotted line. Vertical solid lines indicate the start and end time of the event; remaining data are plotted to make the events more apparent.

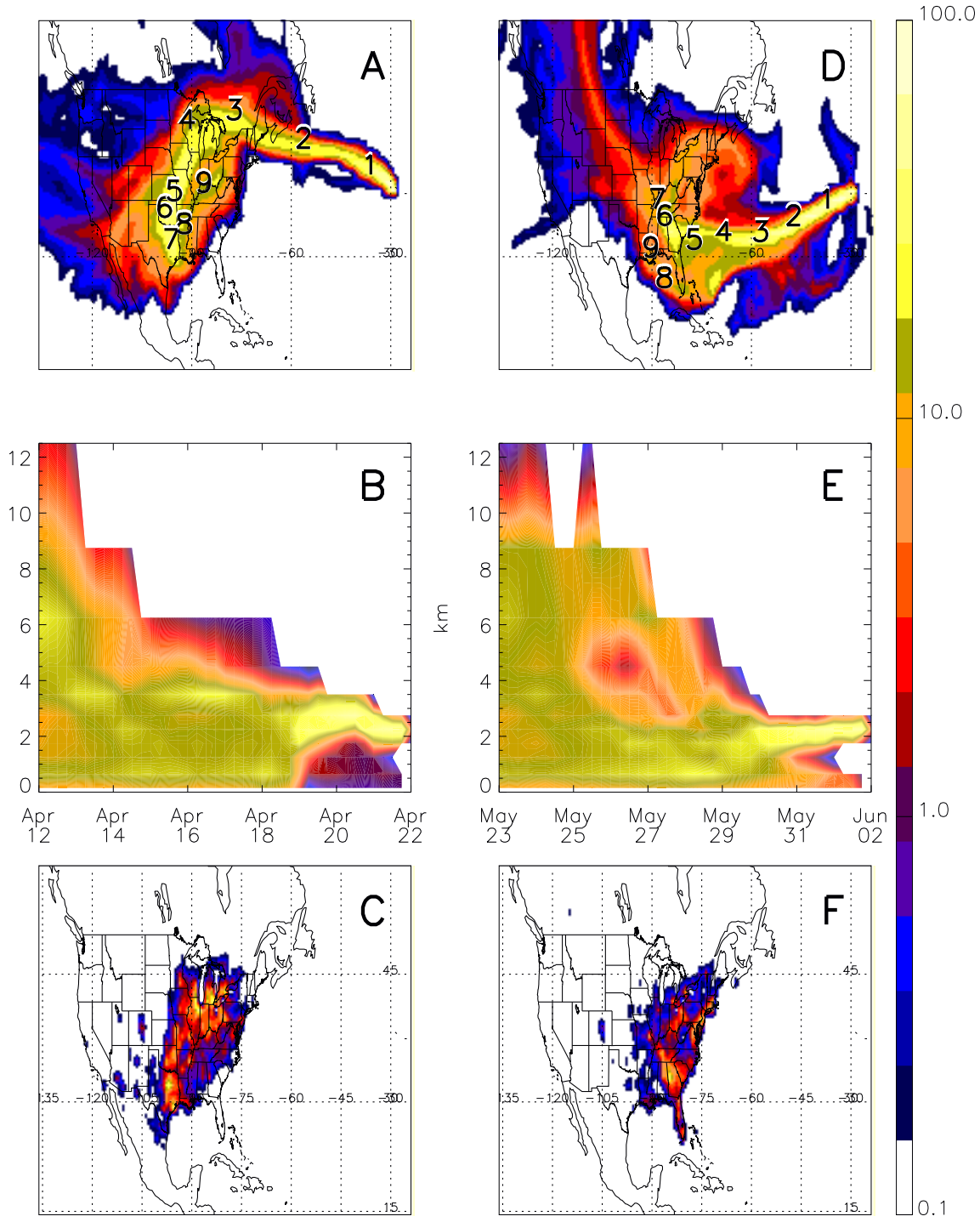

Figure 2.8 Results for retroplumes with release times centered on 18 UTC on April 22, 2005 (A, B and C) and 12 UTC on June 2, 2005 (D, E and F). The top row shows the total column (0–15km) SVWRT. Black numerals indicate the location of maximum column-integrated SVWRT at each integral day upwind. The middle row shows the SVWRT height distribution at each time upwind. The bottom row shows the footprint layer (0–300m) source contribution. Colors are logarithmically scaled (100–0.1%) according to a maximum value for each plot type (8×10^4 seconds*$m^3 kg^{-1}$ for the column-integrated SVWRT, 2.05×10^5 seconds*$m^3 kg^{-1}$ for the SVWRT height distribution, and 4.4 ppbv of CO for footprint source contributions), as shown by the scale on the right.

Figure 2.7a shows the time series of the observations for the episode of April 20–24, 2005. This event was the result of emissions from eastern U.S. and Canada as described in detail by *Helmig et al.*, [submitted]. During April 21–24 air from North America impacted the measurement site. As shown in Figure 2.8a-b for the retroplume of April 22 18:00 UTC, airmasses spent at least five days over North America (numerals 4–9 in Figure 2.8a) at altitudes lower than 2 km and were transported over the ocean for three days (numerals 1–3 in Figure 2.8a) at 2–4 km altitudes (April 19–22 in Figure 2.8b). Apparently as a consequence of the U.S. emissions, levels of CO, nitrogen oxides and O_3 were significantly enhanced during this period, and nitrogen oxides and O_3 were well correlated with CO.

Similarly, levels of CO were also considerably elevated during the June 1–3, 2005 episode, as shown in Figure 2.7b. This episode was the result of a sudden switch from airmasses originating at higher latitudes and altitudes to airmasses originating at low altitude over the southeastern U.S.. This episode, however, exhibited generally small enhancements of nitrogen oxides and O_3 and no significant correlation with CO. As shown in Figure 2.8d-e for the retroplume of June 2 18:00 UTC, airmasses passed over southeastern U.S. for at least four days (numerals 6–9 in Figure 2.8d) and were transported during two days (numerals 4–5 in Figure 2.8d) within the marine BL (altitudes below 2 km, May 28–30 in Figure 2.8e) and during three days (numerals 1–3 in Figure 2.8d) at altitudes of about 2 km (May 30–June 2 in Figure 2.8e), before reaching the measurement site. Strong removal of nitrogen oxides and O_3 destruction in the marine BL may have caused these small enhancements of nitrogen oxides and O_3. This conclusion is consistent with previous studies, which indicate rapid removal of HNO_3 within the MBL [*e.g. Roberts et al.*, 1996; *Peterson and Honrath*, 1999; *Dibb et al.*, 2004].

2.3.1.3 Nitrogen Oxides Enhancements in North America Outflow and Estimates of NO_y Transport Efficiency

Figure 2.9 (left and middle columns) presents the relationship of NO_x and NO_y to CO in the overall data and in the identified North America outflow periods, on a seasonal basis. It is apparent that transport events from North America occur all year round and they are responsible for part of the high nitrogen oxides observations during all seasons.

To characterize the amount of NO_x remaining or released into these plumes during transport, we determined enhancement ratios of NO_y and NO_x with respect to CO during each U.S. outflow period [*e.g. Stohl et al.*, 2002; *Parrish et al.*, 2004]. We first calculated the mean values of ΔCO, ΔNO_y and ΔNO_x in each event and then used those mean values to estimate the ratio relative to CO in each anthropogenic event (*e.g.* $\Delta NO_y/\Delta CO$). Here Δ indicates the difference between the concentration of the indicated species and the background concentration (*e.g.* [CO]-$[CO]_{bkgd}$), with background determined as the 20th percentile of all observations for each species, season and year. CO is commonly used as a tracer for NO_x emissions because it is emitted by combustion sources along with NO_x and has a long lifetime, on the order of one to three months depending on the season [*Novelli et al.*, 1992]. The resulting seasonally averaged enhancement ratios are presented in Figure 2.9. Table 2.6 summarizes the corresponding enhancement ratios for the individual anthropogenic events shown in Figure 2.9. To indicate the possible influence of local removal of HNO_3 on the $\Delta NO_y/\Delta CO$ ratios (section 2.2.3.1), we show in Table 2.6 the percentage of the event time in which the RH at the measurement site was above 96%.

Figure 2.9 (left column) and Table 2.6 show that NO_y was significantly enhanced in all the North America outflow plumes relative to the background levels, with the exception of one plume (April 26–27, 2005). However, the $\Delta NO_y/\Delta CO$ ratios were highly variable (0.2–12.0 pptv $ppbv^{-1}$; Table 2.6). There are two causes that are

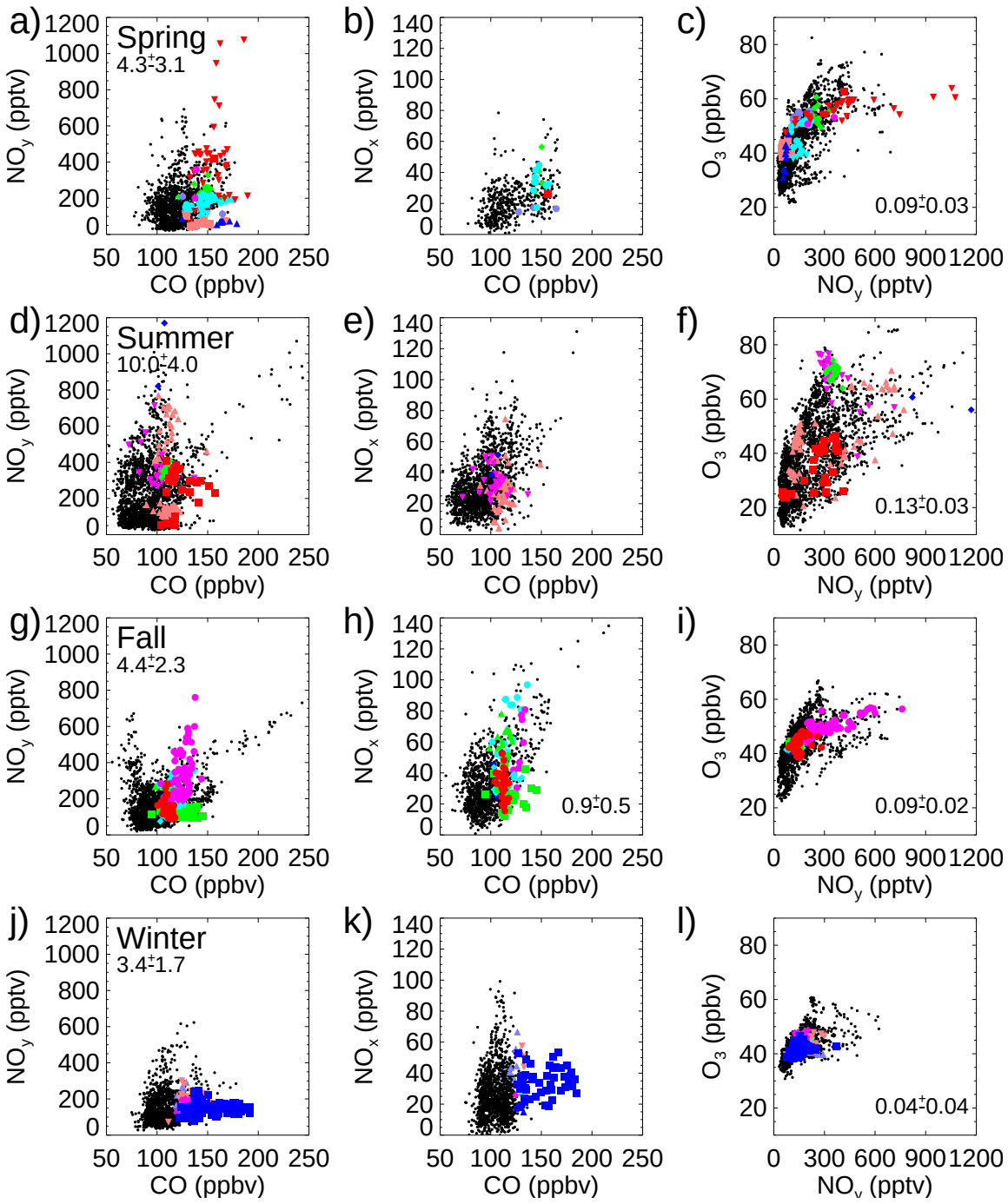

Figure 2.9 Relationship between CO and NO_y, CO and NO_x and NO_y and O_3 in spring (a-c), summer (d-f), fall (g-i) and winter (j-l) during 2002–2005. North America outflow events are plotted with different symbols and colors. Events with fewer than 5 data points are not indicated. Seasonal average enhancement ratios (mean$\pm$2-σ) from the anthropogenic events listed in Table 2.6 are identified in each plot. Units are pptv ppbv^{-1} for $\Delta NO_y/\Delta CO$ and $\Delta NO_x/\Delta CO$ and ppbv pptv^{-1} for $\Delta O_3/\Delta NO_y$. (Averages with fewer than three events are not shown.) All other other observations in 2002–2005 are plotted with small black dots.

Table 2.6 Enhancement ratios of nitrogen oxides during the North American outflow events identified in Figure 2.9. Reported enhancement ratios (calculated as described in text), 2-σ uncertainty and number (N) of simultaneous 30-min average observations of NO_y, NO_x, CO and O_3. Events with N < 5 not shown.

			Cloud[a]	$\Delta NO_y/\Delta CO$		$\Delta NO_x/\Delta CO$		$\Delta O_3/\Delta NO_y$	
Event	Year	Period	(%)	pptv ppbv^{-1}	N	pptv ppbv^{-1}	N	ppbv pptv^{-1}	N
		Spring[b]		4.3 ± 3.1				0.09 ± 0.03	
1	2004	Apr 15 6:15 – Apr 16 11:45	0	3.4 ± 0.2	17			0.14 ± 0.01	59
2	2004	Apr 20 12:15 – Apr 21 23:45						0.07 ± 0.00	70
3	2004	Apr 29 0:15 – Apr 30 23:45 [c]	100	1.3 ± 0.4	7			0.36 ± 0.10	95
4	2005	Mar 27 18:15 – Mar 28 17:45	96	3.9 ± 0.3	29	0.6 ± 0.1	9	0.08 ± 0.01	47
5	2005	Apr 20 18:15 – Apr 24 11:45	47	8.7 ± 1.0	38	NA	NA	0.05 ± 0.01	180
6	2005	Apr 26 18:15 – Apr 27 5:45 [d]	100	0.2 ± 0.2	12	NA	NA	0.37 ± 0.27	24
7	2005	May 18 6:15 – May 18 17:45 [d]	0	0.4 ± 0.1	10	NA	NA	-0.20 ± -0.10	24
		Summer[b]		10.0 ± 4.0				0.13 ± 0.03	
1	2004	Jun 6 0:15 – Jun 8 5:45	60	6.0 ± 0.7	70	0.3 ± 0.1	53	0.10 ± 0.01	108
2	2004	Jun 15 18:15 – Jun 16 11:45	0	12.0 ± 1.5	28	0.7 ± 0.1	26	0.14 ± 0.01	36
3	2005	Jun 1 0:15 – Jun 1 11:45	0	12.0 ± 0.5	16	NA	NA	0.14 ± 0.01	24
4	2005	Jun 1 18:15 – Jun 2 23:45 [d]	0	3.9 ± 0.6	27	NA	NA	0.03 ± 0.01	60
		Fall[b]		4.4 ± 2.3		0.9 ± 0.5		0.09 ± 0.02	
1	2002	Oct 6 18:15 – Oct 7 5:45	0	7.6 ± 0.6	13	1.5 ± 0.2	13	NA	NA
2	2002	Oct 7 6:15 – Oct 7 11:45	0	8.3 ± 0.8	12	1.8 ± 0.2	12	NA	NA
3	2003	Oct 19 12:15 – Oct 21 11:45	54	6.6 ± 0.5	80	1.1 ± 0.2	9	0.06 ± 0.00	96
4	2004	Nov 11 18:15 – Nov 11 23:45	0	2.0 ± 0.3	11	0.5 ± 0.1	11	0.11 ± 0.02	11
5	2004	Nov 22 18:15 – Nov 23 11:45	68	2.1 ± 0.3	19	0.5 ± 0.1	19	0.08 ± 0.01	36
6	2004	Nov 23 12:15 – Nov 24 11:45	14	1.3 ± 0.1	35	0.2 ± 0.1	24	0.13 ± 0.01	48
7	2004	Nov 25 6:15 – Nov 27 11:45	0	2.7 ± 0.2	56	0.5 ± 0.1	35	0.09 ± 0.01	102
		Winter[b]		3.4 ± 1.7				0.04 ± 0.04	
1	2004	Jan 27 12:15 – Jan 27 23:45	0	1.9 ± 0.5	11			0.10 ± 0.03	24
2	2004	Dec 11 0:15 – Dec 11 11:45	100	6.1 ± 0.8	7	1.3 ± 0.18	7	0.00 ± 0.00	19
3	2005	Jan 9 6:15 – Jan 9 17:45	57	4.2 ± 0.4	21			0.02 ± 0.01	24
4	2005	Jan 10 0:15 – Jan 10 5:45	33	3.4 ± 0.3	12			0.07 ± 0.01	12
5	2005	Jan 10 6:15 – Jan 13 17:45	96	1.4 ± 0.1	132	0.39 ± 0.03	49	0.02 ± 0.00	168

NA, Not available.

[a]Percentage of the period with RH above 96%.

[b]Average of all events. Average with fewer than 2 events are not shown. Average enhancement ratios do not include events 6 and 7 in spring and event 4 in summer due to transport in the marine BL, and event 3 in spring due to influence of stratospheric transport.

[c]Event with stratospheric transport influence according to FLEXPART Strat-O_3 tracer and transport at high altitudes indicated by FLEXPART retroplumes.

[d]Events in the marine BL as indicated by FLEXPART retroplumes. (See text for explanation.)

likely to contribute to this variation: different NO_x to CO emission ratios over the continent, which vary as a function of time and type of fuel [*Neuman et al.*, 2006], and varying degree of washout processing during transport. On a seasonal basis, the average $\Delta NO_y/\Delta CO$ was larger in summer (10.0 ± 4.0 pptv ppbv^{-1}; Figure 2.9d) than in winter (3.4 ± 1.7 pptv ppbv^{-1}; Figure 2.9j), suggesting a more efficient export of NO_y from eastern North America during summertime.

To quantify the fraction of NO_x originally emitted that was exported as NO_y in North America outflow (f), we compared the $\Delta NO_y/\Delta CO$ observed at the Pico Mountain station to that from U.S. emissions, using the following approach [*Parrish et al.*, 2004; *Hudman et al.*, 2007]:

$$f = \frac{\Delta NO_y}{\Delta CO} \times R_{emiss} \times \alpha,$$

where R_{emiss} is the CO to NO_x emission molar ratio and α is a factor accounting for chemical sources and sinks of CO. We included a correction factor of 0.88 to account for the increase in the CO export from the U.S. due to oxidation of NMHCs to CO (1.2) [*Chin et al.*, 1994] and to incorporate a 27% decline in the CO mixing ratios during the 5 to 6 day transport time from the U.S. BL to the Pico Mountain station (0.73) [*Honrath et al.*, 2004]. We applied this correction factor only to the summertime observations since biogenic hydrocarbon emissions are reduced during the non-summer seasons and oxidation of CO is not significant ($\sim$5–10% in 5 to 6 day transport, based on the CO+OH rate constant at 800 hPa [*Sander et al.*, 2003] and the estimated zonal average OH at 35°N and 800 hPa [*Spivakovsky et al.*, 2000]) in these seasons. For the U.S. CO to NO_x emission ratio, we used GEOS-Chem input of 5.9 mol mol^{-1} for eastern U.S. [*Hudman et al.*, 2007]. This ratio is similar to that obtained by *Parrish et al.* [2004] (5.1 mol mol^{-1}) using the EPA emission inventory adjusted by a decline in vehicle CO emissions estimated based on field measurements.

We applied this approach to the $\Delta NO_y/\Delta CO$ observed in the North America plumes that traveled above the marine BL. We considered events in the marine BL

those in which FLEXPART retroplumes spent more than one day at altitudes below 2 km (*e.g.*, Figure 2.8e) and excluded them from the analysis, *i.e.*, event 6 and 7 in spring and event 4 in summer (Table 2.6). The resulting average NO_y efficiencies for export and transport are: $3 \pm 2\%$ (mean$\pm$2-standard error of the mean) in spring, $5 \pm 2\%$ in summer, $3 \pm 1\%$ in fall and $2 \pm 1\%$ in winter. The summer season shows an average NO_y transport efficiency about 2 times greater than the other seasons. Although we adjusted the summertime observations by a correction factor, the difference between the summer and non-summer NO_y efficiencies for export and transport is not due to this applied correction as the correction factor changed the summertime values only by about 12%. Table 2.5 on page 46 compares these estimates to previous export efficiencies obtained in U.S. plumes during the NARE and ICARTT campaigns [*e.g. Parrish et al.*, 2004; *Li et al.*, 2004; *Hudman et al.*, 2007]. The Pico Mountain average export efficiencies from spring to fall (3–5%) are similar to the lower limit of the estimates over the western North Atlantic Ocean lower FT ($11 \pm 6\%$ in spring, $18 \pm 11\%$ in summer and $9 \pm 5\%$ in fall [*Parrish et al.*, 2004; *Hudman et al.*, 2007]). Consistent with these previous studies, our observations indicate that the majority (95–97%) of NO_x emitted over eastern U.S. is removed within or during export from the U.S. BL during lofting mechanisms. However, this comparison suggests that about 30% of the nitrogen oxides emissions that escape the eastern North America BL remain after transport to the lower FT over the Azores region.

Consistent with the expectation that export of NO_y may eventually lead to NO_x released from decomposition of PAN and potentially photolysis of HNO_3, Figure 2.9 (middle column) and Table 2.6 show that NO_x was also enhanced in the anthropogenic plumes relative to background during all seasons.

Although NO_x observations in North America outflow were limited, enhancements of NO_x in the North American plumes indicate that North American emissions are a significant source of NO_x to the central North Atlantic lower FT all year round. Larger $\Delta NO_x/\Delta CO$ ratios during fall suggest that the largest supply of NO_x in the central

North Atlantic lower FT occurs during this season. This effect is likely the result of the combination of rapid thermal decomposition of PAN to NO_x and slower conversion of NO_x to HNO_3 in the plumes during this season (section 2.2.3.2). In addition, direct export of NO_x from North America may have also contributed to the NO_x enhancements since some of the fall events were associated with rapid transport from the U.S. ($\lesssim$2 days). Large enhancements of NO_y in spring (4.3±3.1 pptv NO_y/ppbv CO; Figure 2.9a), mostly in the form of PAN (Figure 2.5), suggest a continuing export of nitrogen oxides, which may eventually release NO_x further downwind.

The average NO_x levels observed during airflow from North America were 31 ± 5 pptv (mean±2-standard error of the mean; spring), 31±3 pptv (summer), 41±3 pptv (fall) and 36±3 pptv (winter). These mean values correspond to the 75th percentile of the full distribution each season, with the exception of the summer, which corresponds to the 55th percentile. Lower corresponding percentile during the summer results from the impact of boreal wildfires during this season (section 2.3.2 and Chapter 3). If we exclude the observations impacted by boreal wildfires (section 2.3.2), the NO_x mean in North American outflow corresponds to the 70th percentile of all summertime non-fire impacted observations. Mean levels of daytime NO in these plumes ranged from 8 to 11 pptv, occasionally reaching 20 pptv. Although these levels may be insufficient for a net O_3 production [*Klonecki and Levy*, 1997], they may influence the O_3 chemical tendency through changes in the O_3 production rate [*Mauzerall et al.*, 1996].

2.3.1.4 Implications for the O_3 Production and Budget

We examined the relationship between NO_y and O_3 on a seasonal basis in Figure 2.9 (right column) to investigate the eventual source of O_3 from exported nitrogen oxides. Seasonal average enhancement ratios are presented in Figure 2.9 and Table 2.6 summarizes the $\Delta O_3/\Delta NO_y$ ratios for each anthropogenic event.

The seasonal $\Delta O_3/\Delta NO_y$ averages indicate an approximately 90-fold, 130-fold and 40-fold enrichment of O_3 relative to NO_y (mol mol^{-1}) during spring and fall,

summer, and winter, respectively. The $\Delta O_3/\Delta NO_y$ of 130 ppbv ppbv^{-1} is an order of magnitude higher than what was observed in several rural sites in North America during the summer seasons (8.5–10 ppbv ppbv^{-1} [*Trainer et al.*, 1993; *Olszyna et al.*, 1994]), and is also higher than what was encountered in the FT over North America (∼30–120 ppbv ppbv^{-1} [*Ridley et al.*, 1994]). The larger summer $\Delta O_3/\Delta NO_y$ observed at the Pico Mountain station is thus consistent with the high efficiency with which O_3 is formed in the FT combined with the higher removal rate of NO_y (via HNO_3) compared to that of O_3 during transit to the measurement site. This result contrasts with prior studies over the North Atlantic region, which concluded that the marine BL and lower FT over the North Atlantic are generally on a state of net O_3 destruction all year round [*e.g.*, *Helmig et al.*, submitted;*Parrish et al.*, 1998, *Reeves et al*, 2002]. For example, *Parrish et al.* [1998] indicated that, in the North Atlantic marine BL during the winter, O_3 is mostly removed by reaction with NO_2 and NO and deposition, with a $\Delta O_3/\Delta NO_y$ ratio of -1.5 to -1 mol mol^{-1}.

To evaluate the ultimate impact of the transport of nitrogen oxides on the O_3 budget over the North Atlantic region, we estimated the O_3 production upwind of the Pico Mountain station resulting from the long-range transport of nitrogen oxides during the summer season. Estimates of the O_3 production can be calculated using the flux of transported NO_y and the flux of transported PAN+NO_x, respectively, based on the measured $\Delta NO_y/\Delta CO$ and estimated NO_y speciation (*i.e.*, PAN+NO_x is ∼30% of NO_y; section 2.2.3.1). The use of NO_y enhancement ratios gives approximately an upper estimate in the calculation of O_3 production as it includes HNO_3, which generally does not lead to NO_x generation, while the use of PAN+NO_x gives a lower estimate, as it neglects the O_3 produced upwind of Pico. Both methods are however biased low as the use of our observed $\Delta NO_y/\Delta CO$ ignores the oxidation of NO_x to HNO_3, followed by removal of HNO_3 upwind from the Pico Mountain station. We derived the flux of transported NO_y by multiplying the observed summer average $\Delta NO_y/\Delta CO$ (0.01 ppbv ppbv^{-1} Table 3.3) by the CO emissions for eastern U.S.

in 2005. The daily amount of CO emitted in eastern U.S. (estimated as 2/3 of the total national emissions and adjusted for the 8.8% per year decrease of the on-road CO:NO_x emission ratio [*Parrish et al.*, 2004]) corresponds to 4.7 Gmol day^{-1}. Thus, the resulting long-range-transported NO_y is 0.047 Gmol day^{-1} and, similarly, transported PAN+NO_x is 0.014 Gmol day^{-1}. *Liang et al.* [1998] estimated that 39 and 64 molecules of O_3 are produced for each NO_x or PAN molecule advected downwind from North America at altitudes below and above 2.6 km, respectively. Thus, the resulting O_3 production can be derived by multiplying these O_3 production efficiencies by the amount of PAN+NO_x and NO_y transported to the central North Atlantic region. The result is approximately 1.8–3 Gmol of O_3 produced upwind of the Pico Mountain station per day. The formation of O_3 resulting from transport of nitrogen oxides is quite important. For comparison, the amount of O_3 produced in eastern U.S. BL and directly exported to the North Atlantic is 1.9–2.4 Gmol day^{-1}. (This estimate is based on the $\Delta O_3/\Delta CO$ of 0.4–0.5 ppbv ppbv^{-1} observed downwind from North America [*Hudman et al.*, North American influence on tropospheric ozone and the effects of recent emission reductions: constraints from ICARTT aircraft observations and the daily eastern U.S. emissions, manuscript in preparation] and the daily eastern U.S. CO emissions). It is important to note that, in these calculations, we did not account for chemical loss of O_3 and for chemical sinks and sources of CO, and assume that all PAN decomposes to NO_x.

The occurrence of O_3 formation in the North American plumes observed at the Pico Mountain station and the significant amount of O_3 produced from the long-range transport of nitrogen oxides imply an impact on the regional O_3 budget, even during the wintertime.

2.3.2 Influence of Boreal Wildfires

Transport of North American boreal wildfire emissions significantly impacted the nitrogen oxides measured at the Pico Mountain station during summer 2004 [*Val Martin et al.*, 2006]. On an event-by-event basis, the average levels of nitrogen oxides in boreal wildfire plumes were above levels observed during flow from boreal regions without fire emissions and well above typical summertime background over the central North Atlantic lower FT [*Val Martin et al.*, 2006]. We expand here this previous work and investigate the degree to which boreal wildfire emissions modulate the nitrogen oxides background in the central North Atlantic lower FT. For this purpose, we analyzed nitrogen oxides observations made from June 1 to September 15 in 2004 and 2005. Similar to summer 2004, summer 2005 boreal wildfire emissions from Canada and Alaska frequently impacted the Pico Mountain station [*Lapina, et al.*, (in preparation)]. In summer 2002 and 2003, wildfires emissions from Quebec and Siberia, respectively, impacted the measurement site [*Honrath et al.*, 2004]. However, nitrogen oxides measurements were limited during those summers (Figure 2.1). The time frame of June 1–September 15 was selected since it covers the typical active burning season over northern North America [*Pfister et al.*, 2005] and allows for the 1–2 weeks transport time to the measurement site at the end of the season.

We subdivided the data into two categories: one category representing observations significantly influenced by boreal wildfires ("fire") and a second category representing observations with minimal or no fire impact ("non-fire"). Fire and non-fire observations were selected based on the intensity of North American boreal wildfires impact simulated by the FLEXPART Fire-CO. The 25th and 75th percentiles of all FLEXPART Fire-CO values for each summer were used for the "non-fire" and "fire" cutoffs, respectively. These lower and upper cutoff values were selected to allow both categories to contain a similar number of data points. The cutoff values were different for each year, *i.e.* 1.4 ppbv and 16.4 ppbv for 2004 and 0.9 ppbv and 5.6 ppbv for

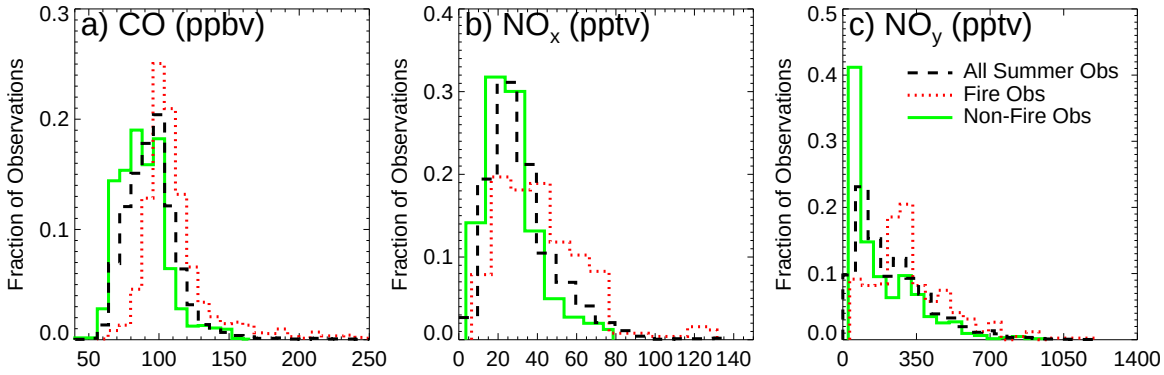

Figure 2.10 Histograms of a) CO, b) NO_x and c) NO_y of all summertime observations (black dashed lines), all fire observations (red dotted lines) and all non-fire observations (green solid lines), in 2004 and 2005.

2005, reflecting the different intensity of the boreal wildfires in 2004 and 2005. Figure 2.10 shows the distribution of NO_x and NO_y for the fire and non-fire periods. We also show the distribution for all summer observations. (The distribution of CO is also shown for comparison.) Table 2.7 summarizes the statistical parameters of each distribution for each summer.

Boreal wildfire emissions significantly affected the summertime distribution of nitrogen oxides at the Pico Mountain station. NO_y median values in the fire subset were 175 pptv and 115 pptv larger than those in the non-fire subset in 2004 and 2005, respectively. Similarly, the difference in the NO_x median values were 30 pptv in 2004 and 9 pptv in 2005. As expected, median values for CO were also larger in the fire subset relative to the non-fire subset, with a difference of 40 ppbv in 2004 and 10 ppbv in 2005. A non-parametric Wilcoxon Sum-rank and a student *t*-test indicated that all distributions and the means of distributions were significantly different at a 0.01 level of significance. Larger differences in the median values were observed in 2004 relative to 2005. This is due to the higher fire activity over the North American boreal region in 2004 than in 2005: total CO emissions estimated using the Boreal Wildland-Fire Emissions Model were 37 Tg in summer 2004, whereas they were 24 Tg in 2005 [*Lapina et al.,* (in preparation)].

To verify that the difference in the medians was the result of boreal wildfire emis-

Table 2.7 Statistics of summertime NO_y, NO_x and CO distribution. Reported are mean, median and number (N) of 30-min average observations, in pptv for NO_x and NO_y and ppbv for CO.

	NO_y, pptv				NO_x, pptv				CO, ppbv			
Year	Mean	Median	N	Δmedian[a]	Mean	Median	N	Δmedian[a]	Mean	Median	N	Δmedian[a]
2004				175				30				40
All	229	169	1529		31	27	888		94	91	3943	
Fire	328	264	150		53	53	174		124	113	548	
Non-Fire	131	89	271		27	23	202		77	73	516	
2005				117				9				11
All	243	234	1006		31	28	645		97	97	3908	
Fire	294	288	238		36	34	174		105	103	863	
Non-Fire	228	171	358		26	25	202		94	92	1267	

[a]Δmedian: difference between the medians in the fire and the non-fire subsets. (See text for description.)

sions, we inspected the periods selected in each category. While the non-fire subset contained observations made in a mixture of both non-boreal and boreal air without wildfire emissions, the fire subset included mainly periods when boreal outflow reached the Pico Mountain station during the active burning season [*Val Martin et al.*, 2006; *Lapina et al.*, in preparation]. Thus, we conclude that the difference in both subsets may be attributed to the presence of boreal wildfire emissions.

The impact of boreal wildfire emissions on the nitrogen oxides levels may have important implications for the global tropospheric O_3 budget [*e.g. Val Martin et al.*, 2006; *Pfister et al.*, 2006; *Real et al.*, 2007]. *Lapina et al.* [2006] showed evidence of the significant impact of boreal wildfire emissions on the O_3 background over the North Atlantic region. Consistent with *Lapina et al.* [2006], the difference between the median values in the non-fire and fire subsets for O_3 were 26 ppbv in 2004 and 17 ppbv in 2005 (not shown).

Overall, these analyses indicate that boreal wildfires were responsible for the shift in the nitrogen oxides distributions toward higher mixing ratios. Given the long distance from the boreal region to the Pico Mountain station, this implies very large-scale impacts on the background NO_x and NO_y levels in the midlatitude lower FT.

2.4 Summary and Conclusions

Measurements of nitrogen oxides made at the Pico Mountain station from July 2002 to August 2005 were used to estimate the magnitude and seasonal variability of nitrogen oxides over the central North Atlantic lower FT and to determine the processes that contribute to this variability.

These measurements reveal the presence of a well-defined seasonal cycle of nitrogen oxides in the background central North Atlantic lower FT, with larger mixing ratios during the summertime. Median NO_x and NO_y of 17–31 pptv and 125–338 pptv observed at the Pico Mountain station were lower than those previously observed

over the western North Atlantic region and more similar to those observed at the remote marine North Pacific MLO station. The observed NO_x and NO_y levels were consistent with long-range transport of emissions with significant removal upwind of the measurement site.

Observations of NO_x and NO_y and estimates of PAN and HNO_3 indicate that reactive nitrogen over the central North Atlantic lower FT largely exists in the form of HNO_3 and PAN, independent of the season. A shift from dominance of PAN in winter–spring to dominance of HNO_3 in summer–fall that occurs over this region is attributed to strong decomposition of PAN to NO_x and efficient formation of HNO_3 from rapid reaction of NO_x with OH during the summer and fall seasons.

Nitric acid contributes 53–71% of NO_y during the summer. Given the significant removal of NO_y during transport, this suggests that the oxidation of NO_x resulting from decomposition of PAN in the airmasses during subsidence, or advection over the ocean with minimal removal, results in a significant source of HNO_3 to the central North Atlantic lower FT. The decomposition of PAN in the airmasses has important implications for O_3 formation, since released NO_x is available to form O_3 before oxidation to HNO_3 during transport to the central North Atlantic lower FT.

North American anthropogenic emissions impacted the measurement site all year round. Enhancements of NO_y in North America outflow show that, consistent with previous observations, the majority (95–97%) of NO_x emitted over the U.S. is removed before or during export out of the U.S. BL. However, these fractions imply that about 30% of the emissions that escapes the U.S. BL is efficiently transported as NO_y to the lower FT over the central North Atlantic region. Enhancements of NO_x in these plumes indicate that decomposition of PAN to NO_x and potentially photolysis of HNO_3 occurring in the airmasses during subsidence and/or advection westward to the Azores constitute a significant source of NO_x to the central North Atlantic lower FT, in particular during the fall. Observed $\Delta O_3/\Delta NO_y$ and large NO_y levels remaining in the North American plumes suggest a potential for O_3 formation well downwind

from North America. For example, during the summer, O_3 formation downwind from North America resulting from the transport of nitrogen oxides may be as important as the direct export of O_3 produced within the U.S. BL.

Boreal wildfire emissions were responsible for significant shifts in the nitrogen oxides distributions toward higher levels, when medians NO_x and NO_y were respectively 117–175 pptv and 9–30 pptv, greater with the presence of boreal wildfire emissions. Since our observations were made very far downwind from the boreal region, we conclude that aged boreal fire emissions significantly altered the background NO_x and NO_y levels over a large region of the Northern Hemisphere. During the summer, boreal wildfire emissions appear to cover the impact caused by North American emissions. This highlights the need to understand the impact of boreal wildfires on tropospheric NO_x levels and the resulting implications for O_3, in order to evaluate the influence of anthropogenic emissions on the NO_x and O_3 budgets during the summer season.

A comparison of nitrogen oxides observations with GEOS-Chem simulations indicates that GEOS-Chem reproduces the seasonal variation of nitrogen oxides over the central North Atlantic lower FT. However, it does not capture the magnitude of the cycles. Important differences were found for PAN, a critical species in the global formation of O_3 via dispersal and release of NO_x. Over recent decades, there have been significant changes in global fossil-fuel NO_x emission [*Richter et al.*, 2005], and even larger emissions are expected in the future. In addition, as a result of climate change, more frequent and severe boreal wildfires are also expected, which will result in an increase in the boreal wildfire emissions [*Stocks et al.*, 1998; *Flannigan et al.*, 2000]. Therefore, accurate simulation of the fate and transport of nitrogen oxides is necessary to understand how these emissions have impacted, and will impact, tropospheric NO_x at hemispheric scales and the resulting implications for tropospheric O_3.

Chapter 3

Impacts of North American Boreal Wildfire Emissions on the North Atlantic Lower Free Troposphere[†]

Boreal wildfires are large sources of reactive trace gases and aerosols in the atmosphere [*e.g.*, *Goode et al.*, 2000; *Andreae and Merlet*, 2001]. The large amounts of trace gases and aerosols emitted by boreal forest fires are subject to long-range transport, with the potential to affect air quality from regional to global scales. Boreal wildfire plumes have been detected over continental [*Wotawa and Trainer*, 2000], intercontinental [*Forster et al.*, 2001; *Honrath et al.*, 2004], and even hemispheric [*Damoah et al.*, 2004] distances. It is recognized that boreal wildfires play an important role in the magnitude and interannual variability of tropospheric background CO in the Northern Hemisphere [*e.g.*, *Novelli et al.*, 2003; *Edwards et al.*, 2004; *Kasischke et al.*, 2005]. Recent studies have also shown increased mean background summertime O_3

[†]This chapter is based on material previously published as Val Martín M., R. Honrath, R.C. Owen, G. Pfister, P. Fialho and F. Barata (2006), Significant enhancements of nitrogen oxides, ozone and aerosol black carbon in the North Atlantic lower free troposphere resulting from North American boreal wildfires, *J. Geosphys. Res., 111*, D23S60, doi:10.1029/2006JD007090.

over northwestern North America [*Jaffe et al.*, 2004], the central North Atlantic [*Lapina et al.*, 2006] and Europe [*Simmonds et al.*, 2005] associated with fire emissions transport. This indicates that boreal wildfires may also impact background O_3.

Ozone plays an important role in the chemistry of the atmosphere since it is estimated to be the third most important greenhouse gas [*Alley et al.*, 2007], and is the primary source of tropospheric hydroxyl radical. In addition, O_3 has negative impacts on ecosystems and human health. Typically, tropospheric O_3 production in the Northern Hemisphere is driven by anthropogenic emissions. However, boreal wildfires are an important source of CO, NO_x and NMHCs, resulting in the potential for significant formation of O_3 during the boreal fire season. Large-scale impacts of boreal fire emissions on tropospheric O_3 can occur as a result of dispersion of O_3 formed in boreal wildfire plumes. Alternatively, impacts on CO, NO_x and NMHCs in the remote atmosphere could also lead to impacts on the O_3 budget over a large region.

The magnitude of the resulting impact of boreal wildfire emissions on tropospheric ozone is not yet well quantified. Prior observations in boreal wildfire plumes indicate O_3 enhancements that range from very low in fresh plumes [*e.g.*, *Goode et al.*, 2000; *Tanimoto et al.*, 2000] to low in moderately-aged plumes [*e.g.*, *Wofsy et al.*, 1992; *Mauzerall et al.*, 1996] to high in well-aged plumes [*e.g.*, *Honrath et al.*, 2004; *Bertschi and Jaffe*, 2005]. Boreal wildfire emissions have a large degree of variability, and are a function of fuel type (*e.g.*, peat fires versus crown fires) and/or burning conditions (*e.g.*, smoldering versus flaming) [*Goode et al.*, 2000; *Kasischke et al.*, 2005]. This causes uncertainty and variability in the emissions of NO_x, a critical compound that controls O_3 production rate.

Measurements of a number of reactive nitrogen species over the North American boreal region were made during the ABLE3A and ABLE3B campaigns. These studies showed that the reactive nitrogen distribution over this region was significantly affected by boreal wildfire emissions [*e.g.*, *Sandholm et al.*, 1992; *Singh et al.*, 1994].

However, the photochemical O_3 production resulting from boreal wildfire NO_x emissions was concluded to be a negligible source of O_3 over this region [*Jacob et al.*, 1992; *Mauzerall et al.*, 1996], due to a combination of low NO_x emissions and low estimated total fire magnitude. However, these studies suggested that dispersion of PAN produced in the fire plumes may provide a major source of NO_x, particularly in warmer layers of the troposphere at low altitude [*Jacob et al.*, 1992; *Singh et al.*, 1994], and hence could contribute to O_3 production far downwind from the fires. Consistent with this expectation, *DeBell et al.* [2004] reported significant enhancements of NO_y and O_3 at several surface sites over the eastern U.S. resulting from a Quebec boreal wildfire plume in July 2002. However, most of these measurements were made in the boundary layer, and loss of NO_y and O_3 by surface deposition may have obscured the true magnitude of the fire plume aloft.

In addition to trace gases, boreal wildfires emit large amounts of aerosol black carbon (BC), on average about 10% of the annual anthropogenic BC emissions in the Northern Hemisphere [*Bond et al.*, 2004]. Recently, it has been shown that BC emissions from boreal wildfires and anthropogenic sources can be efficiently transported to remote regions, such as the Arctic [*Stohl et al.*, 2006] and the northwestern Pacific region [*Park et al.*, 2005]. BC emissions are a significant factor in climate change due to their absorption of light in the atmosphere [*Hansen et al.*, 2000; *Bond and Sun*, 2005]. Therefore, the export of BC far downwind from the source emissions may contribute to the radiative forcing of the atmosphere, and thereby affect climate.

During summer 2004, extensive wildfires burned in Alaska—the largest area on record— and western Canada, releasing large amounts of trace gases and aerosols into the atmosphere. For instance, CO emitted from mid-June to August was on the order of the anthropogenic CO emissions for the entire continental U.S. during that same time period [*Pfister et al.*, 2005; *Turquety et al.*, 2007]. Intense plumes of these boreal wildfires were observed over large regions of North America and Europe by research aircraft [*Flocke et al.*, 2005; *Real et al.*, 2007; *de Gouw et al.*, 2006] and at

several sites over the Arctic [*Stohl et al.*, 2006] during the International Consortium for Atmospheric Research on Transport and Transformation (ICARTT) study [*Fehsenfeld et al.*, 2006].

In this chapter, we present measurements of the composition of highly aged plumes from these fires sampled in the North Atlantic lower free troposphere (FT), using measurements at the Pico Mountain station. Measurements of CO, BC, NO_y, NO_x and O_3 made from June to early September, 2004, are analyzed to assess the impact of boreal wildfires on levels of aerosol BC and nitrogen oxides (NO_x and NO_y) over the central North Atlantic lower FT, to characterize the associated enhancements of O_3 in highly aged plumes, and to determine the resulting implications of the North American boreal wildfires for the regional and hemispheric NO_x and O_3 budgets.

3.1 Experimental Methods

3.1.1 Pico Mountain Station

Observations of CO, BC, NO_x, NO_y and O_3 were made at the Pico Mountain observatory from June to September, 2004. The Pico Mountain station is situated on the summit caldera of the inactive volcano Pico (altitude 2.2 km) in the Azores Islands, Portugal (38°N, 28°W). The Azores are frequently impacted by airflow from high latitudes, which can transport emissions from boreal wildfires in Canada, Alaska and Siberia, and bring them to the Azores 6 to 15 days later. The station is located in the lower FT since marine boundary layer heights in this region are typically less than 1 km during the summer. Upslope flow can transport air from lower altitudes to the mountaintop, including occasionally from the boundary layer. However, a detailed assessment of the impact of upslope flow to the station found that upslope flow affects the Pico Mountain station much less than it does many other mountain observatories, and on many summer days tropospheric air is sampled throughout the day [*Kleissl*

et al., 2007]. From June to September 2004, less than 25% of the time presented the meteorological conditions necessary for an air mass from below the mountain to reach the summit, *i.e.*, weak synoptic winds and strong insolation for buoyant driven lifting or strong synoptic winds for mechanically driven lifting. Periods potentially affected by upslope flow were identified as described by *Kleissl et al.* [2007] and removed from the analysis. None of the periods discussed in detail below contain data affected by upslope flow. Further details on the Pico Mountain station and the occurrence of upslope flow to the station are presented elsewhere [*Honrath et al.*, 2004; *Kleissl et al.*, 2007].

3.1.2 Measurements

3.1.2.1 Nitrogen oxides

NO, NO_2, and NO_y were determined by an automated $NO_{x,y}$ system developed at Michigan Technological University. This $NO_{x,y}$ system is an improved version of the instrument previously described by *Peterson and Honrath* [1999]. NO, NO_2, and NO_y were determined using established techniques: NO detection by O_3 chemiluminescence [*Ridley and Grahek*, 1990], NO_2 by conversion to NO via ultraviolet photodissociation [*Kley and McFarland*, 1980; *Parrish et al.*, 1990], and NO_y by Au-catalyzed reduction to NO in the presence of CO [*Bollinger et al.*, 1983; *Fahey et al.*, 1985]. The $NO_{x,y}$ system was operated on an automated cycle, which included twice-daily NIST-traceable calibration with NO and NO_2, regular measurements of NO and NO_2 (twice per week) and NO_y (once per week) artifacts in zero air, and determination of the NO_y conversion efficiency in ambient air of two NO_y compounds (i-propyl nitrate and HNO_3) and one non-NO_y compound (CH_3CN). Measurements were recorded as 30-s averages (NO and NO_2) and 20-s averages (NO_y) every 10 min, and were further averaged to obtain the 30-min averages used in this work. Ambient NO_2 was determined by subtracting the signal due to ambient NO from the NO_2 instrument signal,

and further multiplying this term by the NO_2 sensitivity [*Gao et al.*, 1994]. NO_x was calculated as the sum of the 30-s average measurements of NO and NO_2 during a single measurement cycle.

Total uncertainty of the NO, NO_2 and NO_y measurements at low mixing ratios resulted from measurement precision and uncertainty in the instrument artifact correction, while measurement accuracy was the primary source of uncertainty at higher levels. The precision of individual measurements was mainly attributable to counting noise, which resulted from photon counting statistics. Excluding periods with high ambient variability, the precision (2-σ) of the 30-min averages was less than 6 pptv (median 5 pptv) for NO, less than 13 pptv (median 10 pptv) for NO_2, less than 14 pptv (median 10 pptv) for NO_x, and less than 9 pptv (median 6 pptv) for NO_y. Potential bias resulting from uncertainty in the artifact correction was estimated to be less than 2 pptv for NO, 4 pptv for NO_2, 4 pptv for NO_x and 2 pptv for NO_y. Measurement accuracy was estimated to be 4% based on total uncertainty of the sample and calibration mass flow controllers and the NO standard calibration gas mixing ratio.

Accuracy of the NO_y measurements also depends on the effective conversion of NO_y compounds and the lack of significant conversion of non-NO_y compounds [*Fahey et al.*, 1985; *Kliner et al.*, 1997; *Kondo et al.*, 1997], in addition to the accurate determination of the resulting NO. Based on standard addition tests and regular calibrations, the observed NO_y included 92–100% of the actual NO_2 level (typically 97–100%), with similar values expected for PAN [*Fahey et al.*, 1985], 70–100% of the actual HNO_3 level, and 80–100% of the actual i-propyl nitrate. Measurements of NO_y presented in this work were corrected for non-unity NO_y conversion by using the NO_2 conversion efficiencies measured at the system. A maximum correction of 8% was applied, and mainly affected the NO_y observations made from mid-July to mid-August when a degraded NO_y converter lowered the NO_2 conversion efficiency to 92–95%. A manual wet cleaning procedure was implemented in mid-August, and

the NO_2 conversion efficiency was restored back to the expected value of 97–100%. In addition to the incomplete conversion of the NO_y species, this type of NO_y converter may overestimate true NO_y levels [*Fahey et al.*, 1985; *Kliner et al.*, 1997]. However, that was not a problem during this study. Interference from reduced nitrogen species (such as NH_4, HCN, and CH_3CN) was found to be always less than 0.3% during regular (twice-daily) testing using standard addition of CH_3CN, a potential NO_y interferant present in biomass-burning plumes [*de Gouw et al.*, 2003]. This level of CH_3CN conversion in our system did not significantly contribute to the observations of NO_y gathered during boreal wildfire plumes: using the maximum enhancement of CH_3CN relative to CO (3.52 pptv CH_3CN/ppbv CO) in the boreal fire plumes intercepted by the NOAA WP-3 research aircraft during summer 2004 [*de Gouw et al.*, 2006], we estimate that the maximum impact of CH_3CN on the NO_y/CO enhancement ratios presented below is 0.01 pptv/ppbv CO, less than 0.2% of the lowest NO_y/CO enhancement ratio reported below.

Observations of nitrogen oxides made during periods with near-calm winds and high ambient variability were also excluded from the analysis. This was done for two reasons. First, calm winds may lead to the removal of HNO_3 by deposition on the mountain surface. Therefore, observations of NO_y during these periods may not be representative of the actual upwind NO_y levels. Second, unexpected spikes in ambient NO_x and NO_y were sometimes observed during low-wind periods (usually wind speeds less than 3 m/s), suggesting that a local source may have perturbed the measurements. Based on analysis of air sampled directly at several volcano vents (with NO_x reaching 1 to 8 ppbv), we deduce that volcanic emanations were the cause of the observed spikes. Therefore, to ensure that all the NO_x and NO_y observations were representative of free tropospheric air, we excluded (1) measurements made during low to calm winds (wind speed < 1 m/s), to avoid including NO_y observations with potential HNO_3 removed on the mountain surface, and (2) measurements with high ambient variability, to avoid including nitrogen oxides resulting from volcanic

emissions. For this purpose, periods with high ambient variability were defined as those when the 30-min NO_x standard error was above 10 pptv or the 30-min NO_y standard error exceeded 10 pptv+0.25([NO_y]-90), where the second term was included to allow increased variability during periods of high NO_y. The wind speed criterion removed 7% of the measurements during the study period, and the ambient variability screen removed an additional 23%.

3.1.2.2 CO and O_3

CO was measured by a non-dispersive infrared (NDIR) photometer (Thermo Environmental, Inc. (TEI), Model 48C-TL), modified as described by *Parrish et al.* [1994] and calibrated daily with a CO calibration gas referenced to the NOAA Global Monitoring Division standard. The instrument alternated between two minutes of zero measurement and two minutes of ambient measurement; the first minute of each mode was discarded to ensure equilibration. O_3 was measured with a commercial ultraviolet absorption instrument (Thermo Environmental, Inc., Model 49C). The stability of the zero reading and the absence of O_3 loss in the inlet and line were confirmed on a daily basis. CO and O_3 data were recorded as one minute averages, and were further averaged to obtain the 30 minute averages used in this work. CO measurement uncertainty (2-σ) was estimated to be 7% based on total uncertainty of the sample and calibration mass flow controllers and the CO calibration standard mixing ratio. The 30-min averages used in this work averaged 7 to 8 one-min average points, and had a precision (2-σ) of 9 ppbv from June to mid-July, and 4 ppbv after mid-July. O_3 measurement precision (2-σ) was usually less than 1 ppbv, based on the standard deviation of the 30 one-min measurements included in each 30-min average. More details on the CO and O_3 instruments are presented by *Owen et al.* [2006] and *Honrath et al.* [2004].

3.1.2.3 Aerosol Black Carbon

Measurements of aerosol light absorption at seven wavelengths (0.37, 0.47, 0.52, 0.59, 0.66, 0.88 and 0.95 μm) were conducted using an aethalometer (Magee Scientific, Model AE31). Briefly, this instrument determines the attenuation of light at these wavelengths transmitted through particles accumulated on a quartz filter, relative to a clean spot on the same filter. The change in attenuation as a function of time is used to determined the light absorption coefficient ($\sigma_{aerosol}$). The $\sigma_{aerosol}$ as a function of wavelength is analyzed to identify the presence of non-BC absorbing compounds [*Fialho et al.*, 2005] (none were significant during the period discussed here) and converted to BC using the calibration constant recommended by the manufacturer (14.6 μm m^2 g^{-1}). The detection limit of the aethalometer depends mainly on the stability of the optics, filter spot area errors, flow rate uncertainties and time error, and was estimated to be 25 ng m^{-3} (2-σ) for the integration period of one hour. More details on the aethalometer used in this study and the approach used to determine the BC concentrations are presented elsewhere [*Fialho et al.*, 2005].

3.1.3 Model Simulations and Transport Analysis

To identify periods apparently impacted by upwind boreal wildfire emissions, we examined CO mixing ratios simulated at the Pico Mountain station by the Model for OZone and Related Chemical Tracers (MOZART) global chemical transport model [*Horowitz et al.*, 2003]. MOZART simulations were driven by 6-hourly meteorological fields from the National Centers for Environmental Predictions (NCEP) National Center for Atmospheric Research re-analysis. The spatial resolution of the model is $\sim$2.8° x 2.8° with 28 levels between the surface to 2 hPa. The chemical time step of the model is 20 minutes. Emissions of CO from the 2004 North American boreal wildfires were optimized to match MOPITT CO observations using an inverse modelling technique [*Pfister et al.*, 2005]. Boreal wildfire CO emissions were injected

uniformly from 0 to 9 km. MOZART simulations used in this work are mixing ratios averaged over 2-hr intervals and interpolated to the pressure and location of the Pico Mountain observatory [*Pfister et al.*, 2006]. To assess the magnitude of fire impact at the Pico Mountain station, we used the MOZART-simulated ratio of CO fire tracer (CO emitted from North American boreal wildfires) to total CO mixing ratio (*i.e.*, $[CO]_{fire}/[CO]_{total}$) interpolated to the measurement times (hereinafter termed the "MOZART fire-CO fraction").

A second MOZART tracer was used for U.S. anthropogenic CO emissions to evaluate the contribution of anthropogenic emissions during the fire-impacted observations. For this purpose, we used the MOZART-simulated ratio of U.S. anthropogenic CO tracer to total CO mixing ratio at the Pico Mountain station (*i.e.*, $[CO]_{anthro}/[CO]_{total}$) interpolated to the 30-min average field observations (hereinafter termed the "MOZART anthro-CO fraction").

To complement field observations and MOZART simulations, we used backward trajectories analysis. We calculated backward trajectories with the Hybrid Single-Particle Lagrangian Integrated Trajectories (HYSPLIT-4) model [*Draxler and Rolph*, 2003]. This model uses 6-hourly data from the NCEP global FNL meteorological dataset. Ten-day backward trajectories were calculated every hour. At each hourly arrival time, six backward trajectories ending at six different locations near the Pico Mountain station were calculated: one centered at the station, four separated from the first by 1° latitude and longitude, and one below the station, at 2000 m.

3.2 Results and Discussion

Time series of CO, BC, NO_y, NO_x and O_3 measurements and MOZART fire-CO fraction at the Pico Mountain station from July to September 5, 2004 are shown in Figure 3.1. Frequent periods with elevated CO levels coinciding with maxima of MOZART fire-CO fraction are evident.

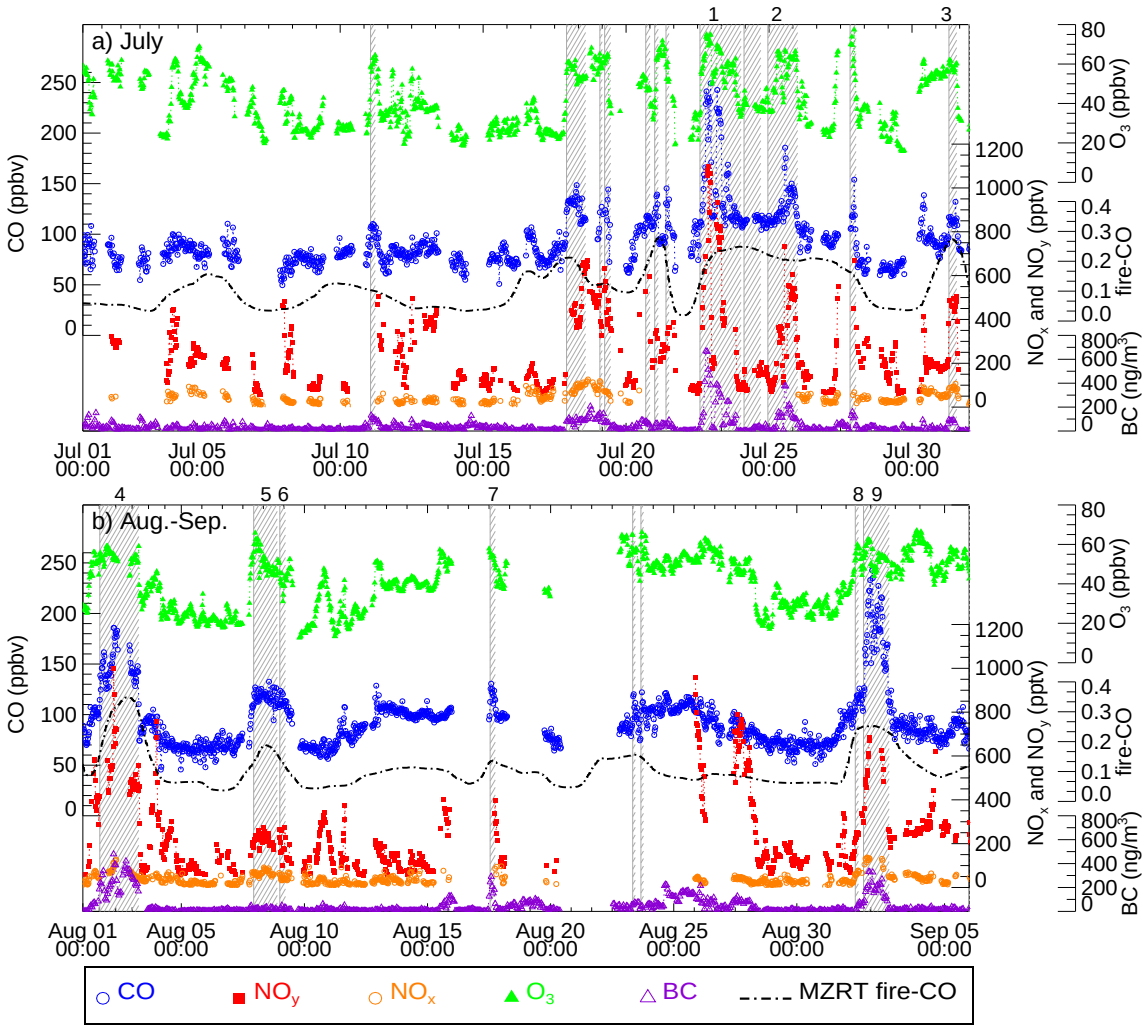

Figure 3.1 Summer 2004 time series of CO, BC, NO_y, NO_x, O_3 measurements, and MOZART fire-CO fraction at the Pico Mountain station. CO is plotted with open blue circles, NO_y with red squares, NO_x with open orange circles, BC with open purple triangles, O_3 with green triangles and MOZART fire-CO fraction with a dash-dotted line. Events identified as potentially boreal fire-impacted periods are identified with hatched areas; events further discussed in the text are numbered above the plot.

3.2.1 Identification of Fire-Impacted Periods

Periods when the hourly average of CO was above 110 ppbv and the MOZART fire-CO fraction was above 0.1 were identified as potentially impacted by upwind boreal wildfire emissions. The CO value of 110 ppbv is well above typical background CO levels at the station and is approximately the maximum value observed in boreal region outflow in the absence of fires, as discussed in section 3.2.3.1 below. (Although we use 30-min averages of CO throughout the remainder of this work, for the purpose of identifying fire-impacted periods we used hourly averages of CO to smooth the CO measurements and compare them with the CO cutoff value.) The MOZART fire-CO fraction cutoff of 0.1 corresponds to approximately the 70th percentile of all model simulated values at the Pico Mountain station for summer 2004. Both of these cutoff values were designed to be conservative and, as a result, may omit some additional periods influenced by boreal wildfire emissions. For example, on August 12 12:00–August 15 23:00, an enhancement of MOZART fire-CO fraction above 0.1 was correlated with an increase in CO, but CO did not exceed the 110 ppbv cutoff value. Conversely, on July 30 7:00–11:00, the hourly average CO increased to 135 ppbv while backward trajectories indicated transport from active fires, but the MOZART fire-CO fraction was lower than 0.07, likely as a result of the model spatial resolution. Although both of these cutoff values are somewhat arbitrarily selected, we find that the use of slightly larger or smaller cutoffs would not significantly affect the results presented below.

In addition to outflow directly from the boreal regions, flow patterns that bring air to the Azores from higher latitudes can travel over the eastern U.S. [*Owen et al.*, 2006]. Therefore transport of boreal wildfire emissions over the Azores may be mixed with air potentially containing North American anthropogenic emissions, which can also be characterized by significant enhancements of CO and O_3 [*Honrath et al.*, 2004]. To determine the magnitude of the impact of anthropogenic emissions during

the boreal wildfire periods, we use the MOZART anthro-CO fraction (not shown in Figure 1). According to the MOZART simulations, anthropogenic emissions may explain some of the enhancements of CO at the station during summer 2004 either alone (*e.g.* August, 25 8:00–19:00) or in combination with boreal wildfire emissions (*e.g.* July 19, 2:00–9:00). To avoid inclusion of observations significantly affected by upwind anthropogenic emissions, we exclude from further analysis all observations with MOZART anthro-CO fraction values above 0.1. This MOZART anthro-CO fraction cutoff corresponded to approximately the 70th percentile of all model values simulated at the site.

To better understand transport patterns during the periods identified as fire-impacted, we examined backward trajectories arriving at the Pico Mountain station altitude. Consistent with MOZART simulations, backward trajectories indicate transport of air that originated from the boreal regions in Alaska and/or Canada as shown in Figures 3.2a and 3.2b. However, the backward trajectories during a few periods indicated intermixing of subtropical and/or tropical air (hereinafter termed tropical air) with the boreal region outflow. Figure 3.2g shows an example of tropical backward trajectories intermixed with boreal region outflow. Observations made during these periods may be affected by clean tropical air and, thus, may not be representative of boreal region outflow. We identified periods potentially affected by tropical air when one or more backward trajectories originated over the Atlantic Ocean south of Pico Island (<35°N) and spent more than 90% of the time over the Atlantic Ocean before arriving at the site. We therefore omit all observations associated with tropical air intermixing from the analysis, with the following exception: during July 23 2:00–18:00, although tropical air masses intermixed with boreal region outflow upwind the station, very large mixing ratios of CO recorded during most of the period ([CO]>180 ppbv) indicate a lack of significant tropical air impact.

Periods identified as potentially affected by boreal wildfire emissions based on CO enhancements and MOZART fire-CO fraction criteria are identified with hatched

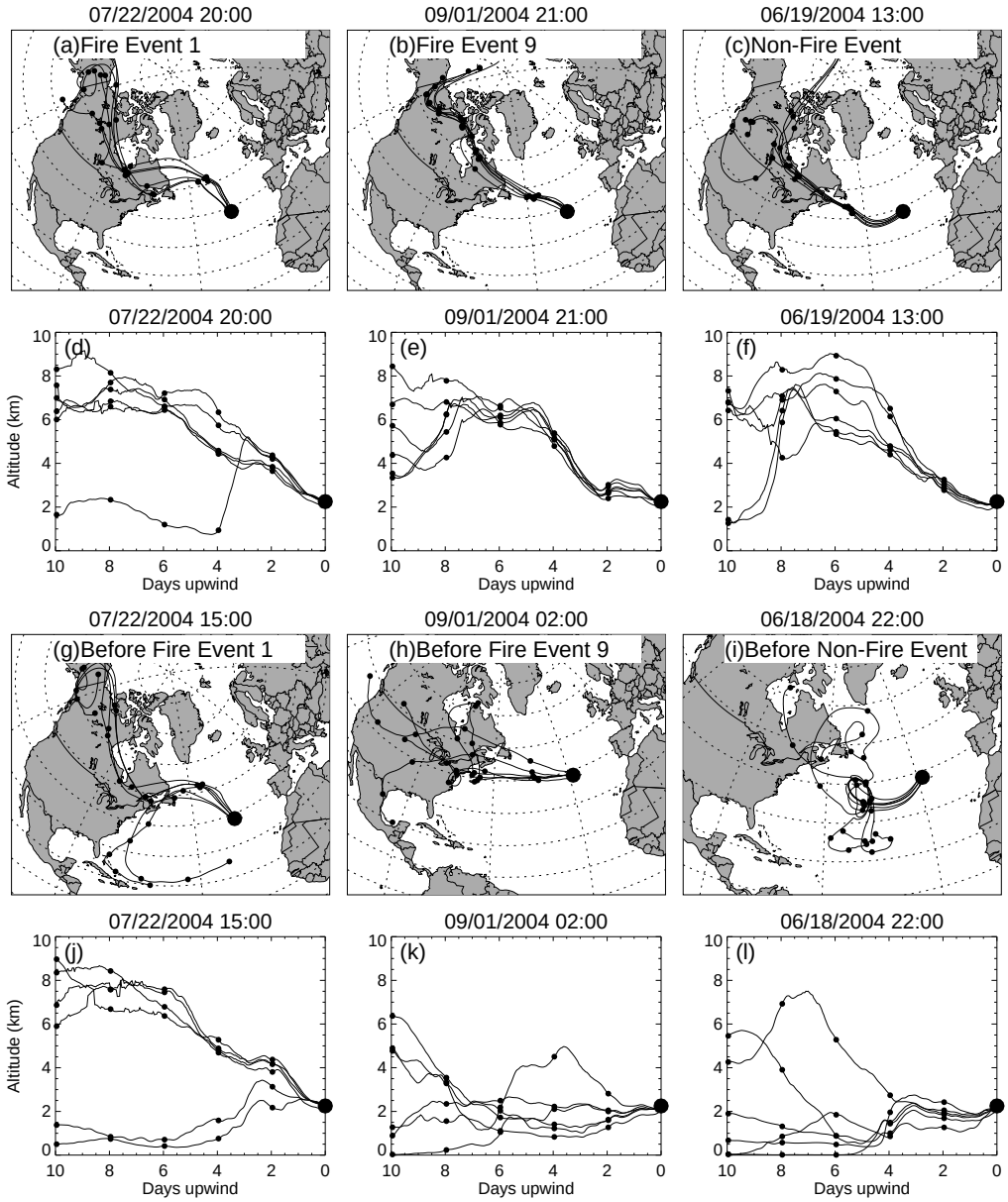

Figure 3.2 Backward trajectories arriving at the measurement site during boreal region outflow: (a, e) boreal region with upwind fire emissions, and (i) boreal region without upwind fire emissions. Backward trajectories before the passage of the boreal region air masses are also shown (c, g, k). Solid lines show the paths of the six trajectories ending on a grid around and below the station; trajectory arrival times are displayed above each pair of plots (a, e, i) and (c, g, k). Plots on the top show the horizontal path of the trajectories [(a, e, i) and (c, g, k)], while plots on the bottom show the altitude profile [(b, d, f) and (d, h, l)]; small dots indicate each 2 days travel time. The location of the Pico Mountain station is marked with a large dot.

areas in Figure 3.1; periods identified with the same criteria, but excluding periods of anthropogenic or tropical influence are also enumerated in Figure 3.1. Table 3.1 provides the statistics of the observations of CO, BC, NO_y, NO_x and O_3 for both criteria, *i.e.* all fire-impacted observations and those excluding anthropogenic or tropical influence.

3.2.2 Overview of Summer 2004 Boreal Wildfire Observations

The impact of boreal wildfire emissions at the Pico Mountain station was very frequent during summer 2004, as shown in Figure 3.1. A total of 21 events with apparent fire impact were identified during the period of study, accounting for 16% of the measurement time from July 1 to September 5. Of these, 9 were unaffected by potential tropical or anthropogenic impacts. We focus only on these fire-impacted periods without anthropogenic or tropical influence, and refer to these periods as boreal wildfire events in the remainder of this paper. These 9 events are numbered in Figure 3.1. During these events, BC, NO_y, NO_x and O_3 levels were also elevated and significantly correlated with CO in most of the cases. MOZART daily CO fire tracer distributions during the ICARTT study (July 10–August 8) indicated the impact of North American fire emissions emitted 6 to 15 days earlier during the events identified during this period (*i.e.* events 1–5).

Figures 3.3a and 3.3b show the time series of 30-min average observations of CO, NO_y, NO_x and O_3, and 1-hr average observations of BC during July 22–24 and September 1–2. These events, labelled respectively event 1 and event 9 in Figure 3.1, represent two of the most intense fire emission episodes observed during the study. Levels of CO, BC, NO_y and O_3 during July 22–24 were extremely enhanced for more than a day, peaking at 249 ppbv, 665 ng m^{-3}, 1100 pptv and 75 ppbv, respectively. (NO_x measurements were not available during this event.) This period had the highest

Table 3.1 Comparison of CO, BC, NO_y, NO_x and O_3 levels during the boreal fire events with observations during periods of flow from boreal region in absence of fires and with all observations during summer 2004. Reported are the average, minimum, maximum and number (N) of 30m-in averages for CO, NO_y, NO_x and O_3, and 1-hr averages for BC.

	Fire Obs.[a]			Non-Fire Obs.[b]			Summer Obs.[c]			
	Mean	Min-Max	N	Mean	Min-Max	N	Mean	Min-Max	Bckgrd[d]	N
CO (ppbv)	139	107–249	379	100	92–111	23	93	46–249	77	3254
w/o anthro, trop air	144	108–249	277							
BC (ng m^{-3})[e]	133	<25–665	188	10	<25	11	38	<25–665	7	1705
w/o anthro, trop air	153	<25–665	133							
NO_y (pptv)	389	71–1100	238	139	127–148	6	270	55–1380	143	1625
w/o anthro, trop air	406	71–1100	178							
NO_x (pptv)	77	33–137	131	35	27–52	6	38	1–137	23	1525
w/o anthro, trop air	77	33–137	98							
O_3 (ppbv)	54	31–77	379	46	42–52	23	41	13–80	30	3428
w/o anthro, trop air	54	31–75	277							

[a]Fire-impacted observations from July to September, 5. First row: all fire-impacted observations; second row (w/o anthro, trop air): fire-impacted observations without anthropogenic or tropical air impact (see text for explanation).

[b]CO, BC and O_3: observations from June 19; NO_y and NO_x: observations from June 7 (see text for explanation).

[c]All observations from June 1–September 5, 2004.

[d]Bckgrd: Background calculated as the 30th percentile of all summer 2004 observations.

[e]"<" indicates BC values below detection limit.

level of CO yet recorded at the Pico Mountain station. Similarly, CO, BC, NO_y, NO_x and O_3 levels were also strongly elevated for more than a day during September 1–2, with peaks of 243 ppbv, 329 ng m^{-3}, 685 pptv, 134 pptv and 62 ppbv, respectively. The MOZART fire-CO fraction was also particularly high during these two events, as shown in Figure 3.1.

Analyses of backward trajectories during events 1 and 9 confirm that the enhancements of these species occurred when airflow from Alaska and/or Canada arrived at the station. Examples of backward trajectories associated with the passage of the boreal fire plumes for these events are shown in Figures 3.2a and 3.2b. For comparison, Figures 3.2g and 3.2h show the airflow before the passage of each boreal fire plume. An important feature of these events is that the levels of these species remained constantly high for more than 24 hours, suggesting the impact of two very large highly aged plumes.

3.2.3 Impacts of Boreal Wildfire Emissions

In this section, we assess the impacts of boreal wildfire emissions by comparing enhancements of CO, BC, NO_y, NO_x and O_3 in fire-impacted boreal outflow to levels under similar conditions but in the absence of fires. First, however, we discuss the estimation of levels during periods of boreal outflow in the absence of fire emissions.

3.2.3.1 Estimation of Levels in Absence of Fires

To estimate the background concentration at the Pico Mountain station in air from the fire source region, but in the absence of fire emissions, we identified two periods when boreal region outflow reached the station prior to the occurrence of the large fires: June 7 5:00–9:00 and June 19 8:00–19:00. Early June was a period with low area burned over northern North America, and as a result, with low boreal wildfire emissions [*Turquety et al.*, 2007]. Therefore, we expect that the contribution of boreal

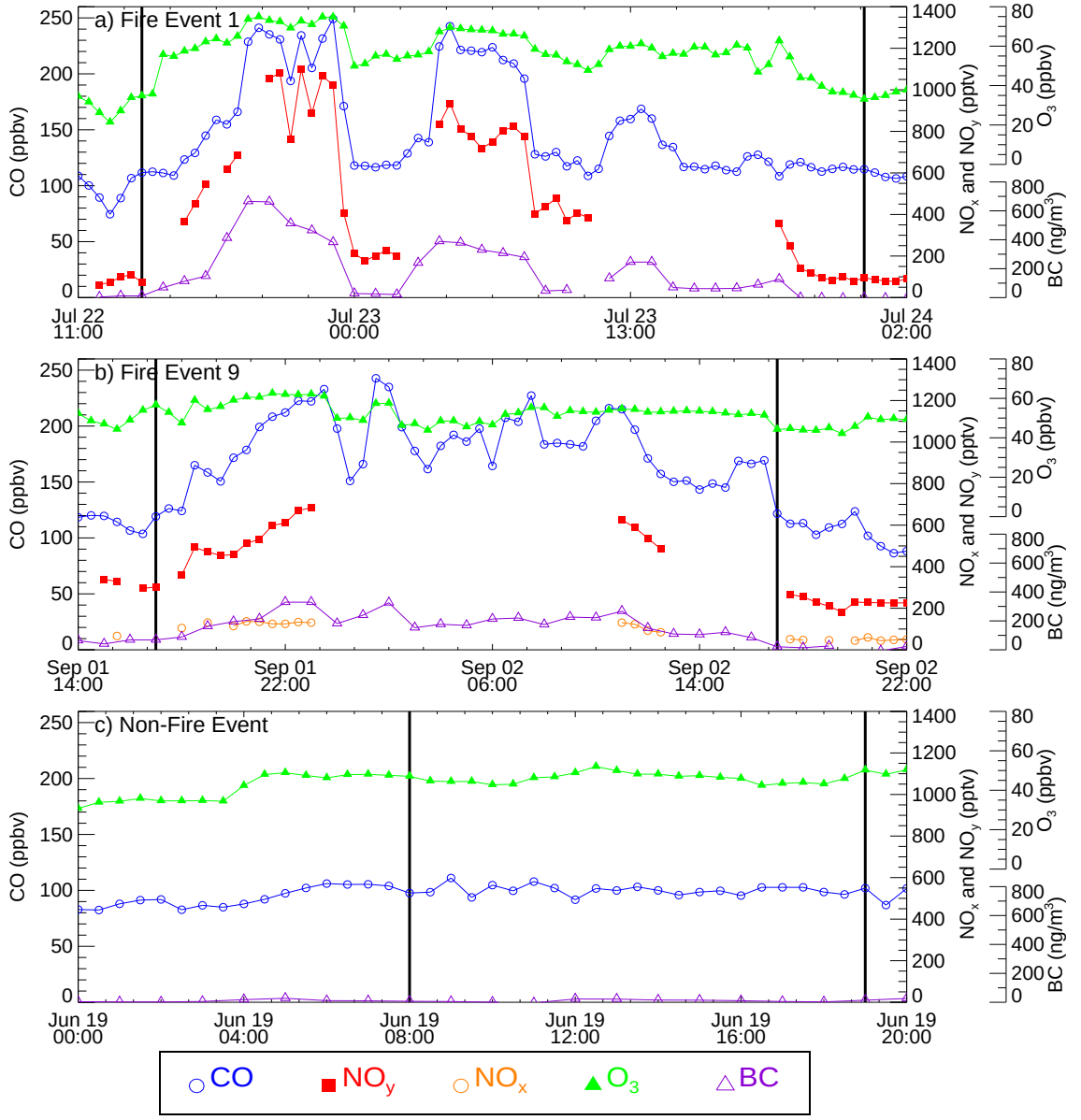

Figure 3.3 Time series of 30-min average CO, NO_x, NO_y and O_3, and 1-hr average BC observations during two boreal wildfire events and one boreal outflow period without upwind fire emissions: a) Fire event 1: July 22 1800–July 23 21:00 (NO_x measurements are not available), b) Fire event 9: September 1 16:30–September 2 16:00 and c) Non-fire event: June 19 8:00–19:00 (NO_x and NO_y measurements are not available). CO is plotted with open blue circles, NO_y with red squares, NO_x with open orange circles, BC with open purple triangles and O_3 with green triangles. Vertical solid lines indicate the start and end time of the event; remaining data are plotted to make the events more apparent.

wildfire emissions to our site was small during these two periods. This is consistent with MOZART simulations, which indicate a maximum fire-CO fraction of 0.05 during these periods.

Figure 3.3c shows the time series of 30-min average observations of CO and O_3 and 1-hr average observations of BC during the longer of these events, June 19 8:00–19:00. (NO_x and NO_y measurements were not available at this time.) Example of the backward trajectories associated with the passage of the air masses during and before this period are shown in Figures 3.2c and 3.2i, respectively. Average levels of CO, BC and O_3 during this period are used as background levels of these species for comparison with fire-impacted periods below. In addition, the maximum level of CO during this event (111 ppbv) was the basis for the 110 ppbv cutoff to select the boreal fire-impacted periods, as discussed in section 3.2.1. (The CO and O_3 background values used in this work are somewhat larger than the levels in non-fire air presented for the same dataset by *Lapina et al.* [2006], because that analysis included periods with a mixture of boreal and non-boreal air).

MOZART simulations during the other non-fire boreal outflow period indicate that anthropogenic emissions may have contributed to these observations (*i.e.*, the MOZART anthro-CO fraction was above 0.1). However, nitrogen oxides measurements in non-fire-impacted boreal outflow were available only during the June 7 event. (Few measurements were available in June 2004 due to testing of the instruments prior the ICARTT campaign.) Average mixing ratios of NO_y and NO_x during this period were used as upper-limit estimates of the background of these species in boreal region outflow in the absence of fires.

The background levels of CO, BC, NO_y, NO_x and O_3 used for boreal region outflow in the study are compared to background levels reported within the North American boreal region in Table 3.2. A wide range of background levels have been reported over the North American boreal region, reflecting differences in the latitude and altitude regions sampled, and the years of study. The values used here are

similar to the background levels reported over the North American boreal region. The enhancement ratios calculated below are dependent on the background values used. This is discussed further in section 3.2.4.

3.2.3.2 Comparison of Levels in Boreal Region Outflow with and without Fire Emissions

Levels of CO, BC, NO_y, NO_x and O_3 during boreal region outflow with fire emissions are summarized and compared to levels observed during boreal region outflow without fire emissions in Table 3.1. Statistics for all summertime observations are also shown. Average CO mixing ratios during the boreal wildfire events (144 ppbv) were above levels observed during flow from boreal region without fire emissions (100 ppbv), and were nearly double the summertime background (estimated as equal to the 30th percentile of all summertime measurements, 77 ppbv). This significant impact is consistent to what it has previously been observed at the Pico Mountain station [*Honrath et al.*, 2004; *Lapina et al.*, 2006], and for the entire Northern Hemisphere in years of high fire activity [*e.g.*, *Novelli et al.*, 2003; *Edwards et al.*, 2004; *Kasischke et al.*, 2005].

Levels of BC, NO_y, NO_x and O_3 were also increased during the fire-impacted events, with levels of these species above those observed in boreal outflow in the absence of fires, and well above the typical summertime background at the site. For example, average NO_x mixing ratios during the boreal wildfire events (77 pptv) were double those observed in boreal outflow without fire emissions (35 pptv) and triple the summertime background at the site (23 pptv).

Figures 3.4a–3.4d show the relationships between CO (used as a tracer of fire emissions) and BC, NO_y, NO_x and O_3. Solid color-coded symbols represent observations obtained during each boreal wildfire event, with one exception: grey circles represent the early June observations made in non-fire boreal outflow discussed in section 3.2.3.1. Most of the fire-impacted observations were above the background

Table 3.2 Estimated background levels over the North American boreal region.

Study	Period	Location	Altitude (km)	CO (ppbv)	NO_y (pptv)	NO_x (pptv)	O_3 (ppbv)	BC (ng m^{-3})
Pico Mountain[a]	June, 04	Pico, Azores	2.2	100	139	35	46	10
ABLE3A[b]	Jul.–Aug., 88	Sub- and Arctic	<1–5.2	91–100	380–600	19–24	47–75[c]	n.r.
ABLE3B[d]	Jul.–Aug., 90	eastern Canada	<1–6.2	80–110	164–542	21–35	25–65[c]	n.r.
Stohl06[e]	Jun.–Aug., 04–05	Summit, Greenland	3	n.r.	n.r.	n.r.	n.r.	20

n.r., Not reported.

[a]Mean values during boreal region outflow in June, used for background levels in enhancement ratio calculations. (See text for explanation.)

[b]Minimum and maximum values reported by *Sandholm et al.* [1992]; *Jacob et al.* [1992].

[c]Large range of O_3 reported reflects mainly O_3 dependence on altitude.

[d]Minimum and maximum values reported by *Talbot et al.* [1994]; *Fan et al.* [1994]; *Wofsy et al.* [1994]; *Mauzerall et al.* [1996].

[e]Median in summer 2004–2005 reported by *Stohl et al.* [2006].

from the boreal regions in the absence of fires, consistent with the average difference noted above. In almost all events, these species were well correlated with CO, although distinct behaviors were observed depending on the levels of CO, in particular for O_3, as discussed further below.

As discussed in section 3.2.1, a number of fire-impacted observations were excluded from the boreal wildfire events due to probable mixing of tropical air or MOZART-simulated anthropogenic emission transport. These observations are also shown in Figure 3.4: observations omitted due to tropical air mixing are represented with open cyan circles and those omitted due to anthropogenic emissions impact are represented with open black squares. Observations omitted due to tropical air mixing fall into two distinct groups of points, suggesting differing degrees of mixing. Of the observations excluded because of anthropogenic impact, some had exceptionally large NO_y, NO_x and O_3 levels, suggesting significant anthropogenic impacts on those species as well. This impact is expect to be small in the events that were not excluded however. During those boreal wildfire events, MOZART-simulated anthropogenic CO was always below 7 ppbv, and usually (60% of the observations) below 3 ppbv.

3.2.4 Analysis of Enhancement Ratios in the Boreal Wildfire Plumes

To characterize the amount of emitted BC and NO_x that still remains in the plumes and the net O_3 production occurring in these plumes during transport to the station, we determined the enhancement ratio of BC, NO_y, NO_x and O_3 with respect to CO during each boreal wildfire event [*e.g.*, *Wofsy et al.*, 1992; *Stohl et al.*, 2002]. CO is commonly used as a tracer because it is emitted from combustion processes in large quantities and has relatively a long lifetime [*Novelli et al.*, 1992]. We consider CO as an inert tracer in this approach. *de Gouw et al.* [2006], based on analysis of VOC measurements, indicated that OH concentrations in the boreal wildfire plumes

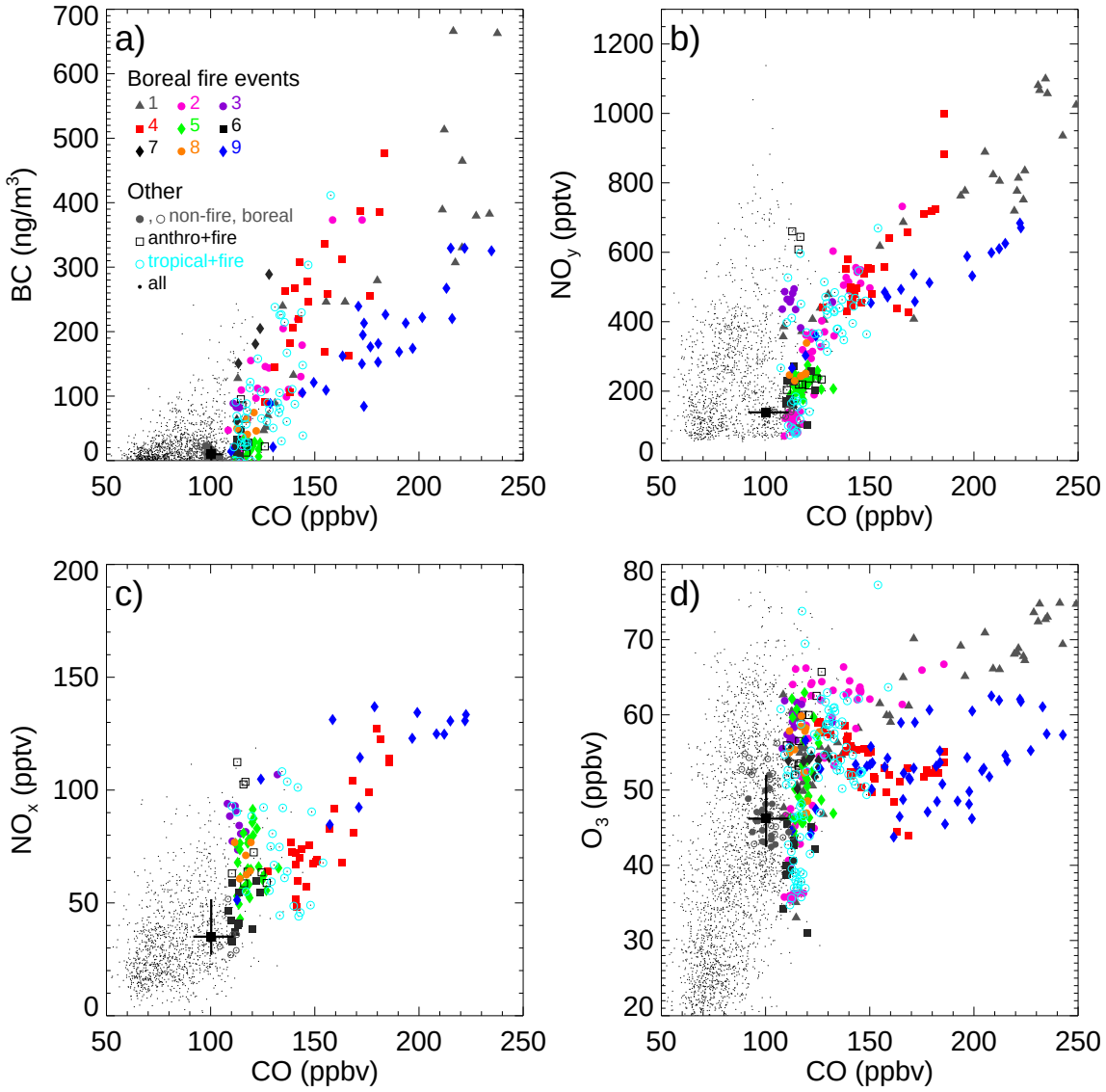

Figure 3.4 Relationship between CO and the indicated species during summer 2004: a) BC versus CO, b) NO_y versus CO, c) NO_y versus CO and d) O_3 versus CO. Boreal wildfire events listed in Table 3.3 and identified in Figure 1 are coded as follows: Event 1 (dark grey triangles), event 2 (magenta circles), event 3 (purple circles), event 4 (red squares), event 5 (green diamonds), event 6 (black squares), event 7 (black diamonds), event 8 (orange circles) and event 9 (blue diamonds). Event 7 is not plotted for NO_y and NO_x because it contained fewer than 5 data points. Fire-impacted observations apparently impacted with tropical air are plotted with open cyan circles; fire-impacted observations apparently impacted with anthropogenic emissions are plotted with open black squares. Observations made during non-fire-impacted boreal outflow are plotted with small solid grey circles; non-fire-impacted boreal outflow observations with anthropogenic impact are plotted with open grey circles. The black square represents the average of non-fire-impacted boreal outflow observations, and black error bars connect minimum and maximum values observed. All other measurements during summer 2004 are plotted with small black dots.

intercepted by the NOAA WP-3 were four times smaller than typical values in the North Atlantic troposphere. Hence, CO reaction with OH is expected to be limited in the boreal fire plumes during the 6–15 days travel time to the station. We calculated mean values of ΔCO, ΔBC, ΔNO_y, ΔNO_x and ΔO_3 during each boreal wildfire event, and calculated enhancement ratios relative to CO for each event using these mean values. Here Δ indicates the difference between the concentration of the indicated species and the background concentration (*e.g.* ΔCO= [CO]-$[CO]_{bkgd}$). Enhancement ratios are critically dependent on the background levels used [*Mauzerall et al.*, 1998]. Our background levels were derived using observations during transport events in June, as discussed in section 3.2.3.1. This results in background levels higher than those that would be estimated using clean marine levels or using the 30th percentile of all summertime measurements. This leads to reduced calculated enhancement ratios for all the species.

Table 3.3 presents the resulting enhancement ratios. A large variability of enhancement ratios was observed. There are two causes that probably contributed to the varying enhancement ratios: different emission rates, which vary as a function of fuel type and burning conditions [*Goode et al.*, 2000; *Reid et al.*, 2005], and varying degrees of removal during transport. We examine both processes in the following sections.

3.2.4.1 Aerosol Black Carbon

The relationships between BC and CO in boreal fire plumes and in background air from boreal regions are shown in Figure 3.4a. Estimated ΔBC/ΔCO ratios for each boreal fire event are shown in Table 3.3. Black carbon was significantly enhanced in all events relative to background from boreal outflow without upwind fire emissions, with the exception of events 5 and 6 (green diamonds and black squares in Figure 3.4a, respectively).

A broad range of BC enhancement ratios (0.5–8.4 ng m^{-3}/ppbv; Table 3.3) were

Table 3.3 Enhancement ratios of the species during the boreal wildfire events identified in Figure 3.1. Reported enhancement ratios (calculated as described in text), 2-σ uncertainty and number (N) of simultaneous 30-min average observations of NO_y, NO_x, O_3 and CO, and simultaneous 1-hr average observations of BC and CO. Events with N < 5 not shown.

		ΔBC/ΔCO		$\Delta NO_y/\Delta$CO		$\Delta NO_x/\Delta$CO		$\Delta O_3/\Delta$CO	
Event	Period	ng m^{-3}/ppbv	N	pptv/ppbv	N	pptv/ppbv	N	ppbv/ppbv	N
1[a]	July 22 14:00 – July 24 0:00	3.60 ± 0.84	26	7.47 ± 1.08	35	NA	NA	0.23 ± 0.03	57
2	July 24 23:00 – July 25 23:30	3.72 ± 0.87	25	6.11 ± 1.09	41	NA	NA	0.31 ± 0.06	50
3	July 31 7:00 – July 31 13:00	4.91 ± 0.48	5	22.10 ± 2.62	10	3.63 ± 0.46	10	0.89 ± 0.11	13
4	Aug. 1 16:30 – Aug. 3 6:00	4.70 ± 0.55	20	8.10 ± 0.62	26	0.85 ± 0.08	25	0.14 ± 0.01	39
5	Aug. 7 22:30 – Aug. 8 17:30	0.47 ± 0.17	14	4.48 ± 0.32	29	1.73 ± 0.14	29	0.26 ± 0.06	33
6	Aug. 9 0:00 – Aug. 9 5:30	1.08 ± 0.42	6	4.17 ± 1.17	10	0.72 ± 0.22	12	-0.42 ± 0.10	12
7	Aug. 17 13:00 – Aug. 17 17:30	8.44 ± 2.26	5					0.37 ± 0.04	10
8	Sep. 1 10:00 – Sep. 1 15:00	2.50 ± 0.41	5	6.74 ± 0.79	7	1.92 ± 0.18	6	0.53 ± 0.08	11
9	Sep. 1 17:00 – Sep. 2 17:30	2.18 ± 0.28	25	4.67 ± 0.34	17	1.02 ± 0.07	14	0.09 ± 0.01	50

NA, Not available

[a]Event with apparent tropical air mixing impact.

observed in the boreal fire plumes. Large variability in BC emissions from boreal wildfires has been reported previously. For example, BC concentrations during smoldering combustion are low, with BC mass fractions typically 2–5% of all carbon particles emitted, while BC mass fractions from flaming combustion are 4 to 28% of all carbon particles emitted [*Reid et al.*, 2005, and references therein].

However, washout processes during transport to the station may also have contributed to this variability. To evaluate this possibility, we examined precipitation during transport and meteorological conditions at Pico during each event. For this purpose, we extracted rainfall rates from the HYSPLIT model output for the backward trajectories during each event and analyzed relative humidity measurements and archived photos of conditions at the station. Average rainfall rates were low (less than 0.05 mm/hr) in all backward trajectories travelling from the boreal region to the station, with the exception of events 5, 6 and 9, which showed average rainfall rates of 0.09, 0.06 and 0.08 mm/hr, respectively. (These events are represented by green diamonds, black squares and blue diamonds in Figure 3.4a, respectively.) Conditions at the station were dry and sunny during all events, with the exception of event 6, when heavy fog, and most likely rain, was present. Therefore, the lower ΔBC/ΔCO ratios during events 5, 6 and 9 compared to those during the other events are consistent with the wet scavenging of a greater fraction of BC during transport and/or at the station location during those events. This is consistent with previous observations of light absorbing aerosols (*e.g.*, BC) in boreal fire plumes, which indicate that a large fraction of aerosols may be removed in the presence of rain and/or clouds [*Bertschi and Jaffe*, 2005; *Stohl et al.*, 2006].

The BC enhancement ratios we report are 8–141% (average 59%, or 78% excluding events 5, 6 and 9) of the BC/CO emission ratio from extra-tropical forest fires (6 ± 3 ng m^{-3}/ppbv) recommended by *Andreae and Merlet* [2001]. (The value of 141% is not significantly different from 100%, considering the uncertainties of the measurements and the recommended value.) These observations indicate that an im-

portant fraction of the total BC emitted into the plumes we sampled was efficiently exported to the Azores, very far downwind from the fires. This underscores other recent work that has documented long-range impacts of the North American wildfire BC emissions [*Stohl et al.*, 2006; *Duck et al.*, 2007]. Since BC effectively absorbs light in the atmosphere [*Hansen et al.*, 2000; *Bond and Sun*, 2005], this implies a potentially significant large-scale impact of boreal wildfire emissions on the direct radiative forcing over the Northern Hemisphere troposphere.

3.2.4.2 NO_y

Figure 3.4b shows the relationship between NO_y and CO in the boreal wildfire plumes and in background air from boreal regions without fire emissions. Table 3.3 provides the $\Delta NO_y/\Delta CO$ ratios estimated for each boreal fire event. Nitrogen oxides were significantly enhanced in all the boreal fire plumes, relative to background levels.

The NO_y enhancement ratios were highly variable, however (4.2–22.1 pptv/ppbv; Table 3.3). In the previous section, we concluded that the variation in BC enhancement ratios could be the result of a combination of emission variation among fires and wet removal during transit to the station. Since NO_x emissions also vary as a function of type of combustion [*e.g. Yokelson et al.*, 1996; *Goode et al.*, 2000] and a part of NO_y (*i.e.* HNO_3) is susceptible to wet deposition, the same processes are expected to contribute to the variation of NO_y enhancement ratios. Consistent with this expectation, the events with the lowest $\Delta BC/\Delta CO$ ratios are also those with the lowest $\Delta NO_y/\Delta CO$ ratios (*i.e.*, events 5, 6 and 9). As a result, a plot of NO_y versus BC is less scattered than the plot of NO_y versus CO, as shown in Figure 3.5, and the correlation of NO_y with BC ($r^2 = 0.82$) is slightly better than that with CO ($r^2 = 0.75$). Additional evidence for efficient HNO_3 removal in some plumes is provided by aircraft measurements over the northwestern Atlantic Ocean, which found very low HNO_3 to NO_y ratios in several 2004 North American fire plumes [*Flocke et al.*, 2005].

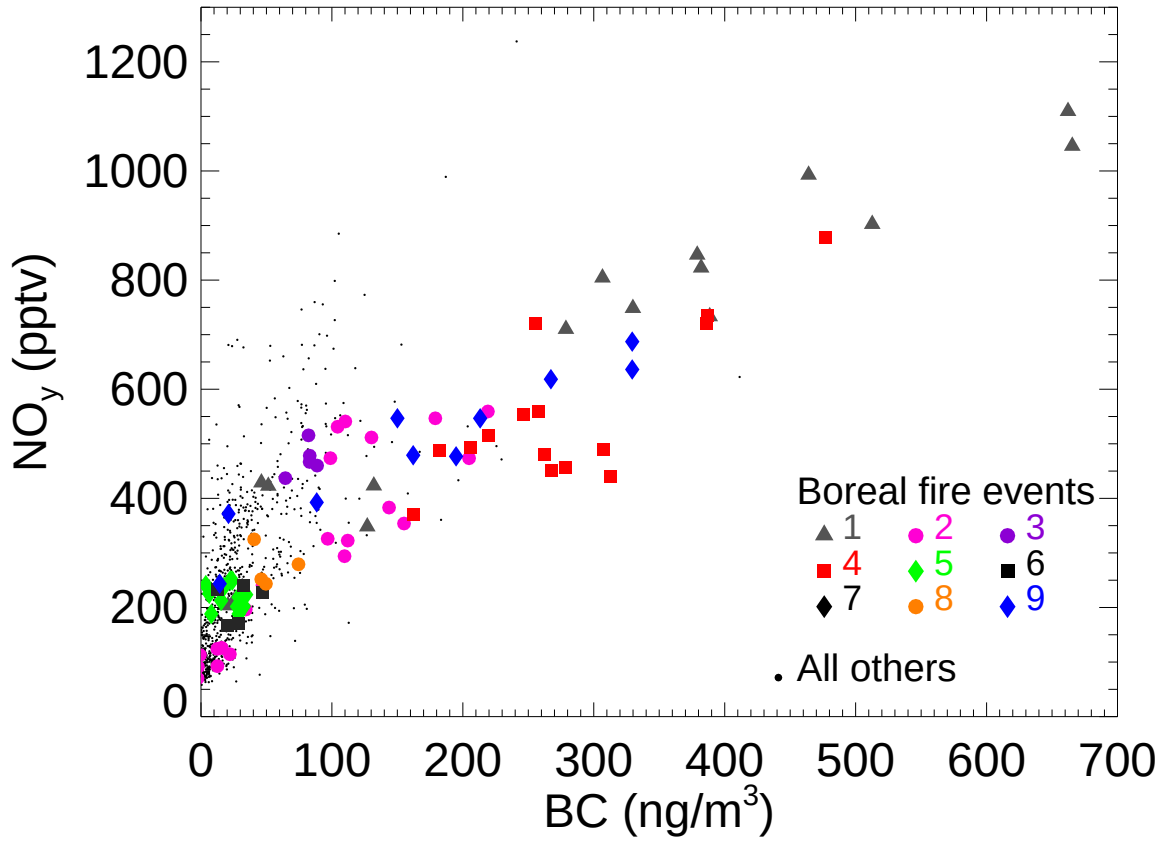

Figure 3.5 Relationship between BC and NO_y during summer 2004. Boreal wildfire events are coded as follows: event 1 (dark grey triangles), event 2 (magenta circles), event 3 (purple circles), event 4 (red squares), event 5 (green diamonds), event 6 (black squares), event 8 (orange circles), event 9 (blue diamonds). Event 7 contained $<$5 simultaneous data points and is not plotted. All other measurements during summer 2004 are plotted with small black dots.

Table 3.4 compares these $\Delta NO_y/\Delta CO$ ratios to previous $\Delta NO_y/\Delta CO$ ratios obtained from previous studies of boreal wildfire plumes. The mean enhancement ratio we observed (8 pptv/ppbv) is within the large range of mean values observed in plumes sampled over North America (5.6–14.1 pptv/ppbv; Table 3.4). The Pico Mountain mean enhancement ratio is also a significant fraction of the available (but poorly constrained) estimates of North American boreal fires NO_x/CO emission ratios, *e.g.* 12 pptv/ppbv [*Jain et al.*, 2006] or 26±15 pptv/ppbv [*Andreae and Merlet*, 2001]. These comparisons indicate that a significant fraction of the NO_x emitted into the sampled plumes was exported as NO_y to the lower FT over the Azores region.

This conclusion contrasts with some prior studies of the export of anthropogenic NO_y to the FT, which conclude that a large majority of surface NO_x emissions (>70%) is removed before or during export from the boundary layer during lofting mechanisms [*e.g.*, *Liang et al.*, 1998; *Stohl et al.*, 2002; *Parrish et al.*, 2004; *Li et al.*, 2004].

However, the boreal fire plumes sampled here differ from typical anthropogenic export in two key ways. First, in boreal wildfires PAN is expected to account for a significant fraction of NO_y [*Jacob et al.*, 1992; *Singh et al.*, 1994] as a result of lower NO_x/hydrocarbon emission ratios [*Jacob et al.*, 1992]. Second, boreal wildfires can often be very energetic, releasing enough thermal energy to create smoke and convection columns that extend rapidly into the troposphere and even into the stratosphere [*e.g. Fromm et al.*, 2005; *Damoah et al.*, 2006]. The rapid vertical transport of emissions in fire-induced convection plumes soon after emission may contribute to the inefficient removal of NO_y during the lofting mechanism, as has been suggested for BC [*Stohl et al.*, 2006]. In addition, as described above, most boreal fire plumes sampled at Pico were associated with low precipitation during transport as well as dry and sunny conditions at the site. Thus, these conditions may have contributed to a more efficient export of NO_y.

Table 3.4 Enhancement ratios of NO_y, NO_x and O_3 relative to CO observed in boreal fire plumes.

Year	Fire Location	Sampling Location	Plume Height (km)	Travel time (day)	$\Delta NO_y/\Delta CO^a$ (pptv/ppbv)	$\Delta NO_x/\Delta CO^a$ (pptv/ppbv)	$\Delta O_3/\Delta CO^a$ (ppbv/ppbv)	Source
2004	AK, Can	Pico, Azores	2.2	6–15	8.0	1.6	0.2^b	[1]
					(4.2–22.1)	(0.7–3.6)	(−0.4–0.9)	
2002	Quebec, Can	eastern U.S.	0–2.5	1–3	4.1	n.r.	0.1	[2]
					(2.4–7.4)		(0.01–0.09)	
1990	Can, AK	eastern Can	1–6.2	< 1	14.1	0.7	0.2	[3]
					(2.5–37.8)	(0–3.8)	(0–0.7)	
1988	Sib, AK, Can	AK, Can	1.5–6.1	near fire	10.9	0.2	0.35	[4]
					(5.7–15.2)	(0–0.52)	(0.1–0.7)	
1988	AK	AK	2.0–4.5	< 1	5.6	n.r.	0.095	[5]
					(3.2–8.4)		(0.014–0.18)	
1997	AK	interior AK	1.6–1.8	∼2hr	n.r.	n.r.	0–0.09	[6]
1998	eastern Sib	north Japan	< 1	<1	n.r.	n.r.	0.01	[7]
1995	Can	South U.S.	0–3.0	2–4	n.r.	n.r.	0.11–0.17	[8]
2004	AK, Can	N Atl, W Eur	5–8	4–9	n.r.	n.r.	-0.01–0.08	[9]
2001–03	Sib, AK, Can	Pico, Azores	2.2	6–15	n.r.	n.r	0.7	[10]
							(0.4–0.9)	
2002–03	Sib	NW U.S/ NE Pacific	0.7–5.0	7–10	n.r.	n.r.	0.4	[11]
							(0.2–0.8)	

n.r.: Not reported; Can: Canada; AK: Alaska; Sib: Siberia; N Atl: North Atlantic; W Eur: Western Europe.

[a]Reported average (minimum–maximum) in each measurement campaign (*e.g.*, ABLE3B). Enhancement ratios were calculated using levels reported in background and biomass burning impacted air masses [*e.g. Sandholm et al.*, 1992] or extracted directly from reported enhancement ratios [*e.g. Wofsy et al.*, 1992]. [1]: *This work*, [2]: *DeBell et al.* [2004], [3]: ABLE3B (*Talbot et al.* [1994]; *Fan et al.* [1994]; *Mauzerall et al.* [1996]), [4]: ABLE3A (*Sandholm et al.* [1992]) [5]: ABLE3A (*Wofsy et al.* [1992]). [6]: *Goode et al.* [2000], [7]: *Tanimoto et al.* [2000], [8]: SOS-95 (*Wotawa and Trainer* [2000]; *McKeen et al.* [2002]), [9]: *Real et al.* [2007], [10]: Pico Mountain (*Honrath et al.* [2004]), and [11]: *Bertschi et al.* [2004]; *Bertschi and Jaffe* [2005].

[b]Average of high-CO-enhancement events 1, 2, 4 and 9, as discussed in section 3.2.4.4.

3.2.4.3 NO_x

Given the presumption of significant PAN content, the export of NO_y is expected to lead to NO_x release downwind from the fires. NO_x mixing ratios were indeed significantly enhanced in these plumes relative to background. Figure 3.4c shows the relationship between NO_x and CO in the boreal wildfire plumes and in background air from boreal regions in absence of fire emissions; $\Delta NO_x/\Delta CO$ ratios for the boreal wildfire events are listed in Table 3.3.

The average of these NO_x enhancement ratios (1.6 pptv/ppbv; Table 3.4) is significantly larger than those reported previously in moderately aged boreal fire plumes (0.2–0.7 pptv/ppbv; Table 3.4 [*e.g.*, *Sandholm et al.*, 1992; *Mauzerall et al.*, 1996]). The occurrence of large enhancements of NO_x and large $\Delta NO_x/\Delta CO$ ratios in these plumes implies that decomposition of PAN to NO_x, occurring as the plumes subside southward to the latitude of the Azores, may be an important source of NO_x to the lower troposphere. This is consistent with the large enhancements of NO_y observed at Pico as well as the large enhancements of NO_y and PAN detected in plumes at higher altitudes than Pico over eastern North America [*Flocke et al.*, 2005] and over western Europe [H. Schlager, Deutsches Zentrum für Luft- und Raumfahrt (DLR), Germany, personal communication, 2006] during the ICARTT campaign.

The overall impact of fire plumes on NO_x levels during summer 2004 was significant. Fire emissions were responsible for 36% of all observations of NO_x above 50 pptv (and 90% of all observations above 100 pptv). Fire plumes also led to a significant impact on NO levels. The 9 boreal wildfire events were responsible for 29% of all observations of NO above 20 pptv, and the average daytime fire-impacted NO was significantly larger (17 ± 2; mean± 2-σ) than the average daytime NO for all summer observations (11 ± 1). The large NO and NO_x mixing ratios present in these well-aged boreal wildfire plumes indicate a significant impact on the regional O_3 budget.

3.2.4.4 Ozone

Figure 3.4d shows the relationship between O_3 and CO in the boreal wildfire plumes and in background air from boreal regions without fire emissions. The estimated O_3 enhancement ratio of each boreal fire event is provided in Table 3.3.

The behaviors of O_3 in the fire plumes varied from significant O_3 enhancement in some plumes (*e.g.* event 1; grey triangles in Figure 3.4d) to O_3 enhancement relative to background, with a negative CO-O_3 slope (*e.g.* event 4; red squares) to a smaller O_3 enhancement (*e.g.* event 9; blue diamonds). Furthermore, several fire plumes presented relatively large $\Delta O_3/\Delta CO$ ratio associated with only moderate CO enhancements (*e.g.* event 3; purple circles in Figure 3.4d; also events 5–8). The moderate CO enhancements during those periods make these events difficult to interpret, and therefore we focus here on the O_3 enhancement ratios in the high-CO-enhancement events.

The significant enhancements of O_3 and large $\Delta O_3/\Delta CO$ ratios (mean 0.2 ppbv/ppbv) in these plumes are consistent with other studies that suggest that significant ozone production occurred downwind from boreal wildfires. For example, ozone enhancements of 20–30 ppbv were observed in boreal wildfire plumes after 5–7 days travel time to southern U.S. [*Wotawa and Trainer*, 2000; *Morris et al.*, 2006] and to Europe [*Forster et al.*, 2001; *Real et al.*, 2007]. Model simulations of the O_3 formation in biomass burning plumes indicate that the slow recycling of PAN, and to a lesser extend HNO_3 and organic nitrates, increases the effective lifetime of NO_x stimulating the continued formation of O_3 in these plumes beyond the typical 1-day NO_2 lifetime [*Chatfield and Delany*, 1990; *Real et al.*, 2007].

However, this mean $\Delta O_3/\Delta CO$ ratio is smaller than some reported previously and listed in Table 3.4 (*e.g.*, 0.4–0.7 ppbv/ppbv [*Honrath et al.*, 2004; *Bertschi and Jaffe*, 2005; *Lapina et al.*, 2006]). This is mainly a result of the background value used here, as discussed in section 3.2.4. The average O_3 enhancement ratio we calculate

increases to 0.3 ppbv/ppbv if the 2004 summertime background (Table 3.1) is used. If, in addition, all boreal wildfire events are considered, *i.e.*, moderate- and high-CO-enhancement events, the average $\Delta O_3/\Delta CO$ ratio increases to 0.5 ppbv/ppbv (range 0.2–0.8 ppbv/ppbv).

The significant O_3 enhancements observed during all but one event indicate O_3 production in most of the sampled boreal wildfire plumes. However, although O_3 levels were above background on average in all these events, the negative O_3–CO slope observed in event 4, and in parts of events 2 and 9, and the very low $\Delta O_3/\Delta CO$ ratio in parts of event 9 imply the removal of O_3 or the suppression of O_3 production as well. This behavior is not fully understood, but may be due to one or a combination of the following causes.

First, a reduction of the O_3 production rates in the plumes would cause a low $\Delta O_3/\Delta CO$, but positive O_3–CO slope. A flat relationship between O_3 and CO, in combination with large enhancements of PAN and little NO_x [*Flocke et al.*, 2005] and large enhancements of VOCs [*de Gouw et al.*, 2006], was observed in some of the boreal fire plumes intercepted by the NOAA W-P3 at higher altitudes than Pico. *de Gouw et al.* [2006] based on the VOCs measurements deduced that OH levels were depressed in these plumes. Similar conditions (*i.e.* large enhancements of PAN and VOCs) were observed at the BAe146 [*Real et al.*, 2007]. As a consequence of low OH concentrations and limited NO_x availability, O_3 production rates may have been reduced. Similarly, *Pfister et al.* [2006] indicated that near the fire regions and, to a lesser extent downwind from the fires, O_3 production may also be reduced due to the combination of a reduction in the production rate and an increase in the loss rate of background O_3, as a result of a decrease in HO_x ($OH+HO_2$) concentrations.

Second, several studies have demonstrated the loss of O_3 by reaction with organic compounds present in aerosols [*e.g.*, *de Gouw and Lovejoy*, 1998; *Griffin et al.*, 1999]. Biomass burning is a large source of smoke particles composed typically of organic carbon (OC) ∼50–60% and BC ∼5–10% [*Reid et al.*, 2005]. Given the significant

levels of BC observed in the boreal fire plumes and the large ratio of OC to BC in biomass burning [*Reid et al.*, 2005], O_3 destruction on organic aerosols may have contributed to the reduced O_3 enhancement ratio or the negative O_3–CO relationship observed in some events.

Finally, nighttime chemistry processes may also result in destruction of O_3. At night, chemical processing of NO_x oxidizes NO_x to HNO_3 via rapid heterogeneous hydrolysis of N_2O_5 in aerosols and initiates nocturnal oxidation of VOCs, with the concurrent destruction of O_3 [*Parrish et al.*, 1998; *Brown et al.*, 2006]. Thus, nocturnal NO_x emissions from boreal wildfires may result in a reduction of O_3 and NO_y, and result in reduced $\Delta O_3/\Delta CO$ ratio or negative O_3–CO relationships.

To further investigate the photochemical properties of the plumes, we present the relationship between O_3 and NO_y in Figure 3.6. With the exception of event 4, O_3 and NO_y showed positive correlations in all plumes ($r^2 = 0.5 - 0.8$). Positive O_3–NO_y correlations are consistent with our expectation of photochemical O_3 production in the plumes, as a result of decomposition of PAN to NO_x occurring in the air masses during subsidence to the station. The sole exception, event 4 (red squares) exhibits no correlation between O_3 and NO_y (Figure 3.6) and a negative O_3–CO relationship (Figure 3.4d) and a larger BC-NO_y relationship than the general trend (Figure 3.5). This situation suggests O_3 destruction from organic aerosols during transport towards the station. However, the data available here are insufficient to test this hypothesis.

Finally, we have evaluated the possibility that stratospheric O_3 contributed to the O_3 enhancements observed during some of these events. Stratospheric O_3 frequently impacted the FT over eastern North America during summer 2004 [*Thompson et al.*, 2007]. Boreal fire plumes that impacted Pico were often associated with subsidence from altitudes of approximately 6–8 km, suggesting a potential stratospheric impact. To assess this, we used FLEXPART stratospheric O_3 tracer values simulated at the station location and altitude during July 1–August 16 [A. Stohl, Norwegian Institute for Air Research (NILU), personal communication, 2006]. Detailed information about

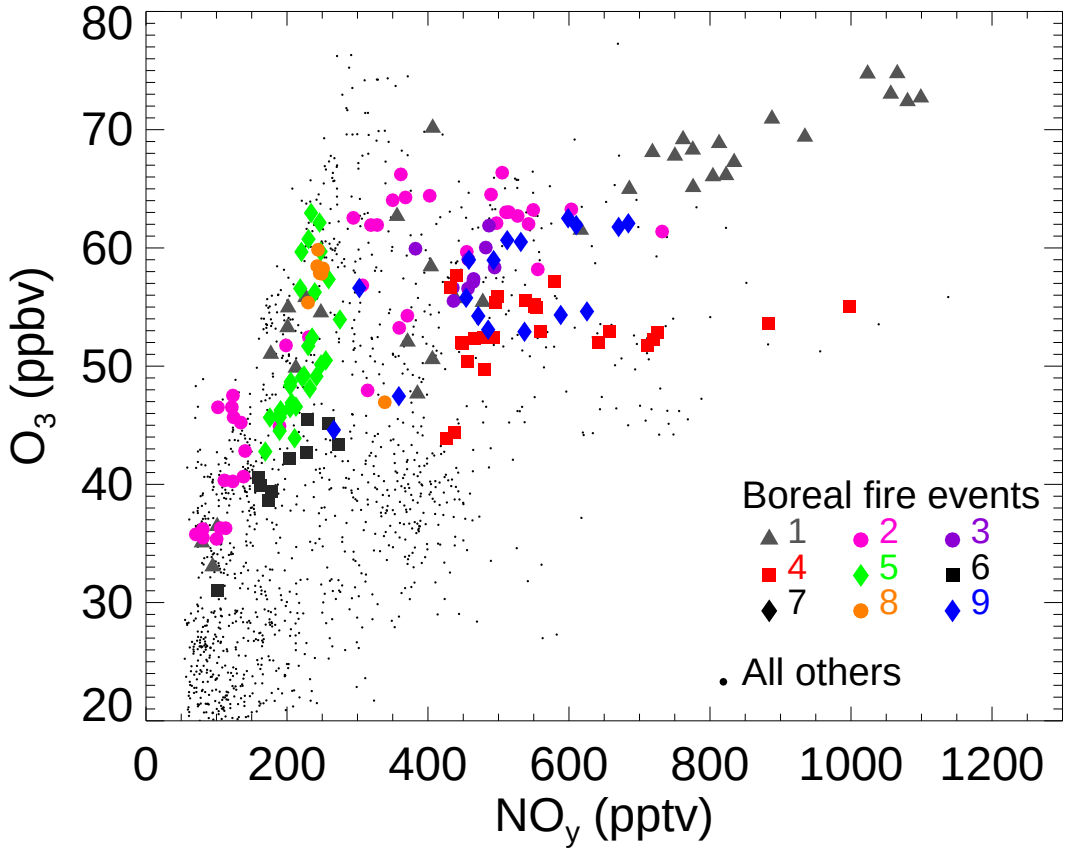

Figure 3.6 As Figure 3.5, but for the relationship between O_3 and NO_y.

the FLEXPART model is present elsewhere [*Stohl et al.*, 2005]. This analysis indicated that stratospheric O_3 occasionally impacted the station during the ICARTT period, but that the overall impact of stratospheric O_3 was rather small: the average ($\pm$ standard deviation) of all stratospheric O_3 tracer values was 8.4 ± 5.2 ppbv. During the fire-impacted events, stratospheric O_3 tracer values were usually reduced, rather than increased, with an average ($\pm$ standard deviation) of 5.8 ± 4.2 ppbv. We found only one episode during the boreal fire events (August 07 23:00–August 08 21:00) when the stratospheric O_3 tracer was large (10 to 18 ppbv). This episode occurred during event 5 (green diamonds in Figure 3.4d). Even during this episode, the O_3

enhancement during the event did not appear to be due to stratospheric O_3, as FLEXPART stratospheric O_3 tracer values did not increase relative to values before or after the event. Therefore, we conclude that stratospheric O_3 was not the cause of the enhancements of O_3 observed during event 5, and that the overall impact of stratospheric O_3 was not significant during the boreal fire plumes analyzed in the study.

3.2.5 Implications of Boreal Wildfires for the NO_x and O_3 Budgets

The NO_y enhancement ratios observed at Pico may be used to estimate the total amount of NO_x emitted from the fires and exported in the plumes by multiplying the observed NO_y/CO enhancement ratio by the fire CO emissions [*Stohl et al.*, 2002; *Parrish et al.*, 2004]. *Pfister et al.* [2005] estimated that 30±5 Tg CO were emitted over the North American boreal region from mid-June to August, 2004, consistent with the estimate of [*Turquety et al.*, 2007]. Using the $\Delta NO_y/\Delta CO$ ratio at the Pico Mountain station (8.0 pptv/ppbv CO; Table 3.4) as an approximation of the impact of long-range-transported fire emissions, this CO emission implies that the fires contributed 0.12 Tg NO_y (as N). If, instead, we use total boreal fire CO emissions in a typical year (∼61 Tg CO; [*Kasischke et al.*, 2005]), *i.e.*, including Siberian emissions as well as North American, the total contribution to long-range-transported NO_y is estimated as 0.24 Tg. These values are quite large. For comparison, the amount of eastern North American NO_x emissions exported to the FT during mid-June through August 2004 was approximately 0.30 Tg NO_y (as N). (This estimate is based on eastern U.S. NO_x emissions equal to two-thirds of the U.S. national emissions during that period, using total NO_x U.S. emissions in 1999 reported by *Parrish et al.* [2004], adjusted for the 8.8% per year decrease of the on-road CO:NO_y emission ratio, and estimated efficiency of export to the FT equal to approximately 25% during sum-

mertime [*e.g.*, *Liang et al.*, 1998; *Stohl et al.*, 2002; *Parrish et al.*, 2004; *Li et al.*, 2004].) These observations imply significant impacts of the boreal wildfires on the NO_y budget over downwind regions distant from the fires.

If the O_3 enhancement ratio at the Pico Mountain station applies to all fire emissions, the average $\Delta O_3/\Delta CO$ ratio (0.2 ppbv/ppbv), combined with the total CO emitted from the North American wildfires (30 Tg) or with the typical CO emitted from boreal wildfires (61 Tg), indicates that the boreal wildfires may have resulted in a source of 10–21 Tg of O_3 during summer 2004. This method is generally consistent with the MOZART analysis of fire-induced O_3 production discussed by *Pfister et al.* [2006]. The monthly mean of our estimate (4–8 Tg O_3/month from mid-June to August) is 10–20% of the July net photochemical O_3 production in the northern middle and high latitudes (30–90° N; surface to 350 hPa) estimated by *Emmons et al.* [2003]. The ultimate impact could be even larger, since additional O_3 is expected to form as a result of the NO_x and PAN still remaining in the transported plumes. Therefore, our observations indicate that boreal wildfires may significantly impact the hemispheric O_3 budget during the fire season.

Given the current uncertainties in the CO emissions from boreal wildfires, the increase in dry and warm conditions over the boreal region [*Hassol*, 2004], and the increase in human-ignited fires [*Mollicone et al.*, 2006], most likely the impact of boreal wildfires is significantly larger than previously believed.

3.3 Conclusions

North American boreal wildfire emissions frequently impacted the Pico Mountain station during summer 2004. Using MOZART simulations and enhancements of CO levels, we identified 21 events of long-range transport of boreal wildfire emissions to the site, which accounted for 16% of the time from July 1 to September 5, 2004. Fire-impacted boreal region outflow resulted in extremely high levels of CO, BC and

nitrogen oxides, relative to other observations at the station, along with significant enhancements of O_3. Analysis of CO, BC, NO_y, NO_x and O_3 observations during the boreal wildfire events showed that levels of all these species were above those in background air from similar outflow in the absence of fires, and well above typical summertime background levels at the site. This indicates a significant contribution from the North American wildfire emissions to background levels of these species over the North Atlantic region during summer 2004.

Enhancement ratios relative to CO were somewhat variable, however. This is attributed to a combination of variation of fire types and emissions and removal during transport to the site. Analyses of $\Delta BC/\Delta CO$ and $\Delta NO_y/\Delta CO$ indicated that a significant fraction of BC and NO_y resulting from the fires was scavenged in some plumes, but on average BC and NO_y were efficiently exported to the lower FT over the North Atlantic region. Analyses of $\Delta NO_x/\Delta CO$ ratios suggested that decomposition of PAN to NO_x, occurring as the plumes subside southward to the Azores, was an important source of NO_x. High levels of NO and NO_x imply continuing O_3 formation in these highly aged plumes.

Ozone levels were also significantly enhanced. Analysis of $\Delta O_3/\Delta CO$ ratios indicated a varying behavior from plume to plume, with significant to moderate O_3 production, and included negative O_3–CO slopes in some plumes. We discussed several mechanisms that may have contributed to the complex behavior of O_3 in the fire plumes, and suggest that further work is needed to better understand this effect. However, the O_3 enhancements present in all but one plume indicate that significant photochemical production occurred during transport, most likely as a result of decomposition of PAN to NO_x. Lower O_3 production in other plumes may have resulted from a reduction in the O_3 production rates due to reduced OH concentrations and limited NO_x, or from destruction of O_3 during transport due to reaction with organic aerosols or nighttime chemistry.

Our analyses demonstrate that boreal wildfire emissions can result in a significant

source of BC, NO_x and O_3 in the central North Atlantic lower FT. Since our observations were made very far downwind from the fires, this suggests very large-scale impacts of boreal wildfires both on direct radiative forcing by BC and on tropospheric NO_x and O_3 budgets. Recent studies have shown a positive trend in the amount of areas burned over recent decades [*Gillett et al.*, 2004; *Kasischke and Turetsky*, 2006], likely as a result of warmer and drier conditions in the boreal region [*Hassol*, 2004], and possibly in combination with direct human impacts [*Mollicone et al.*, 2006]. Global Circulation Models predict more frequent and more severe fires as the climate changes [*Stocks et al.*, 1998; *Flannigan et al.*, 2000]. Thus, the impact of boreal wildfires may become even more important in the near future.

Chapter 4

Summary and Conclusions

This work demonstrates the significance of the impact of long-range transport of boreal wildfire and anthropogenic emissions on the nitrogen oxides levels and their seasonal variation over the central North Atlantic lower FT.

A high-sensitivity instrument developed at Michigan Tech was modified and installed at the Pico Mountain station. The $NO_{x,y}$ system was used to measure the NO, NO_2 and NO_y mixing ratios presented in this work. These measurements were analyzed in combination with simultaneous observations of CO, O_3, aerosol BC and meteorological parameters made at the Pico Mountain station. In addition, HYSPLIT backward trajectories, FLEXPART simulations and results from two GCT models (MOZART and GEOS-Chem) were used to analyze the data.

Measurements of nitrogen oxides from July 2002 to August 2005 at the Pico Mountain observatory provide full seasonal coverage of observations over the central North Atlantic lower FT. The NO, NO_x and NO_y measurements were analyzed to determine the seasonal variation of nitrogen oxides levels over the central North Atlantic lower FT and assess the processes controlling these levels. In particular, the data were analyzed to determine the impacts of transport of emissions from the boreal region and the U.S. on the nitrogen oxides and the further implications for the hemispheric NO_x

and O_3 budgets. The main results of these analyses are presented below, followed by a summary of the overall conclusions and future research.

4.1 Seasonal Variation of Nitrogen Oxides

Measurements at the Pico Mountain station show the presence of a clear seasonal variation of nitrogen oxides over the central North Atlantic lower FT, with higher levels during the summer season. Long-range transport of emissions in combination with removal processes en-route are responsible for the observed NO_x and NO_y levels at the measurement site.

Observations of NO_x and NO_y and estimates of PAN and HNO_3 indicate that reactive nitrogen over the central North Atlantic lower FT largely exist in the form of HNO_3 and PAN ($\sim$80–90% of NO_y). A change in the composition of NO_y from dominance of PAN to dominance of HNO_3 occurs from winter–spring to summer–fall over the central North Atlantic region, as a result of changes in temperature and photochemistry over the region.

The large presence of HNO_3 (53–71% of NO_y) during the summer and a significant removal of NO_y (expected via HNO_3) during transport to the measurement site suggest that oxidation of NO_x released from PAN in the airmasses during subsidence, or advection over the ocean with minimal removal, results in a significant source of HNO_3 over the central North Atlantic lower FT. The decomposition of PAN in the airmasses during transport suggests an important impact on the O_3 production as released NO_x is available to form O_3 before it oxidizes to HNO_3.

4.2 Impacts of Boreal Wildfire Emissions

Boreal wildfire emissions significantly impact the nitrogen oxides levels over the central North Atlantic lower FT. These emissions are responsible for significant shifts in

the nitrogen oxides distributions toward higher levels during the summer. Observations of NO_x and NO_y at the Pico Mountain station show that summertime medians of NO_y and NO_x were, respectively, 117–175 pptv and 9–30 pptv greater with the presence of boreal wildfire emissions. The extreme levels of NO_x (up to 150 pptv) and NO_y (up to 1100 pptv) observed in boreal wildfire plumes suggest that decomposition of PAN to NO_x is a significant source of NO_x, and imply that O_3 formation occurs during transport. Ozone levels are also significantly enhanced in boreal wildfire plumes. However, a complex behavior of O_3 is observed in the plumes, which varies from significant to lower O_3 production to O_3 destruction.

Observed $\Delta NO_y/\Delta CO$ and $\Delta O_3/\Delta CO$ ratios at the Pico Mountain station and estimates of total boreal wildfire CO emissions indicate that boreal wildfires may result in a source of NO_x and O_3 of 0.12–0.24 Tg NO_y (as N) and 19–21 Tg O_3. This estimated source of NO_x emissions from boreal wildfires was comparable to the contribution of U.S. anthropogenic NO_x emissions, and the estimated monthly O_3 production from the wildfires is about 10–20% of the previously estimated net tropospheric O_3 production rate in the northern middle and high latitudes. In addition, aerosol BC measurements were also significantly impacted by boreal wildfires. These results provide evidence of the very large-scale impact on the tropospheric NO_x and O_3 budgets and the direct radiative forcing of the atmosphere by light-absorbing particles.

4.3 Impacts of Anthropogenic Emissions

Transport of pollution from North America causes significant enhancements on nitrogen oxides levels all year round. Enhancements of CO, NO_y and NO_x indicate that, consistent with previous studies, the majority (95–97%) of the NO_x emitted over the eastern U.S. is removed before and during export out of the U.S. BL. However, a comparison of the estimated NO_y transport efficiencies to those previously estimated

upwind from the Pico Mountain station, indicate that about 30% of the emissions exported out of the U.S. boundary layer in the sampled air masses is efficiently transported to the central North Atlantic lower FT. Since the lifetime of NO_x is shorter than the transport timescale, PAN decomposition and potentially photolysis of HNO_3 constitute a supply of NO_x over the central North Atlantic lower FT, in particular during the fall season.

While GCT models indicate that most of the net O_3 production occurs near North America [*e.g. Li et al.*, 2004], the observed $\Delta O_3/\Delta NO_y$ suggests that a substantial amount of additional ozone formation occurs in the anthropogenic plumes during transport to the central North Atlantic lower FT. Large levels of NO_y remaining in the North American plumes suggest a potential O_3 formation well downwind from North America. For example, based on the average $\Delta NO_y/\Delta CO$ ratio observed at the Pico Mountain station, the eastern U.S. CO emissions and estimates of the O_3 production efficiency, this work indicates that 1.8–3 Gmol of O_3 are produced downwind per day as a result of the transport of nitrogen oxides. This estimated source of O_3 may be comparable as the direct export of O_3 produced within the U.S. BL.

4.4 Conclusions and Additional Research

The findings of this work provide an understanding of the seasonal variation and the magnitude of the nitrogen oxides over the central North Atlantic lower FT. In addition, this work provides evidence of the very large-scale impacts of boreal wildfire emissions on the nitrogen oxides and O_3 levels during the summer season, and the significant influence of anthropogenic pollution from North America over the central North Atlantic lower FT all year round.

These measurements, analyses and results motivate future research. First, these measurements suggest that NO_x levels over the central North Atlantic lower FT are significantly influenced by decomposition of PAN, in particular PAN produced

from boreal wildfire NO_x emissions. Therefore, additional measurements of PAN are recommended at the Pico Mountain station in order to determine to what degree the export of PAN from North America and boreal wildfires is responsible for the observed NO_x.

Second, NO_2 observations at the Pico Mountain station show the absence of a negative diurnal variation or no variation of NO_2, which result in the presence of a diurnal cycle for NO_x. This behavior was present all year round and was not well understood, in particular for winter and spring. Thus, additional measurements and analysis are recommended to clarify the unknown source of NO_2 during the daytime.

Third, this study shows the complex behavior of O_3 in the boreal wildfire plumes. An in-situ photochemical modeling analysis using measurements in boreal wildfire plumes at the Pico Mountain station is needed to further understand the behavior of O_3 in the wildfire plumes, and also to determine whether the observed NO_x levels may explain the significant impacts of boreal wildfires on the O_3 background.

Fourth, further research is needed to quantify the ultimate impact of North American outflow on the O_3 photochemical tendency over the central North Atlantic lower FT. An in-situ modeling analysis constrained by measurements and conditions at the Pico Mountain station can be used for this purpose. This analysis could also be applied to understand how the photochemical perturbations caused by boreal wildfire emissions and by anthropogenic emissions differ from one another.

Finally, this work was focused on the impacts of anthropogenic emissions from North America. However, significant emissions from Asia and Europe reach the central North Atlantic region. Additional research is recommended to assess the influence of these sources in the lower FT over the Atlantic and their relative importance.

References

Alley, R., et al., *Climate Change 2007: The Physical Science Basis. Contribution of Working Group I to the Fourth Assessment Report of the Intergovernmental Panel on Climate Change*, in press, 2007.

Andreae, M., and P. Merlet, Emissions from trace gases and aerosols from biomass burning, *Global Biogeochem. Cycles*, *15*, 955–966, 2001.

Atlas, E. L., et al., Partitioning and budget of NO_y species during the Mauna Loa observatory photochemistry experiment, *J. Geophys. Res.*, *97*, 10,449–10,462, 1992.

Auvray, M., and I. Bey, Long-range transport to Europe: Seasonal variations and implications for the European ozone budget, *J. Geophys. Res.*, *110*, 2005.

Auvray, M., I. Bey, E. Llull, M. G. Schultz, and S. Rast, A model investigation of tropospheric ozone chemical tendencies in long-range transported pollution plumes, *J. Geophys. Res.*, *112*, 1–17, 2007, doi:10.1029/2006JD007137.

Bertschi, I. T., and D. A. Jaffe, Long-range transport of ozone, carbon monoxide, and aerosols to the NE Pacific troposphere during the summer of 2003: Observations of smoke plumes from Asian boreal fires, *J. Geophys. Res.*, *110*, 2005.

Bertschi, I. T., D. A. Jaffe, L. Jaeglé, H. U. Price, and J. B. Dennison, PHOBEA/ITCT 2002 airborne observations of transpacific transport of ozone, CO, volatile organic compounds, and aerosols to the northeast Pacific: Impacts of Asian anthropogenic and Siberian boreal fire emissions, *J. Geophys. Res.*, *109*, 2004.

Bey, I., et al., Global modeling of tropospheric chemistry with assimilated meteorology: Model description and evaluation, *J. Geophys. Res.*, *106*, 23,073–23,096, 2001.

Bollinger, M. J., R. E. Sievers, D. W. Fahey, and F. C. Fehsenfeld, Conversion of nitrogen dioxide, nitric acid, and n-propyl nitrate to nitric oxide by gold-catalyzed reduction with carbon monoxide, *Anal. Chem.*, *55*, 1980–1986, 1983.

Bond, T. C., and H. Sun, Can reducing black carbon emissions counteract global warming?, *Environ. Sci. Technol.*, *39*, 5921–5926, 2005, doi:10.1021/es0480421.

Bond, T. C., D. G. Streets, K. F. Yarber, S. M. Nelson, J.-H. Woo, and Z. Klimont, A technology-based global inventory of black and organic carbon emissions from combustion, *J. Geophys. Res.*, *109*, 1–43, 2004, doi:10.1029/2003JD003697.

Bradshaw, J., D. Davis, G. Grodzinsky, R. Newell, S. Sandholm, and S. Liu, Observed distributions of nitrogen oxides in the remote free troposphere from NASA global tropospheric Experiment programs, *Rev. Geophys.*, *38*, 61–116, 2000.

Brown, S. S., et al., Variability in nocturnal nitrogen oxide processing and its role in regional air quality, *Science*, *311*, 67 – 70, 2006.

Carroll, M. A., and A. M. Thompson, NO_x in the non-urban troposphere, in *Problems and Progress in Atmospheric Chemistry*, edited by J. R. Barker, vol. 3, World Scientific Publishing Company, 1995.

Chameides, W. L., The photochemistry of a remote marine stratiform cloud, *J. Geophys. Res.*, *89*, 4739–4755, 1984.

Chandra, S., J. R. Ziemke, X. Tie, and G. Brasseur, Elevated ozone in the troposphere over the Atlantic and Pacific oceans in the Northern Hemisphere, *Geophys. Res. Lett.*, *31*, 1–4, 2004.

Chatfield, R. B., and A. C. Delany, Convection links biomass burning to increased tropical ozone: However, models will tend to overpredict O_3, *J. Geophys. Res.*, *95*, 18,473–18,488, 1990.

Chin, M., D. J. Jacob, J. W. Munger, D. D. Parrish, and B. G. Doddridge, Relationship of ozone and carbon monoxide over North America, *J. Geophys. Res.*, *99*, 14,565–14,573, 1994.

Cox, R. A., Ozone and peroxy radical budgets in the marine boundary layer: Modeling the effect of NO_x, *J. Geophys. Res.*, *104*, 8047–8056, 1999.

Crutzen, P. J., The role of NO and NO_2, *Ann. Rev. Earth Planet. Sci.*, *7*, 443–472, 1979.

Damoah, R., N. Spichtinger, C. Forster, P. James, I. Mattis, U. Wandinger, S. Beirle, T. Wagner, and A. Stohl, Around the world in 17 days–hemispheric-scale transport of forest fire smoke from Russia in May 2003, *Atmos. Chem. and Phys.*, *4*, 1449–1471, 2004.

Damoah, R., et al., A case study of pyro-convection using transport model and remote sensing data, *Atmos. Chem. and Phys.*, *6*, 173–185, 2006.

de Gouw, J., C. Warneke, D. D. Parrish, J. S. Holloway, M. Trainer, and F. C. Fehsenfeld, Emission sources and ocean uptake of acetonitrile (CH_3CN) in the atmosphere, *J. Geophys. Res.*, *108*, 2003.

de Gouw, J. A., and E. R. Lovejoy, Reactive uptake of ozone by liquid organic compounds, *Geophys. Res. Lett.*, *25*, 931 – 934, 1998, doi:10.1029/98GL00515.

de Gouw, J. A., et al., Volatile organic compounds composition of merged and aged forest fire plumes from Alaska and western Canada, *J. Geophys. Res.*, *111*, 2006.

DeBell, L. J., R. W. Talbot, J. E. Dibb, J. W. Munger, E. V. Fischer, and S. E. Frolking, A major regional air pollution event in the northeastern United States caused by extensive forest fires in Quebec, Canada, *J. Geophys. Res.*, *109*, 2004.

Derwent, R., P. J. Simmonds, S. Seuring, and C. Dimmer, Observation and interpretation of the seasonal cycles in the surface concentrations of ozone and carbon monoxide at Mace Head, Ireland from 1990 to 1994, *Atmos. Environ.*, *32*, 145–157, 1998.

Derwent, R., D. Stevenson, W. Collins, and C. Johnson, Intercontinental transport and the origins of the ozone observed at surface sites in Europe, *Atmos. Environ.*, *38*, 1891–1901, 2004.

Dibb, J. E., E. Scheuer, S. I. Whitlow, M. Vozella, E. Williams, and B. M. Lerner, Ship-based nitric acid measurements in the Gulf of Maine during New England Air Quality Study 2002, *J. Geophys. Res.*, *109*, 1–13, 2004, doi:10.1029/2004JD004843.

DiNunno, B., et al., Central/eastern North Pacific photochemical precursors distributions for fall/spring seasons as defined by airborne field studies, *J. Geophys. Res.*, *108*, 10.1029/2001JD0010,044, 2003.

Draxler, R., and G. Rolph, HYSPLIT4 model (HYbrid Single-Particle Lagrangian Integrated Trajectory) model, Web address: http://www.arl.noaa.gov/ready/hysplit4.html, NOAA Air Resources Laboratory, Silver Spring, Maryland, 2003.

Duck, T. J., et al., Transport of forest fire emissions from Alaska and the Yukon Territory to Nova Scotia during summer 2004, *J. Geophys. Res.*, *112*, 1–13, 2007, doi:10.1029/2006JD007716.

Duncan, B., R. Martin, A. Staudt, R. Yevich, , and J. Logan, Interannual and seasonal variability of biomass burning emissions constrained by satellite observations, *J. Geophys. Res.*, *108*, 2003.

ECMWF, Users guide to ECMWF products 4.0, *Tech. Rep. Meteorological Bulletin M3.2*, European Center for Medium-Range Weather Forecasts (ECMWF), Reading, UK, 2005.

Edwards, D. P., et al., Observations of carbon monoxide and aerosols from the Terra satellite: Northern Hemisphere variability, *J. Geophys. Res.*, *109*, 2004.

EMEP, European monitoring and evaluation program (EMEP), transboundary air pollution in Europe I: Emissions, dispersion and trends of acidifying and eutrophying agents, *Tech. Rep. EMEP/MSC-W Rep. 1/97*, EMEP, 1997.

Emmons, L., et al., Climatologies of NO_x and NO_y: A comparison of data and models, *Atmos. Environ.*, *31*, 1851–1904, 1997.

Emmons, L. K., D. A. Hauglustaine, J.-J. Müller, M. A. Carroll, G. P. Brasseur, D. Brunner, J. Staehelin, V. Thouret, and A. Marenco, Data composites of airborne observations of tropospheric ozone and its precursors, *J. Geophys. Res.*, *105*, 20,497–20,538, 2000.

Emmons, L. K., et al., Budget of tropospheric ozone during TOPSE from two chemical transport models, *J. Geophys. Res.*, *108*, 2003.

EPA, National air pollutant emission trends, 1990–1997, *Tech. Rep. EPA 454/R-97-011*, Environmental Protection Agency, 1997.

Fahey, D. W., C. S. Eubank, G. Hubler, and F. C. Fehsenfeld, Evaluation of a catalytic reduction technique for the measurement of total reactive odd-nitrogen NO_y in the atmosphere, *J. Atmos. Chem.*, *3*, 435–468, 1985.

Fan, S., et al., Origin of tropospheric NO_x over subarctic eastern Canada in summer, *J. Geophys. Res.*, *99*, 16,867 – 16,878, 1994, doi:10.1029/94JD01122.

Fehsenfeld, F. C., et al., International Consortium for Atmospheric Research on Transport and Transformation (ICARTT): North America to Europe: Overview of the 2004 summer field study, *J. Geophys. Res.*, *111*, 1–36, 2006, doi:10.1029/2006JD007829.

Fialho, P., A. D. A. Hansen, and R. E. Honrath, Absorption coefficients by aerosols in remote areas: A new approach to decouple dust and black carbon absorption coefficients using seven-wavelength aethalometer data, *J. Aerosol Sci.*, *36*, 267–282, 2005.

Fischer, H., et al., Trace gas measurements during the Oxidizing Capacity of the Tropospheric Atmosphere campaign 1993 at Izaña, *J. Geophys. Res.*, *103*, 13,505–13,518, 2004.

Fishman, J., S. Solomon, and P. J. Crutzen, Observational and theoretical evidence in support of a significant in-situ photochemical source of tropospheric ozone, *Tellus*, *31*, 432–446, 1979.

Flannigan, M., B. Stocks, and B. Wotton, Climate change and forest fires, *Sci. Tot. Env.*, *262*, 221–229, 2000.

Flocke, F., et al., Results from fast airborne measurements of PANs during the 2004 New England Air Quality Study, *Eos Trans. AGU*, *86*, 2005, abstract A54C-03.

Forster, C., et al., Transport of boreal forest fire emissions from Canada to Europe, *J. Geophys. Res.*, *106*, 22,887–22,906, 2001.

Fromm, M., R. Bevilacqua, R. Servranckx, J. Rosen, J. P. Thayer, J. Herman, and D. Larko, Pyro-cumulonimbus injection of smoke to the stratosphere: Observations and impact of a super blowup in northwestern Canada on 3–4 August 1998, *J. Geophys. Res.*, *110*, 1–16, 2005, doi:10.1029/2004JD005350.

Gao, R. S., E. R. Keim, E. L. Woodbridge, S. J. Cicora, M. H. Proffitt, T. L. Thompson, R. J. Mclaughlin, and D. W. Fahey, New photolysis system for NO_2 measurements in the lower stratosphere, *J. Geophys. Res.*, *99*, 20,673–20,681, 1994.

Garrett, T. J., L. Avey, P. I. Palmer, A. Stohl, J. A. Neuman, C. A. Brock, T. B. Ryerson, and J. S. Holloway, Quantifying wet scavenging processes in aircraft observations of nitric acid and cloud condensation nuclei, *J. Geophys. Res.*, *111*, 1–12, 2006, doi:10.1029/2006JD007416.

Gillett, N., A. J. Weaver, F. W. Zwiers, and M. D. Flannigan, Detecting the effect of climate change on Canadian forest fires, *Geophys. Res. Lett.*, *31*, 2004.

Goode, J. G., R. J. Yokelson, D. E. Ward, R. A. Susott, R. E. Babbitt, M. A. Davies, and W. M. Hao, Measurements of excess O_3, CO, CO_2, CH_4, C_2H_6, C_2H_4, HCN, NO, NH_3, HCOOH, CH_3COOH, HCHO and CH_3OH in 1997 Alaskan biomass burning plumes by airborne Fourier transform infrared spectroscopy (AFTIR), *J. Geophys. Res.*, *105*, 22,147–22,166, 2000.

Griffin, R. J., III, R. C. Flagan, and J. H. Seinfeld, Organic aerosol formation from the oxidation of biogenic hydrocarbons, *J. Geophys. Res.*, *104*, 3555–3568, 1999, doi:10.1029/1998JD100049.

Hangal, S., and K. Willeke, Overall efficiency of tubular inlets sampling at 0–90 degrees from horizontal aerosol flows, *Atmos. Environ.*, *24A*, 2379–2386, 1990.

Hansen, J., M. Sato, R. Ruedy, A. Lacis, and V. Oinas, Global warming in the twenty-first century: An alternative scenario, *Proc. Natl. Acad. Sci. USA*, *97*, 9875–9880, 2000.

Hassol, S. J., *Impacts of a warming Arctic: Arctic climate impact assessment*, Cambridge University Press, 2004.

Honrath, R. E., R. C. Owen, M. Val Martín, J. S. Reid, K. Lapina, P. Fialho, M. P. Dziobak, J. Kleissl, and D. L. Westphal, Regional and hemispheric impacts of anthropogenic and biomass burning emissions on summertime CO and O_3 in the North Atlantic lower free troposphere, *J. Geophys. Res.*, *109*, 2004.

Horowitz, L. W., J. Liang, G. M. Gardner, and D. J. Jacob, Export of reactive nitrogen from North America during summertime: Sensitivity to hydrocarbon chemistry, *J. Geophys. Res.*, *103*, 13,451–13,476, 1998.

Horowitz, L. W., et al., A global simulation of tropospheric ozone and related tracers: Description and evaluation of MOZART, version 2, *J. Geophys. Res.*, 2003.

Hudman, R. C., et al., Surface and lightning sources of nitrogen oxides over the United States: magnitudes, chemical evolution, and outflow, *J. Geophys. Res.*, 2007.

Jacob, D., et al., Summertime photochemistry of the troposphere at high northern latitudes, *J. Geophys. Res.*, *97*, 16,421–16,431, 1992.

Jacob, D. J., J. A. Logan, G. M. Gardner, R. M. Yevich, C. M. Spivakovsky, S. C. Wofsy, S. Sillman, and M. J. Prather, Factors regulating ozone over the United States and its export to the global atmosphere, *J. Geophys. Res.*, *98*, 14,817 – 14,826, 1993, doi:10.1029/93JD01224.

Jaeglé, L., L. Steinberger, R. V. Martin, and K. Chance, Global partitioning of NO_x sources using satellite observations: Relative roles of fossil fuel combustion, biomass burning and soil emissions, *Faraday Discuss.*, *130*, 407–423, 2005.

Jaffe, D., H. Price, D. Parrish, A. Goldstein, and J. Harris, Increasing background ozone during spring on the west coast of North America, *Geophys. Res. Lett.*, *30*, 2003.

Jaffe, D., I. Bertschi, L. Jaeglé, P. Novelli, J. S. Reid, H. Tanimoto, R. Vingarzan, and D. L. Westphal, Long-range transport of Siberian biomass burning emissions and impact on surface ozone in western North America, *Geophys. Res. Lett.*, *31*, 2004.

Jain, A. K., Z. Tao, X. Yang, and C. Gillespie, Estimates of global biomass burning emissions for reactive greenhouse gases (CO, NMHCs, and NO_x) and CO_2, *J. Geophys. Res.*, *111*, 2006.

Kasischke, E. S., and M. R. Turetsky, Recent changes in the fire regime across the North American boreal region—Spatial and temporal patterns of burning across Canada and Alaska, *Geophys. Res. Lett.*, *33*, 2006.

Kasischke, E. S., E. J. Hyer, P. C. Novelli, L. P. Bruhwiler, N. H. F. French, A. I. Suckhinin, J. H. Hewson, and B. J. Stocks, Influences of boreal fire emissions on Northern Hemisphere atmospheric carbon and carbon monoxide, *Global Biogeochem. Cycles*, *19*, 2005.

Kleissl, J., R. Honrath, M. Dziobak, D. Tanner, M. Val Martín, R. Owen, and D. Helmig, The occurrence of upslope flows at the Pico mountaintop observatory: A case study of orographic flows on small, volcanic island, *J. Geophys. Res.*, *112*, 2007.

Kley, D., and M. McFarland, Chemiluminescence detector for NO and NO_2, *Atmos. Tech.*, *12*, 63–69, 1980.

Kliner, D., B. Daube, J. Burley, and S. Wofsey, Laboratory investigation of the catalytic reduction technique for measurement of atmospheric NO_y, *J. Geophys. Res.*, *102*, 10,759–10,776, 1997.

Klonecki, A., and H. Levy, Tropospheric chemical ozone tendencies in CO-CH4-NOy-H2O system: Their sensitivity to variations in environmental parameters and their application to a global chemistry transport model study, *J. Geophys. Res.*, *102*, 21,221–21,237, 1997.

Kondo, Y., et al., Profiles and partitioning of reactive nitrogen over the Pacific Ocean in winter and early spring, *J. Geophys. Res.*, *102*, 28,405–28,424, 1997.

Lapina, K., R. E. Honrath, R. C. Owen, M. Val Martín, and G. Pfister, Evidence of significant large-scale impacts of boreal fires on ozone levels in the midlatitude Northern Hemisphere free troposphere, *Geophys. Res. Lett.*, 2006.

Lawrence, M. G., and P. J. Crutzen, The impact of cloud particle gravitational settling on soluble trace gas distributions, *Tellus*, *50B*, 263–289, 1998.

Lawrence, M. G., and P. J. Crutzen, Influence of NO_x emissions from ships on tropospheric photochemistry and climate, *Nature*, *33*, 167–170, 1999.

Leue, C., M. Wenig, T. Wagner, O. Klimm, U. Platt, and B. Jahne, Qualitative analysis of NO_x emissions from global ozone monitoring experiment satellite image sequences, *J. Geophys. Res.*, *106*, 5493–5505, 2001.

Leung, F.-Y. T., J. A. Logan, R. Park, E. Hyer, E. Kasischke, D. Streets, and L. Yurganov, Impacts of enhanced biomass burning in the boreal forests in 1998 on tropospheric chemistry and the sensitivity of model results to the injection height of emissions, *J. Geophys. Res.*, *112*, 1–15, 2007, doi:10.1029/2006JD008132.

Levy II, H., Normal atmosphere: Large radical and formaldehyde concentrations predicted, *Science*, *173*, 141–143, 1971.

Li, Q., D. Jacob, J. Munger, R. Yantosca, and D. Parrish, Export of NO_y from the North American boundary layer: Reconciling aircraft observations and global model budgets, *J. Geophys. Res.*, *109*, 10.1029/2003JD004,086, 2004.

Li, Q., et al., Transatlantic transport of pollution and its effects on surface ozone in Europe and North America, *J. Geophys. Res.*, *107*, 2002.

Liang, J., L. W. Horowitz, D. J. Jacob, Y. Wang, A. M. Fiore, J. A. Logan, G. M. Gardner, and J. W. Munger, Seasonal budgets of reactive nitrogen species and ozone over the United States and export fluxes to the global atmosphere, *J. Geophys. Res.*, *103*, 13,435–13,450, 1998.

Lin, X., M. Trainer, and S. C. Liu, On the nonlinearity of the tropospheric ozone production, *J. Geophys. Res.*, *93*, 15,879–15,888, 1988.

Liu, S. C., M. Trainer, F. C. Fehsenfeld, D. D. Parrish, E. J. Williams, D. W. Fahey, G. Hübler, and P. C. Murphy, Ozone production in the rural troposphere and the implications for regional and global ozone distributions, *J. Geophys. Res.*, *92*, 4191–4207, 1987.

Liu, S. C., et al., A study of the photochemistry and ozone budget during the Mauna Loa Observatory photochemistry experiment, *J. Geophys. Res.*, *97*, 10,463–10,471, 1992.

Liu, X., et al., First directly retrieved global distribution of tropospheric column ozone from GOME: Comparison with the GEOS-CHEM model, *J. Geophys. Res.*, *111*, 1–17, 2006, doi:10.1029/2005JD006564.

Logan, J. A., Nitrogen oxides in the troposphere: Global and regional budgets, *J. Geophys. Res.*, *88*, 10,785–10,807, 1983.

Martin, R. V., et al., Validation of GOME satellite measurements of tropospheric NO_2 and HCHO using regional data from aircraft campaigns in the southeastern United States, *J. Geophys. Res.*, *109*, 2004.

Martin, R. V., et al., Evaluation of space-based constraints on global nitrogen oxide emissions with regional aircraft measurements over and downwind of eastern North America, *J. Geophys. Res.*, *111*, 1–15, 2006, doi:10.1029/2005JD006680.

Mauzerall, D. L., D. J. Jacob, S. M. Fan, J. D. Bradshaw, G. L. Gregory, G. W. Sachse, and D. R. Blake, Origin of tropospheric ozone at remote high northern latitudes in summer, *J. Geophys. Res.*, *101*, 4175–4188, 1996.

Mauzerall, D. L., et al., Photochemistry in biomass burning plumes and implications for tropospheric ozone over the tropical South Atlantic, *J. Geophys. Res.*, *103*, 8401–8423, 1998.

McKeen, S. A., G. Wotawa, D. D. Parrish, J. S. Holloway, M. P. Buhr, G. Hübler, F. C. Fehsenfeld, and J. F. Meagher, Ozone production from Canadian wildfires during June and July of 1995, *J. Geophys. Res.*, *107*, 2002.

Merrill, J. T., and J. L. Moody, Synoptic meteorology and transport during the North Atlantic Regional Experiment (NARE) intensive: Overview, *J. Geophys. Res.*, *101*, 28,903–28,921, 1996.

Miyazaki, Y., et al., Contribution of particulate nitrate to airborne measurements of total reactive nitrogen, *J. Geophys. Res.*, *110*, 1–11, 2005, doi:10.1029/2004JD005502.

Mollicone, D., H. Eva, and F. Achard, Human role in Russian wildfires, *Nature*, *440*, 436–437, 2006.

Morris, G., et al., Alaskan and Canadian forest fires exacerbate ozone pollution over Houston, Texas, on 19 and 20 July 2004, *J. Geophys. Res.*, *111*, 2006.

Moxim, W. J., H. Levy, and P. S. Kasibhatla, Simulated global tropospheric PAN: Its transport and impact, *J. Geophys. Res.*, *101*, 12,621–12,638, 1996.

Nesbitt, S. W., R. Whang, and R. Orville, Seasonal and global no production by lightning estimated from the Optical Transient Detector (OTD), *J. Geophys. Res.*, *52*, 1206–1215, 2000.

Neuman, J. A., et al., Reactive nitrogen transport and photochemistry in urban plumes over the North Atlantic ocean, *J. Geophys. Res.*, *111*, 1–11, 2006, doi:10.1029/2005JD007010.

Novelli, P. C., L. P. Steele, and P. P. Tans, Mixing ratios of carbon monoxide in the troposphere, *J. Geophys. Res.*, *97*, 20,731–20,750, 1992.

Novelli, P. C., K. A. Masarie, P. M. Lang, B. D. Hall, R. C. Myers, and J. W. Elkins, Reanalysis of tropospheric CO trends: Effects of the 1997–1998 wildfires, *J. Geophys. Res.*, *108*, 2003.

Olivier, J., and J. Berdowski, Global emissions sources and sinks, in *The Climate System*, edited by J. Berdowski, R. R. Guicherit, and B. Heij, vol. 33–78, A.A. Balkema Publishers / Swets and Zeitlinger Publishers, Lisse, The Netherlands, 2001.

Olszyna, K. J., E. M. Bailey, R. Simonaitis, and J. F. Meagher, O_3 and NO_y relationships at a rural site, *J. Geophys. Res.*, *99*, 14,557–14,563, 1994.

Owen, R. C., O. R. Cooper, A. Stohl, and R. E. Honrath, An analysis of the mechanisms of North American pollutant transport to the central North Atlantic lower free troposphere, *J. Geophys. Res.*, *111*, 2006.

Park, R. J., et al., Export efficiency of black carbon aerosol in continental outflow: Global implications, *J. Geophys. Res.*, *110*, 1–7, 2005, doi:10.1029/2004JD005432.

Parrish, D. D., and F. C. Fehsenfeld, Methods for gas-phase measurements of ozone, ozone precursors and aerosol precursors, *Atmos. Environ.*, *34*, 1921–1957, 2000.

Parrish, D. D., J. S. Holloway, and F. C. Fehsenfeld, Routine, continuous measurement of carbon monoxide with parts per billion precision, *Environ. Sci. Technol.*, *28*, 1615–1618, 1994.

Parrish, D. D., M. Trainer, J. S. Holloway, J. E. Yee, M. S. Warshawsky, F. C. Fehsenfeld, G. Forbes, and J. L. Moody, Relationships between ozone and carbon monoxide at surface sites in the North Atlantic region, *J. Geophys. Res.*, *103*, 13,357–13,376, 1998.

Parrish, D. D., et al., Measurements of the NO_x-O_3 photostationary state at Niwot Ridge, Colorado, *J. Geophys. Res.*, *91*, 5361–5370, 1986.

Parrish, D. D., et al., Systematic variations in the concentration of NO_x (NO plus NO_2) at Niwot Ridge, Colorado, *J. Geophys. Res.*, *95*, 1817–1836, 1990.

Parrish, D. D., et al., Fraction and composition of NO_y transported in air masses lofted from the North American boundary layer, *J. Geophys. Res.*, *109*, 2004.

Peterson, M. C., and R. E. Honrath, NO_x and NO_y over the northwestern North Atlantic: Measurements and measurement accuracy, *J. Geophys. Res.*, *104*, 11,695–11,707, 1999.

Peterson, M. C., R. E. Honrath, D. D. Parrish, and S. J. Oltmans, Measurements of nitrogen oxides and a simple model of NO_y fate in the remote North Atlantic marine atmosphere, *J. Geophys. Res.*, *103*, 13,489–13,503, 1998.

Pfister, G., P. G. Hess, L. K. Emmons, J. Lamarque, C. Wiedinmyer, D. P. Edwards, G. Petron, J. C. Gille, and G. W. Sachse, Quantifying CO emissions from the 2004 Alaskan wildfires using MOPITT CO data, *Geophys. Res. Lett.*, 2005.

Pfister, G. G., et al., Ozone production from the 2004 North American boreal fires, *J. Geophys. Res.*, *111*, 1–13, 2006, doi:10.1029/2006JD007695.

Real, E., et al., Processes influencing ozone levels in Alaskan forest fire plumes during long-range transport over the North Atlantic, *J. Geophys. Res.*, *112*, 1–19, 2007, doi:10.1029/2006JD007576.

Reeves, C. E., et al., Potential for photochemical ozone formation in the troposphere over the North Atlantic as derived from aircraft observations during ACSOE, *J. Geophys. Res.*, *107*, 10.1029/2002JD002,415, 2002.

Reeves, C. E., et al., Alkyl nitrates in outflow from North America over the North Atlantic during Intercontinental Transport of Ozone and Precursors 2004, *J. Geophys. Res.*, *112*, 1–21, 2007, doi:10.1029/2006JD007567.

Reid, J. S., R. Koppmann, T. F. Eck, and D. P. Eleuterio, A review of biomass burning emissions part II: Intensive physical properties of biomass burning particles, *Atmos. Chem. and Phys.*, *5*, 799–825, 2005.

Richter, A., J. Burrows, H. Nub, C. Granier, and U. Niemeier, Increase in tropospheric nitrogen dioxide over China observed from space, *Nature*, *437*, 129–132, 2005.

Ridley, B., et al., Measurements of NO_x and PAN and estimates of O_3 production over the seasons during Mauna Lao Observatory Photochemistry Experiment 2, *J. Geophys. Res.*, *103*, 8323–8339, 1998.

Ridley, B. A., and F. E. Grahek, A small, low flow, high sensitivity reaction vessel for NO chemiluminescence detectors, *J. Atmos. Tech.*, *7*, 307–311, 1990.

Ridley, B. A., J. G. Walega, J. E. Dye, and F. E. Grahek, Distributions of NO, NO_x, NO_y, and O_3 to 12 km altitude during the summer monsoon season over New Mexico, *J. Geophys. Res.*, *99*, 25,519–25,534, 1994.

Roberts, J. M., et al., Episodic removal of NO_y species from the marine boundary layer over the North Atlantic, *J. Geophys. Res.*, *101*, 28,947–28,960, 1996.

Sander, S. P., et al., Chemical kinetics and photochemical data for use in atmospheric studies evaluation number 14, *Tech. Rep. JPL Publication 02-25*, NASA Jet Propulsion Laboratory, 2003.

Sandholm, S. T., et al., Summertime tropospheric observations related to N_xO_y distributions and partitioning over Alaska: Arctic Boundary Layer Expedition 3A, *J. Geophys. Res.*, *97*, 16,481–16,509, 1992.

Seibert, P., and A. Frank, Source-receptor matric calculation with a Lagrangian particle disperion model in backward mode, *Atmos. Chem. and Phys.*, *4*, 51–63, 2004.

Simmonds, P. G., R. G. Derwent, A. L. Manning, and G. Spain, Significant growth in surface ozone at Mace Head, Ireland, 1987–2003, *Atmos. Environ.*, *38*, 4769–4778, 2004.

Simmonds, P. G., A. J. Manning, R. G. Derwent, P. Ciais, M. Ramonet, V. Kazan, and D. Ryall, A burning question. Can recent growth rate anomalies in the greenhouse gases be attributed to large-scale biomass burning events?, *Atmos. Environ.*, *39*, 2513–2517, 2005.

Singh, H. B., Reactive nitrogen in the troposphere, *Env. Sci. Tech.*, *21*, 320–327, 1987.

Singh, H. B., et al., Summertime distribution of PAN and other reactive nitrogen species in the northern high-latitude atmosphere of eastern Canada, *J. Geophys. Res.*, *99*, 1821–1835, 1994.

Singh, H. B., et al., Reactive nitrogen distribution and partitioning in the North American troposphere and lowermost stratosphere, *J. Geophys. Res.*, *112*, 2007.

Spichtinger, N., M. Wenig, P. James, T. Wagner, U. Platt, and A. Stohl, Satellite detection of a continental-scale plume of nitrogen oxides from boreal forest fires, *Geophys. Res. Lett.*, *28*, 4579–4582, 2001.

Spivakovsky, C. M., et al., Three-dimensional climatological distribution of tropospheric OH: Update and evaluation, *J. Geophys. Res.*, *105*, 8931–8980, 2000.

Stocks, B., et al., Climate change and forest fire potential in Russian and Canadian boreal forests, *Clim. Change*, *38*, 1–13, 1998.

Stohl, A., Computation, accuracy and applications of trajectories—a review and bibliography, *Atmos. Environ.*, *32*, 947–966, 1998.

Stohl, A., M. Trainer, T. Ryerson, J. Hollaway, and D. Parrish, Export of NO_y from the North American boundary layer during 1996 and 1997 North Atlantic Regional Experiments, *J. Geophys. Res.*, *107*, 10.1029/2001JD000,519, 2002.

Stohl, A., C. Forster, A. Frank, P. Seibert, and G. Wotawa, Technical note: The Lagrangian particle dispersion model FLEXPART version 6.2, *Atmos. Chem. and Phys.*, *5*, 2461–2474, 2005, sRef-ID:1680-7324/acp/2005-5-2461.

Stohl, A., et al., The influence of stratospheric intrusions on alpine ozone concentrations, *Atmos. Environ.*, *34*, 1323–1354, 2000.

Stohl, A., et al., Rapid intercontinental air pollution transport associated with a meteorological bomb, *Atmos. Chem. and Phys.*, *3*, 969–985, 2003.

Stohl, A., et al., Pan-arctic enhancements of light absorbing aerosol concentrations due to North American boreal forest fires during summer 2004, *J. Geophys. Res.*, *111*, 1–20, 2006, doi:10.1029/2006JD007216.

Talbot, R. W., et al., Summertime distribution and relations of reactive odd nitrogen species and NO_y in the troposphere over Canada, *J. Geophys. Res.*, *99*, 1863–1885, 1994.

Tanimoto, H., Y. Kajii, J. Hirokawa, H. Akimoto, and N. P. Minko, The atmospheric impact of boreal forest fires in far eastern Siberia on the seasonal variation of carbon monoxide: Observations at Rishiri, a northern remote island in Japan, *J. Geophys. Res.*, *27*, 4073–4076, 2000.

Thakur, A. N., H. B. Singh, P. Mariani, Y. Chen, Y. Wang, D. J. Jacob, G. Brasseur, J.-F. Müller, and M. Lawrence, Distribution of reactive nitrogen species in the remote free troposphere: data and model comparisons, *Atmos. Environ.*, *33*, 1403–1422, 1999.

Thompson, A. M., et al., Intercontinental Chemical Transport Experiment Ozonesonde Network Study (IONS) 2004: 1.Summertime upper troposphere/lower stratosphere ozone over northeastern North America, *J. Geophys. Res.*, *112*, 1–15, 2007, doi:10.1029/2006JD007441.

Trainer, M., et al., Correlation of ozone with NO_y in photochemically aged air, *J. Geophys. Res.*, *98*, 2917–2925, 1993.

Turquety, S., et al., Inventory of boreal fire emissions for North America in 2004: Importance of peat burning and pyroconvective injection, *J. Geophys. Res.*, *112*, 1–13, 2007, doi:10.1029/2006JD007281.

Val Martín, M., Transport of ozone and nitrogen oxides from North America over the North Atlantic region, Master's thesis, Michigan Technological University, 2002.

Val Martin, M., R. Honrath, R. C. Owen, G. Pfister, P. Fialho, and F. Barata, Significant enhancements of nitrogen oxides, ozone and aerosol black carbon in the North Atlantic lower free troposphere resulting from North American boreal wildfires, *J. Geophys. Res.*, *111*, 2006.

Wang, Y., et al., Springtime photochemistry at northern mid and high latitudes, *J. Geophys. Res.*, *108*, 10.1029/2002JD002,227, 2003.

Wenig, M., N. Spichtinger, A. Stohl, G.Held, S. Beirle, T. Wagner, B. Jähne, and U. Platt, Intercontinental transport of nitrogen oxide pollution plumes, *Atmos. Chem. and Phys.*, *3*, 387–393, 2003.

Wofsy, S. C., S.-M. Fan, D. R. Blake, J. D. Bradshaw, S. T. Sandholm, H. B. Singh, G. W. Sachse, and R. C. Harriss, Factors influencing atmospheric composition over subarctic North America during summer, *J. Geophys. Res.*, *99*, 1887–1897, 1994.

Wofsy, S. C., et al., Atmospheric chemistry in the Arctic and subarctic: Influence of natural fires, industrial emissions, and stratospheric inputs, *J. Geophys. Res.*, *97*, 16,731–16,746, 1992.

Wotawa, G., and M. Trainer, The influence of Canadian forest fires on pollutant concentrations in the United States, *Science*, *288(5464)*, 324–328, 2000.

Yamamoto, M., M. Tamaki, H. Bandow, and Y. Maeda, HNO_3 analyzer by scrubber difference and the NO–O_3 chemiluminescence method, *Atmos. Environ.*, *35*, 5339–5346, 2001.

Yang, J., et al., Impacts of snowpack emissions on deduced levels of OH and peroxy radicals at Summit, Greenland, *Atmos. Environ.*, *36*, 2523–2534, 2002.

Yienger, J. J., A. A. Klonecki, H. Levy II, W. J. Moxim, and G. R. Carmichael, An evaluation of chemistry's role in the winter–spring ozone maximum found in the northern midlatitude free troposphere, *J. Geophys. Res.*, *104*, 3655–3667, 1999.

Yokelson, R. J., D. W. T. Griffith, and D. E. Ward, Open-path fourier transform infrared studies of large-scale laboratory biomass fires, *J. Geophys. Res.*, *101*, 21,067–21,080, 1996, doi:10.1029/96JD01800.

Zellweger, C., J. Forrer, P. Hofer, S. Nyeki, B. Schwarzenbach, E.Weingartner, M. Ammann, , and U. Baltensperger, Partitioning of reactive nitrogen (NO_y) and dependence on meteorological conditions in the lower free troposphere, *Atmos. Chem. and Phys.*, *3*, 779–796, 2003.

Appendix A

Data Documentation

This appendix presents the documentation of the NO, NO_2 and NO_y measurements made at the Pico Mountain station from July 2002 to August 2005. The documentation is divided into four files:

1. PRE-ICARTT, which covers the data reduction from July 2002 to April 2004 (*documentation_plots_preicartt.pdf*, 1.3 MB).
2. ICARTT, which presents the data reduction from May 2004 to September 2004 (*documentation_plots_icartt.pdf*, 904 kB).
3. POST-ICARTT, which covers the data reduction from October 2004 to August 2005 (*documentation_plots_posticartt.pdf*, 1.6 MB).
4. ACCURACY, which includes the determination of total accuracy of the instrument (*total_accuracy_measurements.pdf*, 269 kB).

The files are included in the CD attached to this dissertation.